Transcriptional Regulation of Energy Homeostasis and Metabolism in the Central Nervous System

Inaugural-Dissertation

zur

Erlangung des Doktorgrades

der Mathematisch-Naturwissenschaftlichen Fakultät

der Universität zu Köln

vorgelegt von

Marianne Bettina Ernst

aus Bottrop

Köln 2010

"The noblest pleasure is the joy of understanding"

Leonardo da Vinci

für

meine Mutter

Brigitte

TABLE OF CONTENTS

I

Figure Index

Table Index

Abbreviations

°C	degrees Celsius
β-gal	β-galactosidase
3'	three prime end of DNA sequences
5'	five prime end of DNA sequences
A	adenosine
a.m.	ante meridiem
aCSF	artificial cerebrospinal fluid
ACTH	adrenocorticotropin
AgRP	agouti-related peptide
AKT	protein kinase B
Ala	alanine
AP	action potential
ARC	arcuate nucleus
ATP	adenosine triphosphate
Asn	asparagine
Bcl-2	B-cell lymphoma 2
Bim	Bcl-2 interacting mediator of cell death
BMI	body mass index
bp	base pairs
C	cytosine
CaCl$_2$	calcium chloride
CAGGS	*chicken β-actin* promoter
CBP	CREB-binding protein
cDNA	complementary DNA
Ci	Curie
CIS	cytokine-inducible SH2-containing proteins
CNS	central nervous system
cpm	counts per minute
Cre	site-specific recombinase from phage P1 (causes recombination)
CREB	cAMP responsive element-binding protein
DAPI	4',6-diamidino-2-phenylindole
DBD	DNA-binding domain
DIG	digoxigenin
DIO	diet-induced obesity
DMSO	dimethylsulfoxide
DNA	desoxyribonucleic acid
DNase	desoxyribonuclease
dNTP	desoxyribonucleotide-triphosphate

DTT	1,4-Dithio-DL-threitol
E day	embryonic day
E. coli	*Escherichia coli*
e.g.	*exempli gratia*
ECL	enhanced chemiluminescence
EDTA	ethylendiamine tetraacetate
EF	embryonic fibroblasts
eGFP	enhanced green fluorescent protein
EGTA	ethylene glycol tetraacetic acid
ELISA	enzyme-linked immunosorbent assay
EMSA	electrophoretic mobility shift assay
ERK	extracellular signal-regulated kinase
ES	embryonic stem cells
EtBr	ethidium bromide
EtOH	ethanol
F	Farad
FasL	Fas ligand
FCS	fetal calf serum
FLuc	firefly luciferase
FOX	forkhead box-containing protein
FOXO1	forkhead box-containing protein class O 1
FOXO1ADA	constitutively active version of FOXO1
FOXO1DN	dominant negative version of FOXO1
FRE	FOXO recognition element
g	gram
G	guanine
G418	geneticin
G6Pase	glucose-6-phosphatase
GABA	γ-aminobutyric acid
GaCSF	glycerol-based modified artificial cerebrospinal fluid
GAPDH	glyceraldehyde-3-phosphate dehydrogenase
GTP	guanosine triphosphate
GTT	glucose tolerance test
Gusb	glucuronidase beta
h	hour
H_2O_2	hydrogen peroxide
HCl	hydrochloric acid
H&E	hematoxylin/eosin
HEPES	N-2-hydroxyethylpiperazine-N'-2-ethansulfonic acid
HFD	high fat diet
Hprt-1	hypoxanthine guanine phosphoribosyl transferase-1

HR	homologous recombinant
HSV-tk	thymidine kinase of the *Herpes simplex* virus
Hz	Hertz
i.e.	*id est*
IGF1	insulin-like growth factor 1
IGFBP	insulin growth factor-binding protein
IKK	IκB kinase
IL6	interleukin 6
IR	insulin receptor
IRES	internal ribosome entry site
IRS	insulin receptor substrate
ITT	insulin tolerance test
JAK	janus kinase
JNK	c-jun-N-terminal kinase
k	kilo
kb	kilobase
KCl	potassium chloride
K-gluconate	potassium gluconate
KOH	potassium hydroxide
l	liter
LacZ	gene encoding the enzyme *β-galactosidase*
LAH	long arm of homology
LB	Luria-Bertani
LEPR	leptin receptor
LH	lateral hypothalamic area
LIF	leukemia inhibitory factor
*lox*P	recognition sequence for Cre (locus of crossing over phage P1)
m	milli
M	Mol
MAPK	mitogen-activated protein kinase
MCR	melanocortin receptor
MEF	murine embryonic fibroblasts
$MgCl_2$	magnesium chloride
min	minute
mRNA	messenger ribonucleic acid
MSH	melanocyte-stimulating hormone
MST1	mammalian sterile 20-like protein kinase 1
n	nano
Na_2HPO_4	disodium hydrogen phosphate
Na_3O_4V	sodium orthovanadate
NaCl	sodium chloride

Abbreviations

NaF	sodium fluoride
NaH_2PO_4	monosodium phosphate
$NaHCO_3$	sodium bicarbonate
NaOH	sodium hydroxide
NCD	normal chow diet
NeoR	*neomycine resistance* gene
NES	nuclear export signal
NLS	nuclear localisation sequence
NMR	nuclear magnetic resonance
NP-40	nonidet P-40
NPY	neuropeptide Y
ObRb	long isoform of the leptin receptor
OD	optical density
Osm	Osmolarity
P	phosphorylation
p	pico
PAGE	polyacrylamid gel electrophoresis
PBS	phosphate buffered saline
PCR	polymerase chain reaction
PDK1	phosphoinositide-dependent protein kinase 1
PEPCK	phosphoenolpyruvate carboxykinase
PFA	paraformaldehyde
PI3K	phosphatidylinositol 3 kinase
PIAS	protein inhibitor of activated STAT
PIP_2	phosphatidylinositol-4,5-bisphosphate
PIP_3	phosphatidylinositol-3,4,5-trisphosphate
POMC	proopiomelanocortin
PTB	phosphotyrosine binding
PTEN	phosphatase and tensin homolog
PTP	protein tyrosine phosphatase
PVDF	polyvinylidene fluoride
PVN	paraventricular nucleus
R_a	access resistance
RF	radio frequency
RIPA	radioimmunoprecipitation assay
RLuc	*Renilla* luciferase
RNA	ribonucleic acid
RNase	ribonuclease
rpm	rounds per minute
RT	room temperature
SA	splice acceptor

SAH	short arm of homology
Ser	serin
SD	standard deviation
SDS	sodiumdodecylsulfate
sec	second
SEM	standard error of the mean
SH	src homology
SHP2	SH2-domain-containing phosphatase
SIRT1	silent mating type information regulation 2 homolog 1
SOCS3	suppressor of cytokine signalling 3
ss	single-stranded
SSC	sodium chloride/ sodium citrate buffer
STAT3	signal transducer and activator of transcription 3
STAT3-C	constitutively active version of STAT3
SV40	*Simian* virus 40
T2DM	type 2 diabetes mellitus
TAD	transcriptional activation domain
TAE	Tris-acetic acid-EDTA buffer
Taq Pol	polymerase from *Thermus aquaticus*
TBE	Tris/borate/EDTA buffer
TBS	Tris buffered saline
TE	Tris-EDTA buffer
TF	transcription factor
Thr	threonine
TRAIL	tumor necrosis factor-related apoptosis-inducing ligand
Tris	2-amino-2-(hydroxymethyl-)1,3-propandiol
TUNEL	terminal deoxynucleotidyl transferase-mediated dUTP-biotin nick end labelling
TWEEN	polyoxethylene-sorbitan-monolaureate
Tyr	tyrosine
U	Unit
UV	ultraviolet
V	Volt
v/v	volume per volume
VMH	ventromedial nucleus of the hypothalamus
W	Watt
w/o	without
w/v	weight per volume
WHO	World Health Organization
wt	wild-type
ZnSO4	zinc sulfate
µ	micro

1 Introduction

1.1 Obesity and type 2 diabetes mellitus

Obesity is a steadily growing worldwide health problem. Even though initially most abundant in the United States and Western Europe, obesity is now dramatically rising in low- and middle-income countries such as China and Latin America [1, 2]. The most frequently used method to diagnose obesity is the calculation of the body mass index (BMI = body weight in kg/size in meters^2) [3]. The World Health Organization (WHO) defines a BMI ≥ 25 as overweight and a BMI ≥ 30 as obesity. Moreover, the WHO estimated at least 400 million adults globally as obese in 2005 and predicts that in 2015 more than 700 million will be obese [4]. Furthermore, there is an alarming rise in childhood obesity, as at least 20 million children younger than 5 years were overweight worldwide in 2005 [4].

Obesity represents a serious threat to health as it increases the risk of developing various chronic diseases, including type 2 diabetes mellitus (T2DM), cardiovascular diseases, musculoskeletal disorders, certain types of cancer, depression, and sleep apnea [5-7]. For this, obese people have an increased mortality, which rises progressively with increasing BMI within the BMI range above 30 [8, 9]. The cumulative economic costs of obesity are immense and a substantial portion is attributed to T2DM. For instance, it is estimated that 20% of the US health care budget are spent on patients with diabetes mellitus and that the expense will escalate [10]. Recent assessments have indicated 171 million people worldwide with T2DM in 2000 and project an ascent to 366 million by 2030 [11]. T2DM is a progressive disease characterised by chronic hyperglycemia caused by absolute and relative insulin deficiency due to insulin insensitivity in muscle and fat cells, hepatic glucose production during ingestion, and over time regressive β-cell effectiveness [12, 13]. The chronic hyperglycemia leads to severe tissue damage ranging from microvascular disorders such as retinopathy, nephropathy, and neuropathy to macrovascular complications as angina pectoris, myocardial infarction, stroke, and peripheral arterial disease [14, 15]. Therefore, T2DM patients have a reduced quality of life and finally a diminished life expectancy. Diabetes mellitus belongs to the 10 leading causes of death and is responsible for 5% of all deaths globally each year [16, 17].

Various genetic factors have been identified accounting for the development of obesity as mutations in leptin, leptin receptor (LEPR), proopiomelanocortin (POMC), and melanocortin 4 receptor (MC4R) [18]. In addition, a recent genome-wide search has

discovered that common variants of the *fat mass and obesity associated* (FTO) gene are implicated in a higher BMI and the risk of obesity [19, 20]. Due to the fact that single gene mutations have been found in only 5% of all obese patients (BMI ≥ 40) [18], the worldwide prevalence of obesity is more likely caused by environmental and behavioural factors such as high caloric diet and lack of physical activity and is only partially accompanied by genetic predisposition [21].

1.2 Central regulation of energy homeostasis

The continuous increase of body weight and fat mass is caused by a chronic modification of energy balance: energy intake by ingestion versus energy expenditure by exercise, basal metabolism, and thermogenesis. Such an imbalance gives rise to elevated body mass when energy assimilation is in excess of energy utilisation or conversely results in reduced body weight when dissimilation of energy outbalances absorbed energy. Accordingly, elucidating the regulation of energy homeostasis is fundamental to understand the mechanisms of obesity and the development of therapeutic strategies [22, 23].

The central nervous system (CNS) plays an important role in the regulation of energy homeostasis; several brain regions from cortex to brainstem are responsible for controlling energy balance as shown by the effect of factors such as smell and sight of food, and conviviality on food intake in humans [23, 24]. Despite this, most attention has focussed on the hypothalamus, which has already been identified in the 1940s and 1950s to be involved in maintaining energy balance by classical lesion experiments in rodents [25, 26].

1.2.1 The hypothalamus

The hypothalamus marks the ventral part of the diencephalon in vertebrates and is located below the thalamus, just above the brainstem. Neuron populations located in the hypothalamus regulate energy homeostasis, drinking behaviour, body temperature, stress response, reproduction, and the autonomous nervous systems. The hypothalamus is a complex region containing more than 40 anatomically defined neuronal clusters and nuclei including the arcuate nucleus (ARC), the paraventricular nucleus (PVN), the ventromedial nucleus of the hypothalamus (VMH), the dorsomedial hypothalamic nucleus (DMH), and the lateral hypothalamic area (LHA) (Figure 1) [27, 28]. Diverse lesion and electrical studies have shown that destruction of the VMH, DMH or PVN causes severe hyperphagia and obesity in

rats, whereas destruction of the LHA leads to hypophagia. Based on these findings the VMH was identified as the "satiety centre" and the LHA as "hunger centre" [25, 26]. This model was accepted for several decades. Nowadays it is known that the PVN, VMH, DMH, and LHA contain second order neurons which process information regarding energy homeostasis by receiving neuronal projections from the ARC [29].
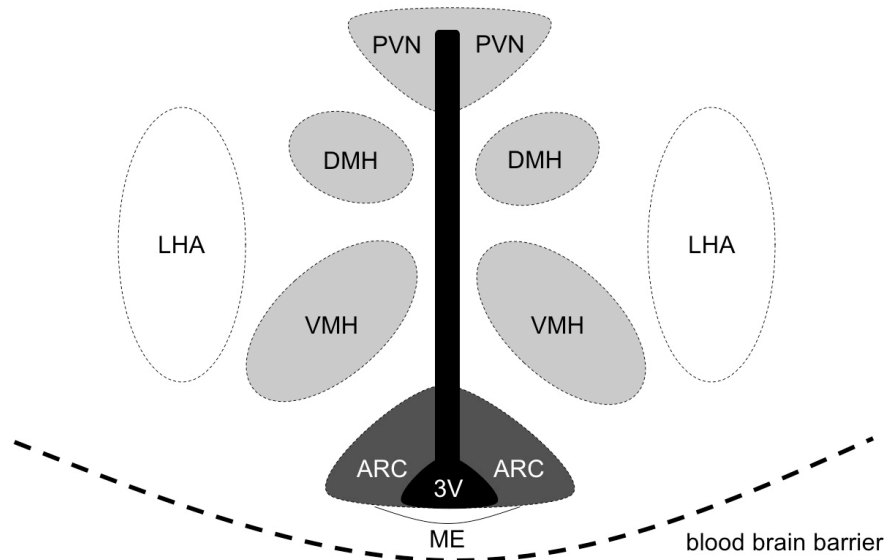
Figure 1: Anatomical structure of the hypothalamic nuclei.
Schematic coronal section of the hypothalamus including main regions involved in the regulation of food intake and energy expenditure. ARC, arcuate nucleus; DMH, dorsomedial hypothalamic nucleus; LHA, lateral hypothalamic area; ME, median eminence; PVN, paraventricular nucleus; VMH, ventromedial nucleus of the hypothalamus; 3V, third ventricle.

1.2.2 The arcuate nucleus of the hypothalamus

The ARC is located in the mediobasal hypothalamus adjacent to the base of the third ventricle directly above the median eminence (ME) (Figure 1) and plays a pivotal role in regulation of energy homeostasis by sensing and integrating signals mediated by nutrients, cytokines, and hormones. Since the ME area is not protected by the blood brain barrier, the entry of circulating peripheral peptides and hormones such as leptin and insulin via saturable mechanisms is permitted [30-32]. Two primary populations of functionally opposing neurons located in the ARC have been studied in detail: the anorexigenic POMC-expressing and the orexigenic agouti-related peptide/neuropeptide Y (AgRP/NPY)-expressing neurons. Whereas the catabolic neuropeptide POMC suppresses food intake and increases energy expenditure, the anabolic neuropeptides AgRP and NPY stimulate food intake and reduce energy expenditure [33-35].

Besides in the ARC, POMC is also expressed in the pituitary, nucleus tractus solitaries of the brainstem, and at low levels in several peripheral tissues such as skin, pancreas, and testis [36-38]. The POMC precursor protein is cleaved posttranslationally in a tissue-specific manner by various prohormone convertases into mature peptide hormones including adrenocorticotropic hormone (ACTH), melanocyte-stimulating hormone (α-MSH, β-MSH, γ-MSH), and β-endorphin [39]. α-MSH is generated by cleavage in POMC neurons as an important participant for regulating energy homeostasis [40]. After its secretion, α-MSH binds to the melanocortin receptors MC3R and MC4R. These G-protein-coupled receptors are expressed in multiple nuclei including PVN, DMH, and VMH and activate the adenylate cyclase [41-43]. Consistently, both POMC-deficiency in humans caused by mutation in the *pomc* gene and POMC-null mutant mice develop severe obesity due to hyperphagia, combined with defective adrenal development and altered pigmentation [44, 45]. Furthermore, expression levels of the anorexigenic POMC reflect the energy state of the body: in fasted animals POMC mRNA is significantly reduced, but is restored with refeeding [46]. In addition, mice lacking MC3R and/or MC4R develop obesity due to a modified energy balance: MC4R-deficient mice show an increased food intake and MC3R-deficiency results in reduced energy expenditure due to hypoactivity without elevated food intake [47-49].

The neuropeptide AgRP is primarily expressed in a distinct neuronal population of the ARC, where it colocalises with NPY. The orexigenic AgRP acts as an inverse agonist of MC3R and MC4R and inhibits the anorectic effect of α-MSH [50]. Accordingly, fasting increases the expression of AgRP mRNA in the ARC and reduction of hypothalamic AgRP mRNA by RNA interference causes an elevated metabolic rate and reduced body weight without affecting feeding [46, 51]. NPY is widely distributed in the brain, but mainly expressed in the ARC [52]. Five G-protein-coupled NPY receptors (Y1, Y2, Y4, Y5, and Y6) with individual distribution patterns have been identified to mediate the diverse effects of this abundant neurotransmitter [53, 54]. The most potent orexigenic factor discovered to date is NPY. Central administration of this peptide causes obesity due to hyperphagia and decreased energy expenditure [55, 56]. Consistently, fasting increases and refeeding decreases NPY mRNA expression [46, 57]. However, disruption of neither NPY nor AgRP or both results in hypophagia [58, 59]. But in contrast, ablation of AgRP/NPY neurons in adult mice causes starvation leading to dramatic reduction in body weight [60, 61]. In addition to orexigenic peptides, AgRP/NPY neurons also release the neurotransmitter γ-aminobutyric acid (GABA) causing inhibitory GABAergic innervation on POMC neurons [62, 63].

Both POMC and AgRP/NPY neurons are located in the ARC and project primarily to the PVN, but also to other MC3R- and MC4R-expressing brain regions [42, 64]. These second order neurons are involved in the regulation of energy expenditure, food intake, and hepatic glucose metabolism (Figure 2) [65].

1.2.3 Regulation of neurons located in the arcuate nucleus

For the regulation of energy homeostasis, the brain senses and integrates peripheral signals of the body energy status by monitoring the levels of hormones such as insulin and leptin as well as of cytokines and nutrients such as glucose and free fatty acids (Figure 2) [66].
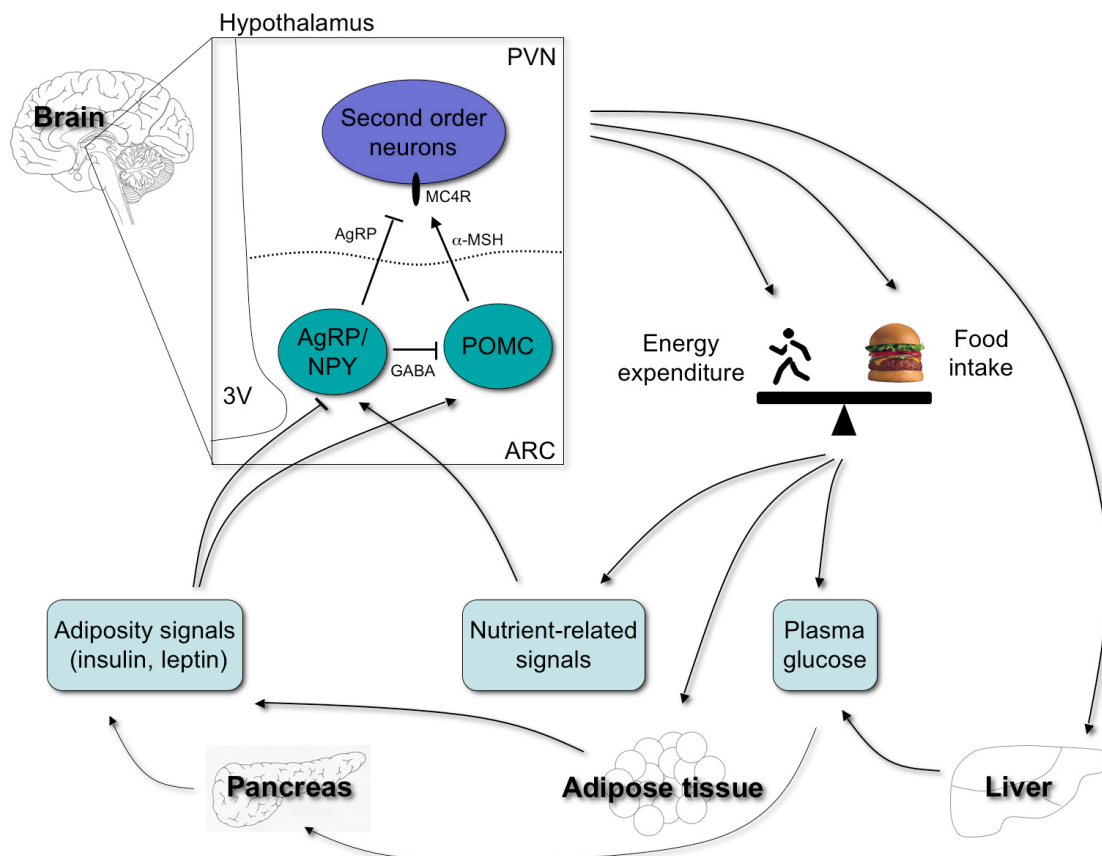
Figure 2: Central regulation of energy homeostasis.
The ARC of the hypothalamus is a critical region that senses and integrates signals regarding the body energy status by monitoring the levels of hormones such as pancreas-derived insulin and adipocyte-secreted leptin, as well as cytokines and nutrients such as glucose and free fatty acids. In the ARC, AgRP/NPY and POMC neurons receive peripheral signals through the unlocked blood brain barrier and regulate energy homeostasis by projecting to second order neurons primarily in the PVN. α-MSH, a cleaved product of POMC binds to MC4R in the PVN and suppresses food intake. In contrast, AgRP as an inverse agonist of MC4R counteracts α-MSH. Furthermore, AgRP/NPY neurons inhibit POMC neurons by synaptic release of GABA. Thus, interplay between POMC and AgRP/NPY neurons is crucial for the regulation of energy homeostasis by monitoring food intake, energy expenditure, and hepatic glucose production. α-MSH, α-melanocyte-stimulating hormone; AgRP, agouti-related peptide; ARC, arcuate nucleus; GABA, γ-aminobutyric acid; MC4R, melanocortin 4 receptor; NPY, neuropeptide Y; POMC, proopiomelanocortin; PVN, paraventricular nucleus; 3V, third ventricle (adapted from [22]).

In the ARC, both POMC and AgRP/NPY neuron populations coexpress the insulin and leptin receptor and are regulated by these hormones in an opposing manner [67, 68]. While the anorexigenic POMC-expressing neurons are activated, the orexigenic AgRP/NPY-expressing neurons are inhibited by insulin [69-71]. Similarly to insulin, leptin activates POMC neurons and inhibits AgRP/NPY neurons [62, 72]. Thus, central leptin administration increases POMC and decreases AgRP and NPY expression. Consistently, central insulin administration activates POMC and inhibits NPY production, without affecting AgRP expression [73-75]. In addition, the administration of a MC4R antagonist inhibits the anorexigenic effect of leptin [62, 76]. Consistently, leptin-deficient (*ob/ob*) and leptin receptor-deficient (*db/db*) mice exhibit decreased levels of POMC and elevated levels of AgRP and NPY mRNA [77, 78].

1.3 Leptin

The peptide hormone leptin was originally identified as the product of the *obese (ob)* gene by J. Friedman in 1994 [79]. Besides its role in controlling energy homeostasis by reflecting the body energy status to the brain [80], leptin is also involved in the regulation of pancreatic β-cells, reproduction, growth, immune system, sympathetic nervous system, thyroid axis, and adrenal corticosteroids [81-86].

Leptin is predominantly expressed in adipocytes and at lower levels in the gastric epithelium, placenta, and testis [79, 87-89]. Adipocytes serve as energy stores of the body and produce leptin in proportion to adipose tissue mass, dependent on number and size of adipose cells [90, 91]. Leptin expression in adipocytes is stimulated by glucose and insulin, but inhibited by fatty acids and by an increased rate of lipolysis in adipocytes [92-95]. Therefore, fasting decreases and refeeding restores leptin level in humans [90, 93]. Secreted leptin circulates in the blood and enters the brain across the blood brain barrier via a saturable mechanism [31]. Binding of leptin to its receptor leads to body weight loss as a consequence of decreased food intake and increased energy expenditure due to enhanced thermogenesis [96, 97]. Consistently, both *ob/ob* and *db/db* mice develop extreme obesity due to hyperphagia and reduced energy expenditure [98, 99]. Analogue, humans carrying loss-of-function mutations in *leptin* or *lepr* genes exhibit hyperphagia resulting in severe obesity [100, 101]. Peripheral and central administration of leptin to *ob/ob* mice reverses the obese phenotype [98, 102, 103]. Moreover, wild-type rodents under long-term treatment with leptin show a decreased food intake, loss of body weight and fat mass [98, 102, 103]. In line

with these findings, a recombinant leptin therapy of leptin-deficient patients can ameliorate the early-onset morbid obesity in both children and adults and emphasises the role of leptin as key molecule in maintaining energy balance [104, 105].

Only a minority of obese patients suffers from relative leptin deficiency, whereas the majority of obese humans and rodents exhibit proportionally high circulating leptin levels, pointing to leptin resistance in these cases: the body is not able to respond adequately to high leptin levels by reducing food intake and increasing energy expenditure [90, 106, 107]. Therefore, recombinant leptin therapy leads only to a modest reduction of body weight in most obese patients [108, 109]. Accordingly, centrally administered leptin has a reduced capacity to inhibit food intake in diet-induced obese mice, while peripheral leptin administration exhibit no influence on feeding behaviour to those mice [110]. The development of leptin resistance is likely caused by different mechanisms including defects in leptin transport into the brain and leptin signalling in hypothalamic neurons [107].

1.3.1 Leptin receptor signalling

Leptin exerts its effect by binding to the cell-surface LEPR, which belongs to the type 1 cytokine receptor family [111]. Alternative splicing of the single *lepr* gene and/or proteolytic processing generate multiple isoforms of the LEPR with an identical ligand-binding-domain, but variations in transmembrane and cytoplasmic domains [112, 113]. Among the different isoforms, intracellular signalling is mediated only by the long form of the LEPR (ObRb), which contains the full-length intracellular domain comprising several docking sites for proteins critical for signal transduction [111, 113]. The ObRb is expressed at basal levels in multiple tissues including lung, kidney, liver, adipose tissue, and pancreatic β-cells, but is most abundant in the brain, especially in the hypothalamus where it influences the control of energy balance [114, 115].

Binding of leptin to ObRb leads to the homodimerisation of the receptor and subsequently results in the activation of the Janus kinase/signal transducer and activator of transcription (JAK/STAT) signalling pathway (Figure 3) [116-118]. The dimerised ObRb causes activation and autophosphorylation of the constitutively associated JAK2. This tyrosine kinase in turn phosphorylates the ObRb within the cytoplasmic domain at the residues Tyr^{985}, Tyr^{1077}, and Tyr^{1138}, which act as docking sites for downstream signalling molecules [116, 119, 120]. Each phosphorylated tyrosine site of the ObRb is recognised by specific proteins containing a specialised phosphotyrosine-binding-domain, the SH2-domain

[121]. Phosphorylated Tyr^{985} leads to recruitment and phosphorylation of the SH2-domain-containing phosphatase (SHP) 2 and thereby mediates the activation of the extracellular signal-regulated kinase (ERK) pathway, which is known to be involved in energy homeostasis and metabolism [122, 123]. Recently, it has been demonstrated that upon phosphorylation of Tyr^{1077}, STAT5 is activated, translocates in the nucleus, and regulates gene expression [120, 124]. Tyr^{1138} of the ObRb lies within a consensus YXXQ-binding site for STAT3. Leptin-induced binding to phosphorylated Tyr^{1138} causes STAT3 phosphorylation and activation by JAK2 [125, 126].
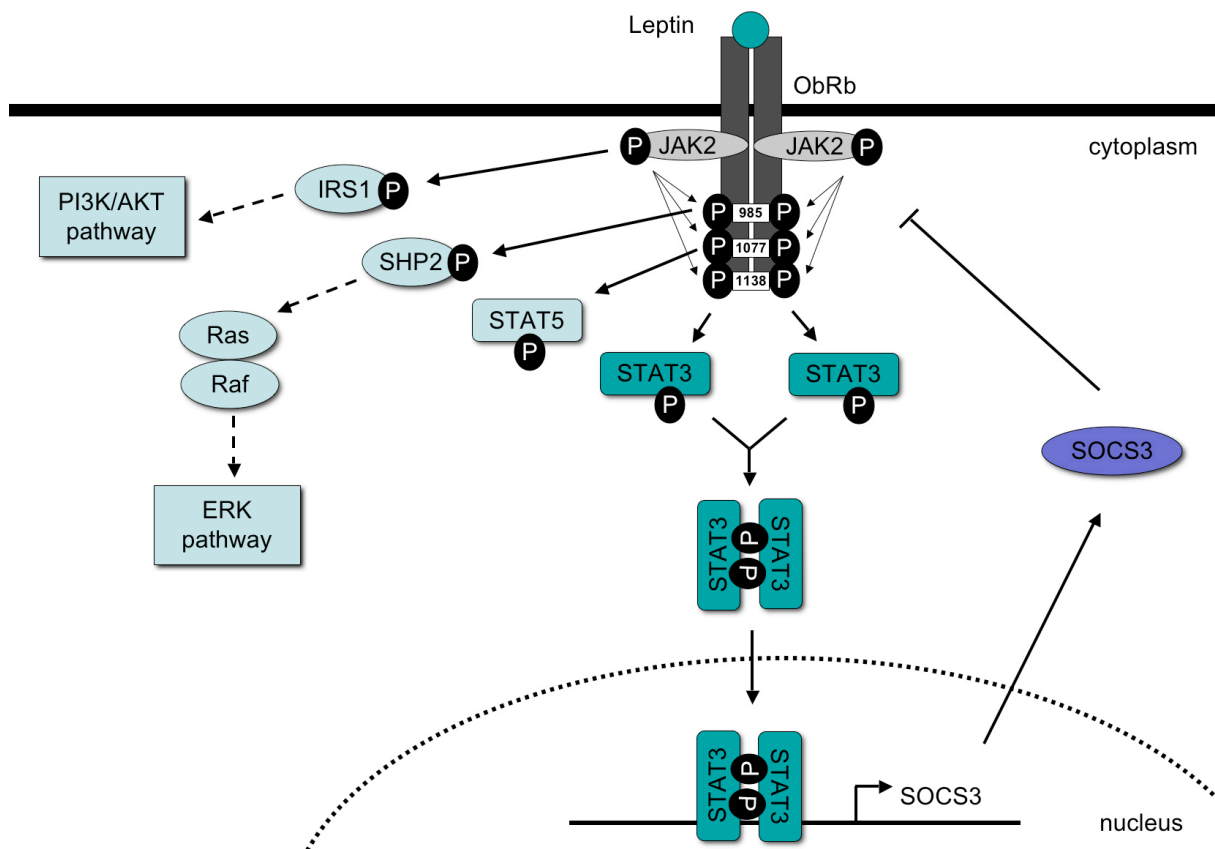
Figure 3: Leptin receptor signalling.
Binding of leptin to the ObRb results in activation of JAK2 and subsequently leads to JAK2-mediated phosphorylation of the intracellular residues Tyr^{985}, Tyr^{1077}, and Tyr^{1138} of the receptor. Phosphorylated Tyr^{985} activates the ERK pathway via SHP2, phosphorylation of Tyr^{1077} leads to activation of STAT5, and phosphorylated Tyr^{1138} causes phosphorylation and activation of STAT3. Activated STAT3 dimerises, translocates into the nucleus and regulates transcription of target genes such as SOCS3, which acts as negative regulator of JAK/STAT signalling. Additionally, phosphorylated JAK2 directly activates PI3K signalling by IRS1. AKT, protein kinase B; ERK, extracellular signal-regulated kinase; IRS1, insulin receptor substrate 1; JAK2, Janus kinase 2; ObRb, long form of leptin receptor; P, phosphorylation; Raf, ras-activated factor; Ras, rat sarcoma virus protein; SHP2, SH2-domain-containing phosphatase; STAT3, signal transducer and activator of transcription 3; SOCS3, suppressor of cytokine signalling 3; Tyr, tyrosine; PI3K, phosphatidylinositol 3 kinase.

Phosphorylated STAT3 dimerises, translocates from the cytoplasm into the nucleus, and regulates transcription of target genes contributing to the regulation of energy homeostasis [127, 128]. Furthermore, STAT3 activates the transcription of suppressor of

cytokine signalling (SOCS) 3, which acts as a negative feedback regulator of JAK/STAT signalling [129, 130]. Disruption of the STAT3-binding site in ObRb as well as neuronal deletion of STAT3 causes severe hyperphagia and morbid obesity indicating that the ObRb/JAK/STAT pathway in the brain is essential to transmit leptin's capacity to reduce food intake and increase energy expenditure [131-134].

In addition to the JAK/STAT and the ERK pathways, leptin also activates phosphatidylinositol 3 kinase (PI3K) signalling due to direct tyrosine phosphorylation of insulin receptor substrate (IRS) 1 by JAK2 (Figure 3). However, this activation is independent of phosphorylated immunoreceptor tyrosine-based activation motifs (ITAM) in the ObRb [116, 135]. These findings support the assumption of synergism and convergence of leptin and insulin signalling pathways [136].

1.3.2 STAT transcription factors

The first two STAT transcription factors (TFs) were discovered in the early 1990s as DNA-binding proteins that mediate interferon (IFN) signalling [137]. Seven mammalian STAT proteins (STAT1, 2, 3, 4, 5a, 5b and 6) encoded by individual genes have been identified [127]. All STATs are activated by cytokines and share characteristic domains: a coiled-coil-domain for interaction with other proteins, a DNA-binding-domain (DBD), a SH2-domain for dimerisation, a tyrosine activation-domain, and a C-terminal transcriptional activation-domain (TAD) [138].

"Knock-out" mice lacking an individual *stat* gene gave new insights of STATs in a variety of biological processes [139]. In short, STAT1 participates in anti-viral and anti-bacterial responses, growth inhibition, apoptosis, and tumour suppression [140, 141], while STAT4 and STAT6 are essential for T-helper 1 and 2 development [142, 143]. STAT5a and STAT5b regulate proliferation, cell cycle progression, and prolactin response [144, 145] and STAT3 is essential for early development as evidenced by embryonic lethality of STAT3-deficient mice [146]. However, tissue-specific disruption of STAT3 revealed its various functions including wound healing, mammary involution, anti-inflammatory responses in macrophages and neutrophils, and survival of different cell types [147-150]. In general, STAT3 activation has been associated with the prevention of apoptosis and promotion of survival, proliferation, and cellular transformation including oncogenesis [151]. STAT3 also regulates energy homeostasis, as ablation of STAT3 in the CNS causes obesity combined with decreased POMC expression [133]. Moreover, STAT3 directly mediates the

feeding repressing effects of leptin by transcriptional regulation of orexigenic AgRP and anorexigenic POMC. The effect of STAT3 to increase POMC and decrease AgRP expression is counter-regulated by forkhead box-containing protein class O 1 (FOXO1) through transcriptional squelching [73, 152, 153].

1.3.2.1 Negative regulation of STAT signalling

The latent cytoplasmic STAT TFs are activated by a multitude of cytokines including IFN and interleukins (IL) as well as growth factors and hormones such as leptin and insulin. While STAT2, STAT4, and STAT6 are activated by a limited number of cytokines, STAT1, STAT3, STAT5a, and STAT5b are mobilised by diverse distinct and in part overlapping ligands [154, 155]. Four different mechanisms have been identified to activate STAT proteins via tyrosine phosphorylation. First, STATs become activated by the classical JAK tyrosine phosphorylation (1.3.1), which is initiated by receptor-binding of cytokines such as IL6, IFN, leukemia inhibitory factor (LIF), or ciliary neurotrophic factor (CNTF) [156]. Second, receptors containing intrinsic tyrosine kinase activity such as epidermal growth factor (EGF), platelet-derived growth factor (PDGF), and fibroblast growth factor (FGF) receptor directly activate STAT proteins [155]. Third, G-protein-coupled receptors including chemokine receptors for mitogen-activated protein (MAP) 1 and RANTES cause JAK activation leading to STAT phosphorylation [157]. Fourth, non-receptor tyrosine kinases such as the viral oncoproteins v-src, v-Sis, v-Fps, v-abl and polyoma virus middle T antigen lead to persistent STAT activation [158]. Phosphorylation of STATs leads to formation of homodimers or heterodimers by reciprocal binding of the SH2-domain of one monomer to the crucial phosphotyrosine of the partner molecule. In case of STAT3, the dimerisation is initiated by phosphorylation of Tyr^{705}, while Ser^{727} phosphorylation by kinases including ERK and c-jun-N-terminal kinase (JNK) negatively modulates Tyr^{705} phosphorylation [159, 160]. The resulting STAT dimers translocate via importin into the nucleus [161], where they bind to specific DNA sequences and activate transcription of target genes [138, 155].

The negative regulation of STATs is controlled by constitutively expressed and cytokine-induced proteins including SOCS, cytokine-inducible SH2-containing proteins (CIS), protein inhibitor of activated STAT (PIAS), and phosphatases (Figure 4) [162, 163].
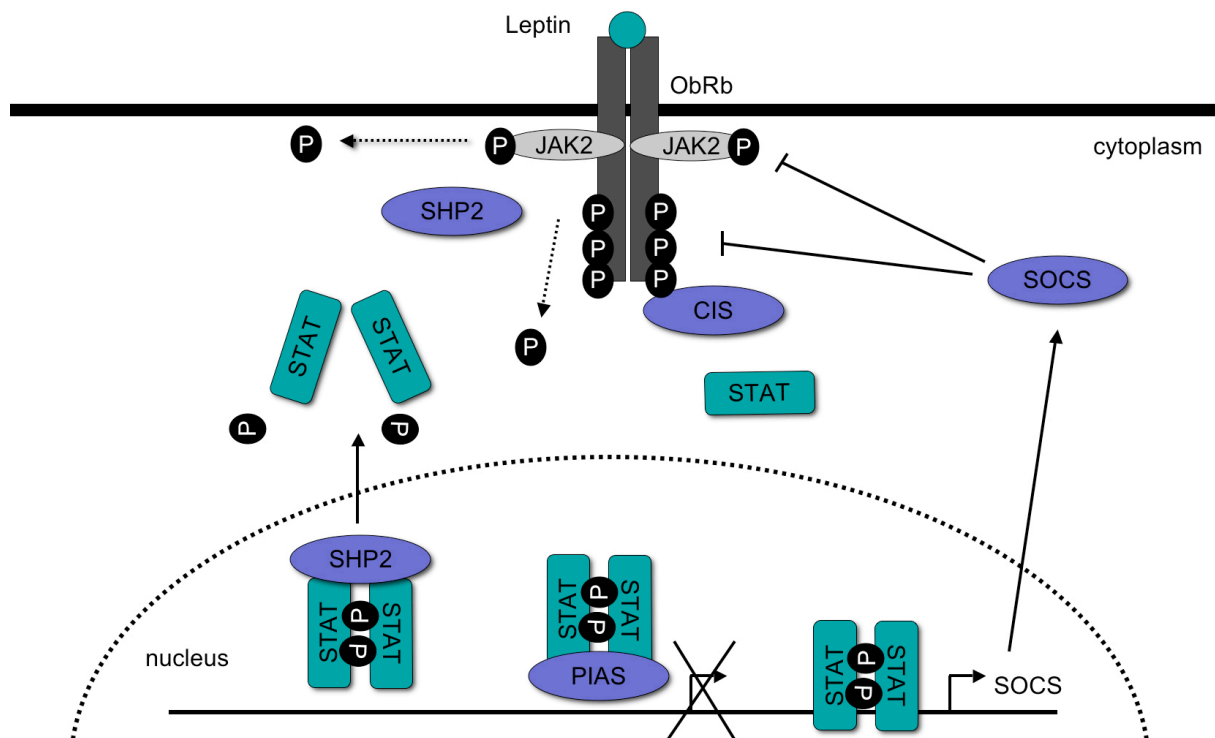
Figure 4: Negative regulation of STAT signalling.
The phosphorylation and dimerisation of STAT causes translocation to the nucleus and transcriptional activation of target genes including SOCS acting as a negative regulator of STAT activation. SOCS suppresses JAK activity by interacting with both phosphorylated receptor and JAK. CIS competes with STAT proteins for the same docking sites at the phosphorylated receptor. PIAS binds to dimerised STAT and blocks the DNA-binding and transcriptional activity of the TF. Phosphatases such as SHP2 inactivate STAT by dephosphorylation of receptor, JAK, and STAT. CIS, cytokine-inducible SH2-containing proteins; JAK2, Janus kinase 2; ObRb, long form of leptin receptor; P, phosphorylation; PIAS, protein inhibitor of activated STAT; SHP2, SH2-domain-containing phosphatase; STAT, signal transducer and activator of transcription; SOCS, suppressor of cytokine signalling.

SOCS and CIS proteins belong to the family of STAT target genes, which directly antagonise STAT activation. STAT3-activated SOCS3 interacts with phosphorylated receptors as well as with JAK proteins as a classical feedback loop of cytokine signalling [164, 165]. Moreover, CIS blocks STAT receptor recruitment by competing for the same

docking site on phosphorylated receptors [166]. By contrast, PIAS proteins are constitutively expressed and directly interact with STATs in the nucleus. PIAS3 binds to STAT3 dimers and thereby blocks DNA-binding and transcriptional activity of the TF [167]. In addition, phosphatases such as SHP2 and protein tyrosine phosphatase (PTP) 1B permanently dephosphorylate the receptor, JAK, and STAT [168, 169].

1.3.2.2 Constitutively active STAT3 mutant

Constitutively active STATs are associated with oncogenesis. Persistently activated STAT3 and STAT5 proteins - potentially evoked by viral oncoproteins - were identified in a variety of clinical samples such as lymphoma, leukemia, multiple myeloma, or cancer of brain, prostate, breast, lung, and neck, respectively [151]. Consistently, it was shown that STAT3 proteins regulate the transcription of proto-oncogenes such as c-myc and interact with c-jun [170, 171].

A constitutively active version of STAT3 (STAT3-C) was created by substitution of the residues Ala^{661} and Asn^{663} to cysteins in the SH2-domain, thereby producing a mutant which dimerises spontaneously via disulfide bonds, thus activating transcription independent of signal-dependent Tyr^{705} phosphorylation [172]. The functionality of this STAT3-C mutant to constitutively activate target genes was demonstrated in several studies [173-176], as STAT3-C expression in cultured fibroblasts leads to transformed cells, which are capable of forming tumours in nude mice [172].

1.4 Insulin

Insulin is a peptide hormone that plays a key role in the regulation of glucose metabolism and energy homeostasis [177]. The anabolic insulin is produced by the β-cells of the pancreatic islets of Langerhans; it is synthesised as the inactive precursor proinsulin and then cleaved by peptidases giving rise to the native insulin capable to interact with the insulin receptor (IR) [178-180]. Insulin secretion is increased rapidly after ingestion due to rises in blood glucose levels, whereas the circulating insulin level is directly correlated to the body fat mass [181, 182].

Circulating insulin promotes the influx of nutrients and simultaneously blocks the release of stored energy forms by binding to the IR, which is expressed in the primary insulin target tissues: fat, muscle, and liver [183]. In particular, insulin increases the glucose uptake

in muscle cells and adipocytes by translocation of the glucose transporter to the cell membrane [183-185]. Furthermore, insulin promotes anabolic processes such as amino acid uptake and protein synthesis in muscle, glycogen synthesis in liver and muscle, as well as lipogenesis in adipocytes. In contrast, catabolic processes such as gluconeogenesis, glycogenolysis, lipolysis, and proteolysis are suppressed by insulin [186, 187]. Besides the effect of insulin on peripheral tissues, circulating insulin passes the blood brain barrier via a

saturable mechanism, binds to the IR, which is centrally widely expressed and regulates energy homeostasis [188-191].

Central administration of insulin causes reduction of body weight by decreasing food intake and increasing energy expenditure [69]. Consequently, neuron-specific IR-deficient mice show diet-sensitive obesity and mild insulin resistance [192]. Moreover, it was shown that insulin action in AgRP neurons is required to suppress hepatic glucose production, further supporting the important role of insulin signalling in the CNS to regulate energy homeostasis [193].

1.4.1 Insulin receptor signalling

Insulin mediates its pleiotropic effects by binding to the IR, which is predominantly expressed in the primary insulin target tissues, but also in other tissues such as the CNS, pancreas, kidney and lymphatic cells [188, 192, 194-197]. The heterotetrameric IR belongs to the family of ligand-activated receptor tyrosine kinases and forms a bifunctional complex consisting of two extracellular α-subunits and two transmembrane β-subunits [198-200].

After binding of insulin to the α-subunits, a conformational change is induced thereby activating the intrinsic tyrosine kinase activity of the β-subunits, which leads to autophosphorylation of the receptor [201, 202]. Subsequently, IRS1-4 are recruited via phosphotyrosine-binding (PTB)-domains and in turn tyrosine phosphorylated to serve as docking platforms for further downstream signalling events [203-205]. Recruitment of growth factor receptor-binding protein (GRB) 2, SHP2, and the regulatory subunit of PI3K activates two important branches of the IRS pathway [206-208]: on one hand the mitogen-activated protein kinase (MAPK) pathway enhances growth and differentiation [209, 210], while on the other hand the PI3K pathway mediates the majority of insulin's metabolic actions (Figure 5) [208, 211, 212].

The PI3K is a heterodimer, which comprises a catalytic subunit p110 and a regulatory subunit p55 or p85, whereas p85 is the most highly expressed regulatory subunit [213]. The binding of p85 or p55 to phosphorylated tyrosine residues of IRS leads to conformational changes and activation of p110 by translocating p110 to the plasma membrane [208, 211]. At the membrane, PI3K catalyses the conversion of phosphatidylinositiol-4,5-bisphosphate (PIP_2) to phosphatidylinositol-3,4,5-trisphosphate (PIP_3) [214, 215]. However, PI3K is counter-regulated by the phosphatase and tensin homolog (PTEN) [216]. Accumulation of PIP_3 at the plasma membrane recruits phosphoinositide-dependent protein kinase (PDK) 1,

which in turn phosphorylates and activates protein kinase B (AKT) [217]. Activated AKT phosphorylates downstream targets such as AKT substrate (AS) 160, glycogen synthase kinase (GSK) 3, mammalian target of rapamycin (mTOR), and FOXO proteins to mediate the diverse effects of insulin including stimulation of glucose uptake, glycogen and protein synthesis, and the regulation of transcription (Figure 5) [218, 219].
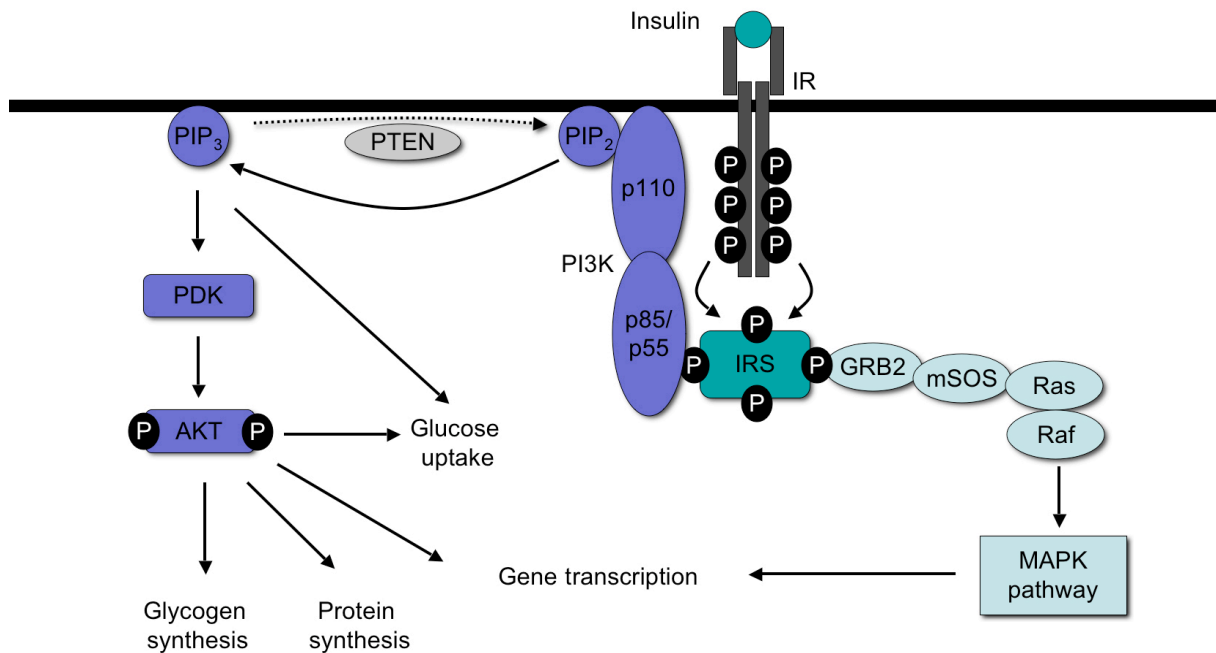
Figure 5: Insulin receptor signalling.
Binding of insulin causes a conformational change of the IR, resulting in activation of the intrinsic tyrosine kinase and autophosphorylation of the intracellular subunits of the IR. Subsequently, IRS proteins are tyrosine phosphorylated to serve as docking platforms for SH2-domain-containing proteins such as GRB2 and the regulatory subunit of the PI3K. Binding and activation of these proteins elicit activation of signalling cascades such as the Ras-Raf-MAPK and the PI3K pathway. The activation of PI3K catalyses formation of PIP_3 leading to PDK-mediated phosphorylation and activation of AKT. These signals result in the diverse effects of insulin signalling including glucose transport, glycogen and protein synthesis, and gene transcription. AKT, protein kinase B; IR, insulin receptor; IRS, insulin receptor substrate; GRB2, growth factor-binding protein 2; mSOS, son of sevenless; Raf, ras-activated factor; Ras, rat sarcoma virus protein; MAPK, mitogen-activated protein kinase; p55, regulatory subunit of PI3K; p85, regulatory subunit of PI3K; p110, catalytic subunit of PI3K; PDK1, phosphoinositide-dependent kinase 1; PI3K, phosphatidylinositol 3 kinase; PIP_2, phosphatidyl-inositol-4,5-bisphosphate; PIP_3, phosphatidylinositol-3,4,5-trisphosphate; PTEN, phosphatase and tensin homolog; SH2, src-homology 2.

1.4.2 FOXO transcription factors

The forkhead box-containing (FOX) proteins are a group of TFs characterised by a highly conserved monomeric DBD, the forkhead-domain, which displays a variation of the helix-turn-helix motif [220, 221]. The TFs were named after the first in 1989 identified FOX protein, the *forkhead* gene of *Drosophila melanogaster* [222]. Up to the present, more than 100 FOXs have been identified in species ranging from yeast to human. After the introduction of a standard nomenclature in 2000 they were divided in 19 subclasses [223].

The subclass O, the FOXO proteins, contains four members in mammals: FOXO1 (FKHR), FOXO3a (FKHRL1), FOXO4 (AFX), and FOXO6 that act as transcriptional activators or repressors dependent on the target gene [224-227]. FOXO1, FOXO3a, and FOXO4 are ubiquitously expressed at varying levels depending on the cell type. FOXO1 and FOXO4 are highly expressed in adipocytes and muscle cells, respectively; FOXO3a is expressed at abundant levels in liver, brain, heart, kidney, and spleen. By contrast, FOXO6 expression is restricted to the developing and adult brain [227-230]. All FOXOs consist of a N-terminal forkhead-domain and a C-terminal TAD, as well as a nuclear localisation signal (NLS) and a nuclear export signal (NES) facilitating nucleocytoplasmic shuttling [231, 232]. Based on the shared DBD, FOXOs bind to similar DNA sequences, identified as consensus FOXO recognition element (FRE) 5′(G/C)(T/A)AA(C/T)AA3′ [228, 231, 233]. The FRE can be detected in promoters of FOXO target genes such as insulin growth factor-binding protein (IGFBP) 1, Fas ligand (FasL), and Bcl-2 interacting mediator of cell death (Bim) [234, 235]. In principle, due to the ability to bind to similar DNA sequences, all FOXOs could regulate the same set of target genes. Nevertheless, they act with specificity, which is likely mediated by posttranscriptional modifications and interactions with coregulators and binding partners [236, 237]. The individual function of the FOXO proteins has been demonstrated in mouse models: FOXO1 deficiency causes embryonic lethality due to an impaired angiogenesis, mice lacking FOXO3a are viable, but females have an abnormal ovarian follicular development leading to age-dependent infertility, and FOXO4-deficient mice exhibit no consistent abnormalities [238].

By now, it is shown that the FOXOs are involved in a multitude of biological processes including cell cycle, differentiation, apoptosis, repair of damaged DNA, detoxification of ROS, immune system, aging, and cancer [234, 239-242]. In addition, FOXO proteins have a crucial role in the regulation of energy metabolism and glucose homeostasis. Under fasting conditions, FOXO1 promotes hepatic gluconeogenesis by transcriptional activation of phosphoenolpyruvate carboxykinase (PEPCK) and glucose-6-phosphatase (G6Pase) [243]. Consistently, the loss of insulin sensitivity in IR-haploinsufficient mice can be rescued by FOXO1 haploinsufficiency-mediated reduced expression of gluconeogenic enzymes [244]. Furthermore, it was reported that FOXO1 mediates hepatic expression of genes involved in lipid/sterol synthesis. Consequently, adenoviral delivery of a constitutively active FOXO1 (FOXO1AAA) variant to the liver causes lipogenesis, liver steatosis, and reduced fatty acid oxidation [245]. Additionally, it was demonstrated that FOXO1 inhibits β-cell proliferation by negatively regulated expression of the TF pancreatic and duodenal

homeobox factor (PDX) 1, which plays an important role in pancreas development [246]. The diabetic phenotype of IRS2-deficient mice caused by combined peripheral insulin resistance and β-cell failure is restored by FOXO1 haploinsufficiency-mediated proliferation of β-cells [246, 247]. Moreover FOXO1 has a crucial role in both muscle differentiation by regulating myotube formation and in muscle atrophy by breaking down muscle fibers. Expression of a constitutively active version of FOXO1 (FOXO1ADA) in myoblasts completely inhibits muscle differentiation [248]. In contrast, skeletal muscle-specific expression of a dominant negative FOXO1 mutant (FOXO1DN) inhibits starvation-mediated muscle atrophy by upregulating atrogin 1 expression in mice [249-251]. Likewise, FOXO1 is involved in adipocyte differentiation through transcriptional activation of cyclin-dependent kinase inhibitors such as p27 and p21, and repression of G1-phase cyclins D1 and D2, and G2-M-phase cyclin B [252, 253]. Consistently, expression of FOXO1ADA leads to an increase of p21 and suppression of adipocyte differentiation, whereas FOXO1DN causes adipogenesis [254]. As mentioned above (1.3.2), FOXO1 directly influences food intake by regulating expression of anorexigenic POMC and orexigenic AgRP. Controlled by insulin, FOXO1 inhibits POMC, but promotes AgRP transcription and interferes with STAT3 due to overlapping binding sites in the *pomc* and *agrp* promoter [73, 152]. Furthermore, it was recently shown that FOXO1 controls expression of carboxypeptidase E (CPE), mediating post-transcriptional cleavage of POMC and generation of α-MSH and β-endorphin [255].

1.4.2.1 Posttranslational modifications of FOXO proteins

The FOXO TFs are regulated by various stimuli including insulin, insulin growth factor-1 (IGF-1), growth factors, cytokines, nutrients, neurotrophins, and oxidative stress. These stimuli change the posttranslational modifications at the TFs such as phosphorylation, acetylation, and ubiquitination, thus altering cellular localisation, DNA-binding, transcriptional activity, and protein level of the FOXO proteins (Figure 6) [256, 257].

With exception of FOXO6, subcellular localisation of FOXOs is achieved by phosphorylation resulting in nucleocytoplasmic shuttling [227, 258]. The activation of the PI3K/AKT pathway causes negative regulation of FOXO´s transcriptional activity by cytoplasmic sequestration. AKT, as well as serum and glucocorticoid-inducible kinase (SGK) phosphorylate FOXO at three conserved sites (*e.g.* murine FOXO1 Thr^{24}, Ser^{256}, Ser^{319}) allowing recruitment of two 14-3-3 proteins, thus inhibiting binding to DNA consensus sequences [231, 259-261]. The accompanied conformational change of FOXO facilitates the

interaction of NES with exportin/Crm1 and ultimately leads to rapid relocalisation from the nucleus to the cytoplasm [260, 262]. Moreover, phosphorylation of Ser[319] in FOXO1 triggers Ser[322] and Ser[325] phosphorylation by casein kinase (CK) 1 followed by phosphorylation of Ser[329] through dual tyrosine phosphorylated regulated kinase (DYRK) 1A [263, 264]. The simultaneous phosphorylation of these four adjacent residues forms a negatively charged patch interacting with exportin/Crm1 and supporting AKT-mediated translocation of FOXOs to the cytoplasm [263]. In contrast to growth factors, stress triggers the relocalisation of FOXOs from the cytoplasm to the nucleus, thus overriding the sequestration of FOXO by growth factors [265]. Stress-activated protein kinases such as JNK and mammalian sterile 20-like protein kinase (MST) 1 phosphorylate FOXOs as well as FOXO-interacting protein 14-3-3, ultimately leading to dissociation of FOXO and 14-3-3 proteins thus allowing FOXO entry into the nucleus [266-268]. Additionally, the JNK-mediated phosphorylation of residues located in the TAD of FOXO seems to increase transcriptional activity of the TFs [266].

Moreover, it was shown that in response to oxidative stress the transcriptional coactivators cAMP responsive element-binding protein (CREB)-binding protein (CBP), p300 and p300/CREB associated factor (PCAF) bind and acetylate FOXO proteins at several lysine residues in the DBD and TAD [265, 269]. In contrast, protein acetylases such as silent mating type information regulation 2 homolog (SIRT) 1 reverse this process by deacetylation of FOXO factors [265, 270]. However, the acetylation-mediated effect on transcriptional activity of FOXOs is controversially debated, however the majority of studies indicate that acetylation paradoxically inhibits the transcriptional activity [271, 272].

Furthermore, oxidative stress triggers monoubiquitination of lysine residues in the C-terminus of FOXOs resulting in relocalisation into the nucleus and acceleration of their transcriptional activity. The detailed mechanisms are still unclear, but the ubiquitin-specific protease (USP) 7 binds and deubiquitinates FOXO proteins and thereby inhibits the stress-enhanced transcriptional activity of FOXOs [273]. In contrast, the polyubiquitination of FOXOs subsequently leads to the proteosomal degradation of the TFs [274]. Both the SKP2, a subunit of the E3 ubiquitin ligase complex and the IκB kinase (IKK) β were identified to initiate polyubiquitination-mediated degradation [275-277]. While AKT-mediated phosphorylation and cytoplasmic localisation are required for the direct ubiquitination of FOXOs by SKP2 [276, 278], IKKβ causes C-terminal phosphorylation of FOXO TFs ultimately leading to polyubiquitination and degradation [275].
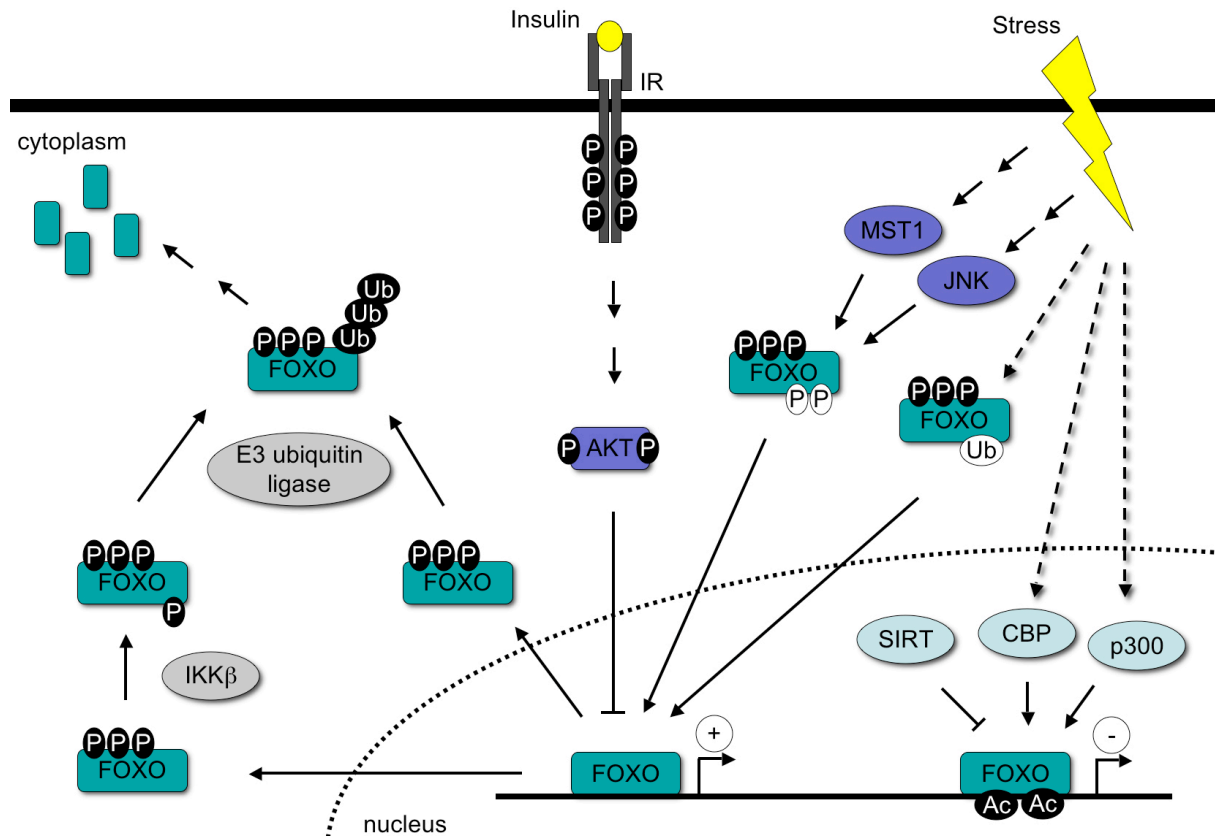
Figure 6: Posttranslational modifications of FOXO proteins.
After binding to the DNA, FOXO proteins act predominantly as transcriptional activators than repressors. Insulin signalling negatively regulates FOXO by AKT-mediated phosphorylation leading to translocation from the nucleus to the cytoplasm. In contrast, stress-activated JNK and MST1 phosphorylate FOXO, trigger relocalisation to the nucleus and enhance transcriptional activity. In addition, oxidative stress-mediated monoubiquitination of FOXO forces nucleus relocalisation. However, stress-mediated acetylation of FOXO by CREB or p300 mainly causes transcriptional inhibition and deacetylation by SIRT transcriptional activation of FOXOs. After cytoplasmic sequestration, FOXO proteins are polyubiquitinated by E3 ubiquitin ligase or phosphorylated by IKKβ and proteosomally degraded. Ac, acetylation; AKT, protein kinase B; CBP, cAMP responsive element-binding protein (CREB)-binding protein; FOXO, forkhead box-containing protein class O; IKKβ, IκB kinase β; IR, insulin receptor; JNK, c-jun-N-terminal kinase; MST1, mammalian sterile 20-like protein kinase 1; P, phosphorylation; SIRT, silent mating type information regulation 2 homolog; Ub, ubiquitination.

1.4.2.2 Dominant negative and constitutively active FOXO1 mutants

To analyse the biological function of FOXO1 in detail, various FOXO1 mutants have been generated including a gain- and loss-of-function version. FOXO1DN is a C-terminal truncated variant of FOXO1, which lacks the TAD (Δ256) including residues essential for nuclear export and acts as a dominant negative inhibitor of transcription. Independent of PI3K/AKT signalling, FOXO1DN binds to FRE and blocks the endogenous FOXO1 and presumably other FOXO proteins to bind to DNA consensus sequences [279].

In contrast, FOXO1ADA is an AKT/SGK phosphorylation-defective mutant, which functions as constitutive activator of transcription independent of insulin or other growth

factor signals. Due to the replacement of the three AKT/SGK phosphorylation sites to nonphosphorylatable amino acids (T24A, S256D, S319A), FOXO1ADA is unable to shuttle between the nucleus and the cytoplasm thereby constitutively activating the transcription of FRE-containing genes [280]. Recent studies have demonstrated the functionality of FOXO1DN and FOXO1ADA constructs *in vitro* as well as *in vivo* [244, 248, 254, 279-281].

1.5 Objectives

Obesity and type 2 diabetes are intimately connected diseases and their incidences are steadily increasing worldwide. Thus, there is an urgent need for the development of new therapeutic strategies to prevent and treat the obesity epidemic. Several studies over the last decade have demonstrated the crucial role of central leptin and insulin signalling to control body weight and glucose homeostasis. Therefore, this study aimed at investigating the central function of leptin- and insulin-regulated transcription factors STAT3 and FOXO1 by cell type-specific transgenesis in conditional mouse mutants.

First, POMC neuron-specific overactivation of STAT3 as present during obesity should be achieved by crossing POMC-Cre mice with mouse mutants carrying a Cre-inducible constitutively active *stat3* transgene (STAT3-C) in the *ROSA2*6 locus. These STAT3-C^{POMC} mice should be physiologically characterised with regard to energy and glucose homeostasis. Although, the STAT3-C mouse strain was generated by Sergei Koralov and Klaus Rajewsky, and the STAT3-C mutant was extensively used for constitutive STAT3 signalling *in vivo* and *in vitro*, the STAT3-C construct should also be functionally validated in ES cells and mice.

Second, two novel mouse mutants should be generated allowing cell type-specific expression of a dominant negative FOXO1 (FOXO1DN) and a constitutively active FOXO1 (FOXO1ADA) construct. To this end, FOXO1DN and FOXO1ADA cDNAs will be inserted into the STOP-eGFP-ROSA-CAGGS targeting vector to create Cre-inducible ROSA26 FOXO1DN and FOXO1ADA mouse strains. After functional verification of the FOXO1DN and FOXO1ADA constructs in MEFs, the FOXO1DN and FOXO1ADA mice should be subsequently crossed with mice expressing the Cre recombinase in neurons of the central nervous system to determine the impact of a central transcriptional block and overactivation of FOXO1 on the regulation of energy and glucose homeostasis.

2 Material and Methods

2.1 Chemicals and Biological Material

Size markers for agarose gel electrophoresis (Gene Ruler^{TM} DNA Ladder Mix, Lambda DNA/*Hind*III) and for SDS-PAGE (Page Ruler^{TM} Prestained Protein Ladder Mix) were obtained from MBI Fermentas, St. Leon-Rot, Germany. All chemicals used in this work are listed in table 1 and all enzymes used in this work are listed in table 2. Solutions were prepared with double distilled water. Bacterial media were autoclaved prior to use.

Table 1: Chemicals

Chemical	Supplier
α^{32}P-Desoxy Cytosine Triphosphates (dCTPs)	Amersham, Freiburg, Germany
γ^{32}P-Desoxy Adenosine Triphosphates (dATPs)	Amersham, Freiburg, Germany
β-Mercaptoethanol	AppliChem, Darmstadt, Germany
β-Mercaptoethanol	Gibco, Karlsruhe, Germany
0.9% saline (sterile)	Delta Select, Pfullingen, Germany
1,4-Dithio-DL-threitol (DTT)	Sigma-Aldrich, Seelze, Germany
2,2,2-Tibromethanol (Avertin)	Sigma-Aldrich, Seelze, Germany
2-Propanol (Isopropanol)	Roth, Karlsruhe, Germany
Acetic acid	Merck, Darmstadt, Germany
Acetone	KMF Laborchemie, Lohmar, Germany
Acrylamide Rotiphorese Gel 30	Roth, Karlsruhe, Germany
Agarose, Ultra Pure	Invitrogen, Karlsruhe, Germany
Ammonium persulfate (APS)	Sigma-Aldrich, Seelze, Germany
Amphotericin B	Sigma-Aldrich, Seelze, Germany
Bacillol$^{®}$	Bode Chemie, Hamburg, Germany
Bovine serum albumin (BSA)	Sigma-Aldrich, Seelze, Germany
Bromphenol blue	Merck, Darmstadt, Germany
Calcium chloride ($CaCl_2$)	Merck, Darmstadt, Germany
Chloroform	Merck, Darmstadt, Germany
Complete mini protease inhibitor cocktail tablets	Roche, Basel, Switzerland
Count off^{TM}	NEN$^{®}$ Research Products, Boston, USA
Desoxy Ribonucleotid Triphosphates (dNTPs)	Amersham, Freiburg, Germany
Dextran sulfate	Sigma-Aldrich, Seelze, Germany
Dimethylsulfoxide (DMSO)	Merck, Darmstadt, Germany
di-Sodiumhydrogenphosphate	Merck, Darmstadt, Germany
DMEM with stable Glutamin (Glutamax)	Invitrogen, Karlsruhe, Germany

Chemical	Supplier
Dulbecco's modified Eagle Medium (DMEM)	Invitrogen, Karlsruhe, Germany
Enhanced chemiluminescence (ECL) Kit	Perbio Science, Bonn, Germany
Eosin	Sigma, Steinheim, Germany
Ethanol (EtOH), absolute	AppliChem, Darmstadt, Germany
Ethidium bromide	Sigma-Aldrich, Seelze, Germany
Ethylendiamine tetraacetate (EDTA)	AppliChem, Darmstadt, Germany
Ethylene glycol tetraacetic acid (EGTA)	Sigma-Aldrich, Seelze, Germany
Fetal calf serum (FCS) for EF cells	Invitrogen, Karlsruhe, Deutschland
FCS for ES cells	PAA, Pasching, Austria
Gelatine, type B	Sigma, Steinheim, Germany
Geneticin (G418)	Gibco, Karlsruhe, Germany
Glucose 20%	DeltaSelect, Pfullingen, Germany
Glycerol	Serva, Heidelberg, Germany
Glycine	AppliChem, Darmstadt, Germany
Halothane	Sigma-Aldrich, Seelze, Germany
Hematoxylin	Sigma, Steinheim, Germany
Hydrochloric acid (37%)	KMF Laborchemie, Lohmar, Germany
Hydrogen peroxide	Sigma-Aldrich, Seelze, Germany
Insulin, human	Novo Nordisk, Bagsværd, Denmark
Insulin, human	Sigma-Aldrich, Seelze, Germany
Isopropyl-β-D-Thiogalacto-Pyranoside (IPTG)	Biomol, Hamburg, Germany
Kaisers Glycerol Gelatine	Merck, Darmstadt, Germany
Leptin	Sigma-Aldrich, Seelze, Germany
Leukemia inhibiting factor (LIF)	homemade
L-Glutamine	Invitrogen, Karlsruhe, Germany
LIF ESGRO®	Millipore, Billeria, USA
Luria Bertani agar	Sigma, Steinheim, Germany
Luria Bertani medium	AppliChem, Darmstadt, Germany
Magnesium chloride (MgCl$_2$)	Merck, Darmstadt, Germany
Methanol (MeOH)	Roth, Karlsruhe, Germany
Mitomycin-C from *Streptomyces caespitosus*	Sigma, Steinheim, Germany
Monosodium phosphate (NaH$_2$PO$_4$)	AppliChem, Darmstadt, Germany
N-2-hydroxyethylpiperazine-N'-2-ethansulfonic acid (HEPES)	AppliChem, Darmstadt, Germany
Nitrogen (liquid)	Linde, Pullach, Germany
Non essential amino acids	Invitrogen, Karlsruhe, Germany
Nonidet P-40 (NP-40)	Roche, Basel, Switzerland
Paraformaldehyde (PFA)	Fluka, Sigma-Aldrich, Seelze, Germany
Phenol	AppliChem, Darmstadt, Germany
Phenylmethylsulfonylfluoride (PMSF)	Sigma-Aldrich, Seelze, Germany

Chemical	Supplier
Phosphate buffered saline (PBS)	Gibco BRL, Eggenstein, Germany
Poly(deoxyinosinic-deoxycytidylic) acid sodium (poly(dI-dC))	Pharmacia, Freiburg, Germany
Potassium chloride (KCl)	Merck, Darmstadt, Germany
Potassium gluconate (K-gluconate)	Sigma-Aldrich, Seelze, Germany
Potassium hydroxide (KOH)	Merck, Darmstadt, Germany
Ready Safe^{TM}, Liquid Scintillation Cocktail	Beckman Coulter, Fullerton, USA
Roswell Park Memorial Institute Medium (RPMI) w/o phenol red	Gibco, Karlsruhe, Germany
Sodium acetate	AppliChem, Darmstadt, Germany
Sodium bicarbonate (NaHCO$_3$)	AppliChem, Darmstadt, Germany
Sodium chloride (NaCl)	AppliChem, Darmstadt, Germany
Sodium citrate	Merck, Darmstadt, Germany
Sodium dodecyl sulfate (SDS)	AppliChem, Darmstadt, Germany
Sodium fluoride	Merck, Darmstadt, Germany
Sodium hydroxide (NaOH)	AppliChem, Darmstadt, Germany
Sodium orthovanadate (Na$_3$VO$_4$)	Sigma-Aldrich, Seelze, Germany
Sodium pyrophosphate (Na$_4$P$_2$O$_7$)	Sigma-Aldrich, Seelze, Germany
Sodium pyruvate	Invitrogen, Karlsruhe, Germany
Spermidine	Sigma, Steinheim, Germany
Sucrose	AppliChem, Darmstadt, Germany
Tetramethylethylenediamine (TEMED)	Sigma-Aldrich, Seelze, Germany
Tissue Freezing Medium	Jung, Heidelberg, Germany
Tolbutamide	Sigma-Aldrich, Seelze, Germany
Trishydroxymethylaminomethane (Tris)	AppliChem, Darmstadt, Germany
Triton X-100	AppliChem, Darmstadt, Germany
Trypsin/EDTA	Gibco, Karlsruhe, Germany
Tween 20	AppliChem, Darmstadt, Germany
Denhardt´s solution	AppliChem, Darmstadt, Germany
Western Blocking Reagent	Roche, Basel, Switzerland

Table 2: Enzymes

Enzym	Supplier
*Asc*I	New England Biolabs, Schwalbach, Germany
*Bam*HI	Fermentas, St. Leon-Rot, Germany
Bca DNA polymerase	Takara, Otsu, Japan
*Bsg*I	New England Biolabs, Schwalbach, Germany
*Bsm*I	New England Biolabs, Schwalbach, Germany
DNase, RNase-free	Promega, Madison, USA
*Dpn*I	New England Biolabs, Schwalbach, Germany

Enzym	Supplier
Dream Taq^{TM} DNA polymerase	Fermentas, St. Leon-Rot, Germany
*Eco*RI	New England Biolabs, Schwalbach, Germany
*Eco*RV	Fermentas, St. Leon-Rot, Germany
EuroScript reverse transcriptase	Eurogentec, Seraing, Belgium
*Nsi*I	New England Biolabs, Schwalbach, Germany
Pfu Turbo polymerase	Stratagene, Cedar Creek, USA
Proteinase K	Roche, Basel, Switzerland
Red Taq® DNA polymerase	Roche, Sigma-Aldrich, Seelze, Germany
RNase A, DNase-free	Fermentas, St. Leon-Rot, Germany
RNase inbibtor	Eurogentec, Seraing, Belgium
*Sac*II	Fermentas, St. Leon-Rot, Germany
T4 DNA ligase	New England Biolabs, Schwalbach, Germany
T4 polynucleotide kinase	New England Biolabs, Schwalbach, Germany
T7 polymerase	Roche, Basel, Switzerland
*Xba*I	Fermentas, St. Leon-Rot, Germany

2.2 Molecular biology

Standard methods of molecular biology were performed according to protocols described by Sambrook and Russell [282], unless otherwise stated.

2.2.1 Competent *E. coli* and isolation of plasmid DNA

Competent *Escherichia coli* (*E. coli*) DH5α cells were prepared according to a standard protocol [283] and used in heat shock transformation of plasmid DNA. Isolation of plasmid DNA was performed using an alkaline lysis method [284] (E.Z.N.A.® Plasmid Miniprep Kit 1, Peqlab, Erlangen, Germany) according to the protocol of Zhou *et al.* [285]. Plasmid DNA of higher purity was obtained using Qiagen columns (Qiagen, Hilden, Germany) following the supplier's instructions. DNA ligation was performed with T4 DNA ligase according to manufacturer's instructions.

2.2.2 Cloning of targeting vectors

Oligonucleotides used for cloning of FOXO1DN and FOXO1ADA targeting vectors and SOCS3 and POMC *in situ* hybridisation probe synthesis vectors are listed in table 3. All constructs used for plasmid generation were confirmed by sequencing (2.2.8).

Table 3: Oligonucleotides used in cloning procedures.

Name	Sequence (5´-3´)	Application
3foxoDN_Asc	TTT GGC GCG CCT AGT CCA TGG ACG CAG CTC TTC TCC G	amplification of FOXO1DN
5Sphfoxo	GCA TGC GGC GCG CCA CCA TGG CCG AAG CGC CCC AGG TGG TGG AGA CCG ACC CGG ACT TCG AGC CGC TGC CCC GGC AGC GCT CCT GTG CCT GG	site-directed mutagenesis of pCMV5-FOXO1ADA
ADA_Mut_anti	CCA GGG CTG TCT CCA GGA CCC TCT TGC	site-directed mutagenesis of pCMV5-FOXO1ADA
ADA_Mut_sense	GCA AGA GGG TCC TGG AGA CAG CCC TGG	site-directed mutagenesis of pCMV5-FOXO1ADA
foxo1m_Asc3	AAG GCG CGC CTT AGC CTG ACA CCC AGC TGT	amplification of FOXO1
foxo1m_Asc5	AAG GCG CGC CAC CAT GGC CGA AGC GCC CCA GGT	amplification of FOXO1and FOXO1DN

2.2.2.1 Generation of FOXO1DN targeting vector

In order to generate a FOXO1DN targeting vector, the open reading frame of FOXO1 was amplified by PCR from mouse macrophage cDNA using primer foxo1m_Asc5 and foxo1m_Asc3. The 1.9 kb PCR fragment was cloned into a pGEM®-T Vector using the pGEM®-T Vector System (Promega, Madison, USA) according to manufacturer's instructions. The resulting pGEM-FOXO1wt plasmid served as template to create the 0.75 kb FOXO1DN PCR fragment by means of primer foxo1m_Asc5 and 3 foxoDN_Asc containing *Asc*I restriction sites. After subcloning into a pGEM®-T Vector (Promega, Madison, USA), FOXO1DN was inserted into the *Asc*I restriction site of the STOP-eGFP-ROSA-CAGGS targeting vector [286] (Figure 7). This plasmid is a variant of the targeting vector STOP-eGFP-ROSA [287], which contains an additional CAGGS promoter [288].
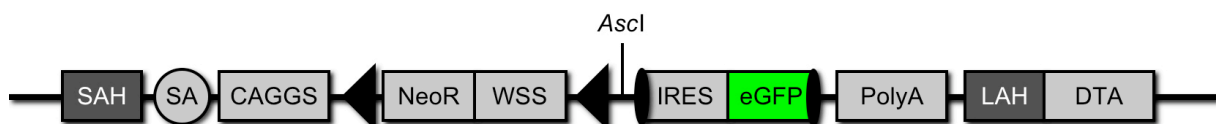
Figure 7: Map of STOP-eGFP-ROSA-CAGGS targeting vector.
Scheme of the ROSA26 targeting vector STOP-eGFP-ROSA-CAGGS. CAGGS, *chicken β actin* promoter; DTA, *diphtheria toxin A* gene driven by *pGK* promoter; eGFP, enhanced *green fluorescent protein* gene; IRES, internal ribosome entry site; LAH, 4.2 kb long arm of homology; NeoR, *neomycine resistance* gene driven by *TK* promoter; PolyA, polyadenylation signal; SA, adenoviral splice acceptor; SAH, 1.0 kb short arm of homology; WSS, Westphal stop sequence; filled triangles, *lox*P; closed ellipses, FRT sites.

2.2.2.2 Generation of FOXO1ADA targeting vector

To create a FOXO1ADA targeting vector, the plasmid pCMV5-FOXO1ADA [289], containing a mutated version of FOXO1ADA was used to generate FOXO1ADA, which harbours the pointmutations T24A, S256D, and S319A. The point mutation G282R was eliminated by the usage of QuikChange® Site-Directed Mutagenesis Kit (Stratagene, Cedar Creek, USA) and primers ADA_Mut_anti and ADA_Mut_sense as described in 2.2.10. After *Bsg*I and *Bsm*I digestion of the resulting plasmid pCMV5-FOXO1ADA_R282G, a 330 bp fragment of FOXO1ADA including S256D and S319A was exchanged with the equivalent fragment of the plasmid pGEM-FOXO1wt (2.2.2.1) to generate pGEM-FOXO1DA. The third point mutation T24A was introduced by PCR using primers 5Sphfoxo containing nucleotide exchange T24A and foxo1m_Asc3. After subcloning of the 1.9 kb fragment into a pGEM®-T Vector (Promega, Madison, USA), FOXO1ADA was inserted into the *Asc*I restriction site of the STOP-eGFP-ROSA-CAGGS targeting vector (2.2.2.1).

2.2.3 Construction of *in situ* hybridisation probes

Oligonucleotides used for generation of SOCS3 or POMC *in situ* hybridisation probes are listed in table 4.

Table 4: Oligonucleotides used in construction of *in situ* hybridisation probes.

Name	Sequence (5´-3´)
SOCS-5'	GGC GCG CCA CCA TGG TCA CCC ACA GCA AGT TTC C
SOCS-3'	ATT TAA ATT AAA GTG GAG CAT CAT ACT G
POMC-5'	ATG CCG AGA TTC TGC TAC AG
POMC-3'	TGC TGC TGT TCC TGG GGC

2.2.3.1 Generation of SOCS3 *in situ* hybridisation probe synthesis vector

To generate a plasmid for SOCS3 *in situ* hybridisation probe synthesis, a 678 bp PCR fragment was amplified from mouse hypothalamic cDNA using respective primer SOCS-3' and SOCS-5'. The PCR fragment was cloned into the *T7* promoter containing pGEM®-T Vector using the pGEM®-T Vector System (Promega, Madison, USA) according to manufacturer's instructions.

2.2.3.2 Generation of POMC *in situ* hybridisation probe synthesis vector

To generate a plasmid for POMC *in situ* hybridisation probe synthesis, a 280 bp PCR fragment was amplified from mouse hypothalamic cDNA using respective primers POMC-3' and POMC-5' and cloned into pGEM®-T Vector by the use of the pGEM®-T Vector System (Promega, Madison, USA) according to manufacturer's instructions.

2.2.4 Isolation of genomic DNA

For preparation of DNA from mouse liver or tail biopsies, the tissue was incubated in lysis buffer (10 mM Tris-HCl [pH 8], 10 mM EDTA, 150 mM NaCl, 0.2% (w/v) SDS, 400 mg/ml proteinase K) at 56°C for several hours. The debris was pelleted, the supernatant mixed with an equal volume of isopropanol and the DNA was precipitated by centrifugation. After washing with 70% (v/v) EtOH, the pellet was dried at room temperature (RT) and resuspended in TE buffer (10 mM Tris-HCl [pH 8], 1 mM EDTA).

DNA from ES cell clones grown in 96-well tissue culture dishes was extracted and prepared as described previously [290].

2.2.5 Agarose gel electrophoresis and DNA gel extraction

PCR-amplified and digested DNA fragments were separated by size using agarose gel electrophoresis (0.8 to 2% (w/v) agarose (dependent on fragment size), 1x TAE, 0.5 mg/ml EtBr, 1x TAE electrophoresis buffer). The fragments were excised and the DNA was eluted using the QIAEX II or the QIAquick Gel Extraction Kit (Qiagen, Hilden, Germany) according to manufacturer's instructions.

2.2.6 Phenol chlorophorm extraction

DNA in solution was purified for transfection or Southern blot analysis using phenol chloroform extraction. The aqueous solution was mixed with an equal volume of phenol and centrifuged to separate the phases. To guarantee a high degree of purity, nucleic acids were extracted once more from the aqueous phase by chloroform addition. DNA was precipitated from the aqueous phase by adding an equal volume of 100% (v/v) EtOH, washed with 70% (v/v) ethanol and resuspended in RPMI w/o phenol red for transfection or in TE buffer (10 mM Tris-HCl [pH 8], 1 mM EDTA).

2.2.7 Quantification of nucleic acids

The concentration of DNA and RNA was determined by measuring the sample absorption at 260 nm with a NanoDrop$^®$ ND-1000 UV-Vis Spectrophotometer (Peqlab, Erlangen, Germany). An OD_{260} of 1 corresponds to approximately 50 µg/ml of double stranded DNA and to 38 µg/ml of RNA. To assess purity of nucleic acids, the ratio of absorption at 260 nm versus 280 nm was calculated, as proteins absorb maximum at 280 nm. An OD_{260}/OD_{280} ratio of 2 refers to pure nucleic acids, lower values display protein contaminations.

Alternatively, the DNA was electrophoresed in an agarose gel, and the concentration was approximated from the band intensity in comparison with a standard.

2.2.8 DNA sequencing

DNA was sequenced with the ABI Big Dye Terminator Sequencing Kit (Applied Biosystems, Foster City, USA) according to Sanger *et al.* [291]. The fluorescently labelled DNA fragments were analysed with an ABI Prism 3730 DNA analyser (Applied Biosystems, Foster City, USA).

2.2.9 Polymerase chain reaction (PCR)

The polymerase chain reaction [292, 293] was performed to amplify cDNA fragments for cloning and to detect targeted alleles or transgenes for genotyping of mice and cells. Reactions were performed in a Triothermocycler (Biometra, Göttingen, Germany), Thermocycler iCycler PCR machine (Bio-Rad, München, Germany) or Peltier Thermal Cycler PTC-200 (MJ Reasearch, Waltham, USA) and all primers were purchased from Eurogentec, Cologne, Germany.

Genotyping of mice, ES cells, and MEFs or synthesis of the neo probe were performed in a total reaction volume of 25 µl, containing a minimum of 50 ng template DNA, 25 pM of each primer (Table 5, 6), 25 µM dNTPs mix, 3 to 6% (v/v) DMSO, either 10x RedTaq$^®$ reaction buffer and 1 unit of RedTaq$^®$ DNA Polymerase (Sigma, Steinheim, Germany) or 10x Dream Taq^{TM} Green Buffer and 1 unit of DreamTaq^{TM} DNA Polymerase (Fermentas, St. Leon-Rot, Germany). Standard PCR programs started with 4 min of denaturation at 95°C, followed by 30 to 35 cycles consisting of denaturation at 95°C for 45 sec, annealing at 54 to 60°C for 30 sec and elongation at 72°C for 30 sec. The PCR was finished with a final extension step at 72°C for 10 min.

Table 5: Oligonucleotides used for genotyping.

Transgene	Name	Sequence (5´-3´)
stat3-c	Typ_forward	AAA GTC GCT CTG AGT TGT TAT C
	Typ_reverse	GAT ATG AAG TAC TGG GCT CTT
	NeoRT	CGG ACC GCT ATC AGG ACA TA
pomc cre	N16R	TGG CTC AAT GTC CTT CCT GG
	N57R	CAC ATA AGC TGC ATC GTT AAG
	AA03	GAG ATA TCT TTA ACC TGA TC
foxo1dn foxo1ada	Typ_forward	AAA GTC GCT CTG AGT TGT TAT C
	Typ_reverse	GAT ATG AAG TAC TGG GCT CTT
	Typ_rev_CAGS	TGT CGC AAA TTA ACT GTG AAT C
Δfoxo1dn Δfoxo1ada	ROSA1	AG GGT TTC CTT GAT GAT GTC A
	3 NeoStat	CAT CAG GGG CTC GCG CC
	3FOXORT4	CTG GGG CGC TTC GGC CAT
nestin cre	NestinCre5	TGC TGG AGT TCT CCG CTT CCG
	NestinCre3	ATG TTT AGC TGG CCC AAA TGT

Table 6: Oligonucleotides used for synthesis of neo probe.

probe	Name	Sequence (5´-3´)
Neo	neo5pPNT	TGA ATG AAC TGC AGG ACG AGG CA
	neo3pPNT	GCC GCC AAG CTC TTC AGC AAT AT

For cloning procedures, DNA fragments were amplified from cDNA or plasmid DNA using the High Fidelity PCR Master Kit (Roche, Basel, Switzerland) containing a *Tgo* DNA polymerase with proofreading activity according to manufacturer's guidelines with 500 ng template cDNA, 25 pM of each primer (Table 3, 4) and 3 to 9% (v/v) DMSO. After an initial denaturation step at 94°C for 4 min, 15 cycles of denaturation at 94°C for 30 sec, annealing at 54 to 60°C for 30 sec and elongation at 68°C for 90 sec were followed by another 25 cycles of denaturation at 94°C for 45 sec, annealing at 54 to 60°C for 45 sec and elongation at 68°C for 3 min. The PCR was finished with a final extension step at 68°C for 10 min.

2.2.10 Site-directed mutagenesis

To exchange one nucleotide of a plasmid, site-directed mutagenesis was performed by usage of QuikChange® Site-Directed Mutagenesis Kit (Stratagene, Cedar Creek, USA) according to manufacturer's instructions.

2.2.11 RNA extraction and reverse transcriptase-PCR (RT-PCR)

Hypothalamic tissue and MEFs were homogenised using an Ultra Turrax homogeniser (IKA, Staufen, Germany) or QIAshredder spin columns (Qiagen, Hilden, Germany), respectively. Total RNA was extracted using the RNeasy system (Qiagen, Hilden, Germany) according to manufacturer's guidelines. After treatment with RNase-free DNase, 200 ng of each RNA sample were reversely transcribed with EuroScript Reverse Transcriptase (Eurogentec, Cologne, Germany) according to manufacturer's instructions. Fragments of STAT3-C, endogenous STAT3, and glyceraldehyde-3-phosphate dehydrogenase (GAPDH) were amplified using specific primers (Table 7).

Table 7: Oligonucleotides used for amplification of cDNA fragments.

amplified cDNA fragment	Name	Sequence (5´-3´)
STAT3-C	Rosa512	GCC GTT CTG TGA GAC AG
	3StatRT	AGG ACA TTG GAC TCT TGC AG
endogenous STAT	5StatRT	CAG TCG GGC CTC AGC CC
	3StatRT	AGG ACA TTG GAC TCT TGC AG
GAPDH	GAPDH5´	ACC ACA GTC CAT GCC ATC AC
	GAPDH3´	TCC ACC ACC CTG TTG CTG TA

2.2.12 Analysis of RNA expression

Expression of mRNA was analysed using quantitative realtime PCR. cDNA was obtained from hypothalamic tissue as described above (2.2.11) and amplified using TaqMan® Universal PCR-Master Mix, NO AmpErase® UNG with TaqMan® Assay on demand kits for AgRP (agouti-related protein), Gusb (glucuronidase beta), Hprt-1 (hypoxanthine guanine phosphoribosyl transferase 1), NPY (neuropeptide Y), PIAS (protein inhibitor of activated STAT), and SOCS3 (suppressor of cytokine signalling 3) (Applied Biosystems, Foster City, USA). Analysis of POMC mRNA expression was performed with customised primers (Table 8). Relative expression of samples was adjusted for total RNA content by Gusb and Hprt-1 RNA quantitative realtime PCR. Calculations were performed by a comparative method (2-ddCT). Quantitative PCR was performed on an ABI-PRISM 7700 Sequence Detector (Applied Biosystems, Foster City, USA). Assays were linear over 4 orders of magnitude.

Table 8: Oligonucleotides used for analysis of POMC mRNA expression.

Name	Sequence (5´-3´)
POMC sense	GAC ACG TGG AAG ATG CCG AG
POMC anti-sense	CAG CGA GAG GTC GAG TTT GC
probe sequence	FAM-CAA CCT GCT GGC TTG CAT CCG G-TAMRA

2.2.13 Southern blot analysis

Digestion of 5 - 15 µg genomic DNA isolated from ES cells was performed overnight with 100 U of the appropriate restriction enzyme (Table 9). Subsequently, DNA fragments were separated by agarose gel electrophoresis and transferred onto Hybond™-N+ (Amersham, Braunschweig, Germany) nylon membranes by alkaline capillary transfer [294]. Membranes were incubated at 80°C for 40 min to fix the DNA, equilibrated in 2x SSC [282] and then prehybridised at 65°C for 4 h in hybridisation solution (1 M NaCl, 1% (w/v) SDS, 10% (w/v) dextran sulfate, 50 mM Tris-HCl [pH 7.5], 250 µg/ml sonicated salmon sperm DNA). 50 ng of probe DNA (Table 9) were radioactively labelled with 2.5 µCi α^{32}P-dCTP using the Ladderman™ Labelling Kit (Takara, Otsu, Japan) based on the principle of random primed oligolabelling [295].

Table 9: Probes used for Southern blot analysis.

Name	Description of probe	genomic DNA digestion
Rosa26 probe	1200 bp *Eco*RI/*Bam*HI fragment from A-04 plasmid [296]	*Eco*RI
Neo probe	500 bp PCR fragment (2.2.9)	*Nsi*I

Non-incorporated radiolabelled nucleotides were removed with MicroSpin™ S-200HR columns (GE Healthcare, Munich, Germany). Probes were denatured for 5 min in a boiling waterbath and then cooled on ice, before addition to the hybridisation solution. Hybridisation was performed at 65°C overnight in a rotation cylinder (Hybaid, Thermo Fisher Scientific, Waltham, USA). After hybridisation, stringency washes were initially performed twice in 2x SSC/0.1% (w/v) SDS followed by washes in 1x SSC/0.1% (w/v) SDS, 0.5x˘SSC/0.1% (w/v) SDS and 0.1x SSC/0.1% SDS at 65°C under gentle shaking. Radioactivity on the membranes was monitored with a Geiger counter until specific signals reached 20 to 100 cps. Afterwards, membranes were sealed in a plastic bag and exposed to X-ray films (BioMAX MS, Eastman Kodak, Rochester, USA) at -80°C. Films were developed in an automatic developer (Agfa, Mortsel, Belgium). Alternatively, the membranes

were exposed to PhosphoImager screens (Fujifilm, Tokyo, Japan) at RT and analysed on BAS1000 PhosphoImager (Fujifilm, Tokyo, Japan).

2.3 Cell biology

2.3.1 Embryonic fibroblast cell cultur

Murine embryonic fibroblasts (MEF) were isolated from E14.5 embryos [297]. After setting up matings, the females were checked for the presence of vaginal plug every morning. 14.5 days after copulation, mice were sacrificed by cervical dislocation and disinfected with Bacillol®. After dissection of the uterus, embryos were washed in PBS. Liver, heart, and brain of every embryo were removed and used for genotyping. The remaining part of the embryo was washed in PBS, homogenised by a 70 μm nylon cell strainer (Falcon, Belford, USA), and washed with EF medium (DMEM supplemented with 10% FCS, stable Glutamin (Glutamax) and 1 mM sodium pyruvate). MEFs were expanded in EF medium in tissue culture dishes (Falcon, Belford, USA) at 37°C under humid atmosphere with 10% CO_2.

For immortalisation, $2x10^5$ MEFs were transfected with 1 μg SV40 genomic DNA [298] using Lipofectamine^TM 2000 transfection reagent (Invitrogen, Karlsruhe, Germany) according to manufacturer's protocol. Next day, MEFs were trypsinised and serial diluted to reach single colonies, starting from 12.5, 25, 50, 100 to 200 cells per well of a 96-well tissue culture dish (Falcon, Belford, USA). After changing EF medium every fourth day for the next 14 days, MEF clones were expanded.

2.3.2 Embryonic stem cell culture

All gene targetings were performed in V6.5 (129SV x C57BL/6, F1 Hybrid) embryonic stem (ES) cells [299]. Culturing and transfection of ES cells were performed according to published protocols [290, 300]. ES cells were grown in ES cell medium (DMEM supplemented with 15% FCS, 1 mM sodium pyruvate, 2 mM L-glutamine, 1x non essential amino acids, 10 U/ml LIF, 0.1 mM 2-β-mercaptoethanol) and kept at 37°C under humid atmosphere with 10% CO_2. ES cells were cultured on a layer of embryonic fibroblast (EF) cells, which were never passaged more than three times and mitotically inactivated by mitomycin-C treatment (10 μg/ml for 2 to 4 h) before seeding with ES cells. ES cell colony growth was stopped before they became confluent by washing the colonies twice with PBS and short treatment with trypsin at 37°C. ES cell suspension was then used for passaging,

freezing or transfection. ES cells were frozen in 90% FCS, 10% DMSO at -80°C and later transferred into liquid nitrogen for long-term storage.

For transfection, 1×10^7 ES cells were mixed with 40 µg DNA in 800 µL RPMI w/o phenol red and electroporated at RT (500 mF, 240 V). After 5 min incubation, ES cells were transferred onto an EF layer and after 48 h placed under selection with 250 µg/ml G418. On day 9 after transfection, resistant colonies were picked and split into EF-containing 96-well tissue culture dishes for expansion. After 3 days, ES cells were frozen and parallel further expanded for genomic DNA extraction and Southern blot analysis of each clone.

Microinjection and transfer of 3.5 day-old embryos were performed in the Centre for Mouse Genetics, University of Cologne.

2.3.3 His-TAT-NLS-Cre (HTNC) treatment

ES cells were treated with HTNC [301] to delete *lox*P-flanked gene segments. 2×10^5 ES cells or 3×10^5 MEFs were plated into a well of a 6-well tissue culture dish. After 5 h, cells were washed twice with PBS and then incubated in 4 to 10 µM HTNC in DMEM w/o FCS/PBS (1:1) for 20 h. Thereafter the cells were washed with PBS and cultured as described before.

2.3.4 Dual luciferase assay

STAT3-C and control ES cells were transiently transfected with 30 µg pSTAT3-TA-Luc (Clontech Laboratories, Mountain View, USA) and 10 µg pRLnull vector (Promega, Madison, USA) by electroporation as described in 2.3.2. After transfection, ES cells were suspended in growth medium and plated onto 24-well culture plates. 24 h after transfection, ES cells were washed with PBS and incubated for 24 h with DMEM w/o FCS or ES cell medium supplemented with 30 U/ml LIF ESGRO. ES cells were then washed in PBS and lysed in 100 µl passive lysis buffer (Promega, Madison, USA) and centrifuged at 4°C. Supernatant was assayed for FLuc activities using the Dual Luciferase Assay (Promega, Madison, USA) according to the manufacturer´s protocol. Each experiment was performed in triplicate and each transfection was repeated four times.

2.3.5 Flow cytometry

ES cells and MEF were analysed on a FACS Calibur and data were evaluated using CellQuest software (Becton Dickinson, Mountain View, USA).

2.3.6 Electrophysiology

All electrophysiology experiments were performed in the Institute of Zoology and Physiology, Group Peter Kloppenburg, University of Cologne, CECAD, Germany.

2.3.6.1 Animals and brain slice preparation

Experiments were performed on brain slices from 18 - 28 day old POMC-EGFP and STAT3-C^{POMC}POMC-EGFP mice that express enhanced green fluorescent protein (eGFP) selectively in POMC neurons [62]. The animals were anaesthetised with halothane and subsequently decapitated. The brains were rapidly removed and a block of tissue containing the hypothalamus was immediately cut out. Coronal slices (250 – 300 μm) containing the ARC were cut with a vibration microtome (HM-650 V; Thermo Scientific, Karlsruhe, Germany) under cold (4°C), carbogenated (95% O_2 and 5% CO_2), glycerol-based modified artificial cerebrospinal fluid (GaCSF) to enhance the viability of neurons. GaCSF contained: 250 mM glycerol, 2.5 mM KCl, 2 mM $MgCl_2$, 2 mM $CaCl_2$, 1.2 mM NaH_2PO_4, 10 mM HEPES, 21 mM $NaHCO_3$, 5 mM glucose adjusted to pH 7.2 (with NaOH) resulting in an osmolarity of ~310 mOsm. Brain slices were transferred into carbogenated artificial cerebrospinal fluid (aCSF). First, they were kept for 20 min in a 35°C 'recovery bath' and then stored at RT for at least 30 min prior to recording. aCSF contained: 125 mM NaCl, 2.5 mM KCl, 2 mM $MgCl_2$, 2 mM $CaCl_2$, 1.2 mM NaH_2PO_4, 21 mM $NaHCO_3$, 10 mM HEPES, and 5 mM glucose adjusted to pH 7.2 (with NaOH) resulting in an osmolarity of ~310 mOsm. Slices were transferred to a recording chamber (~3 ml volume) and continuously superfused with carbogenated aCSF at a flow rate of ~2 ml·min^{-1}. 200 nM insulin and 200 μM of the K_{ATP} channel blocker tolbutamide were bath-applied via the superfusion system. The tolbutamide was dissolved in DMSO and added to aCSF with a final DMSO concentration of 0.25%. The DMSO concentration had no obvious effect on the investigated neurons.

2.3.6.2 Perforated patch recordings

Perforated patch recordings were performed using protocols modified from Horn and Marty [302] and Akaike and Harata [303]. Electrodes with tip resistances between 3 and 5 MW were fashioned from borosilicate glass (0.86 mm inner diameter; 1.5 mm outer diameter; GB150-8P; Science Products, Hofheim, Germany) with a vertical pipette puller (PP-830; Narishige, Tokyo, Japan). Perforated patch recordings were performed with ATP and GTP free pipette solution containing: 128 mM K-gluconate, 10 mM KCl, 10 mM HEPES,

0.1 mM EGTA, 2 mM $MgCl_2$ and adjusted to pH 7.3 (with KOH) resulting in an osmolarity of ~300 mOsm. ATP and GTP were omitted from the intracellular solution to prevent uncontrolled permeabilisation of the cell membrane [304]. The patch pipette was tip filled with internal solution and back filled with amphotericin B-containing internal solution (~200 $\mu g \cdot ml^{-1}$) to achieve perforated patch recordings. Amphotericin B was dissolved in DMSO (final concentration: 0.4 - 0.5%) and added to the modified pipette solution shortly before use [305]. Experiments were carried out at approximately 31°C using an inline solution heater (Warner Instruments, Hamden, USA) operated by a temperature controller (Warner Instruments, Hamden, USA). During the perforation process access resistance (R_a) was constantly monitored and experiments were started after R_a had reached steady state (~15 - 20 min) and the action potential (AP) amplitude was stable. By the use of an ATP-free pipette solution, a change to the whole-cell configuration would be obvious by a spontaneous hyperpolarisation of the neuron due to K_{ATP} activation. Such experiments were rejected. Neurons in the ARC were visualised with a fixed-stage upright microscope (Olympus, Hamburg, Germany), using a 60× water immersion objective (LUMplan FI/IR; 60×; 0.9 numerical aperture; 2 mm working distance; Olympus, Hamburg, Germany) with infrared-differential interference contrast [306] and fluorescence optics. POMC neurons were identified by their eGFP fluorescence that was visualised using a Chroma 41001 filter set (EX: HQ480/40x, BS: Q505LP, EM: HQ535/50m, Chroma, Bellow Falls, USA). Current-clamp recordings were performed with an EPC10 patch-clamp amplifier (HEKA, Lambrecht, Germany) controlled by the PatchMaster software (version 2.32, HEKA, Bellmore, USA). Data were sampled at intervals of 100 μs (10 kHz) and low-pass filtered at 2 kHz with a four-pole Bessel filter. The liquid junction potential between intracellular and extracellular solution was not compensated (14.6 mV, calculated with Patcher's Power Tools plug-in for Igor Pro 6 (Wavemetrics, Lake Oswego, USA)).

2.3.6.3 Data analysis

In agreement with previous studies it was found that the basic electrophysiological properties of POMC neurons and their insulin responsiveness [307, 308] were not homogeneous. Therefore, a 3 standard deviation (SD) criterion was used and considered a neuron insulin responsive when the change in membrane potential before and during insulin application was > 3 SD [309, 310]. For each neuron, the membrane potential averaged from 60 s intervals was taken as one data point. To determine the mean membrane potential with SD 5 data points at stable membrane potentials before and during insulin application were

averaged. Data analysis was performed with Igor Pro 6 (Wavemetrics, Lake Oswego, USA) and Sigma Stat (version 3.1, Systat Software, Chicago, USA).

2.3.7 Histological analysis and immunohistochemistry

2.3.7.1 Immunohistochemistry

For visualisation of eGFP expression after Cre-mediated recombination, STAT3-C^{POMC} mice at the age of 12 weeks were anaesthetised and perfused transcardially with physiologic saline solution followed by 4% (w/v) PFA (in 0.1 M PBS [pH 7.4]). The brains were dissected, postfixed in 4% (w/v) PFA at 4°C for 24 h, transferred to 20% sucrose for 6 h, and frozen in tissue-freezing medium. Subsequently, 25 μm thick free-floating coronal sections were dissected through the ARC using a freezing microtome (Leica, Solms, Germany). The sections were collected in PBS/azide (pH 7.4) and washed extensively to remove cryoprotectant. The sections were stained as described previously [311], using anti-GFP antibody (#A6455; Invitrogen/Molecular Probes, Karlsruhe, Germany).

For X-Gal stainings STAT3-C^{POMC} were mated with ROSAArte26 reporter mice [312]. At the age of 12 weeks animals fasted for 16 h were anaesthetised and perfused transcardially with physiologic saline solution followed by 4% (w/v) PFA. The brains were dissected, postfixed in 4% (w/v) PFA for 4 h, soaked in 20% (w/v) sucrose for 24 h at 4°C and frozen in tissue-freezing medium. 8 μm coronal sections containing the ARC were fixed for 10 min in cold 4% (w/v) PFA, washed three times with PBS, rinsed in distilled water and subjected to X-Gal-staining overnight at 37°C (X-Gal solution: 5 mM $K_3Fe(CN)_6$, 5 mM $K_4Fe(CN)_6$, 2 mM $MgCl_2$, 1 mg/ml X-Gal in PBS [pH 7.4]) [313].

For the staining of pSTAT3 in POMC neurons, STAT3-C^{POMC} mice were crossed with ROSAArte26 reporter mice [312]. At the age of 10 to 12 weeks animals fasted for 16 h were anaesthetised and injected intraperitoneally with either saline or 1 mg/kg leptin for 30 min. Mice were perfused transcardially with physiologic saline solution and the dissected brains were frozen in tissue-freezing medium. The 7 μm coronal sections containing the ARC were stained with β-galactosidase (#9361; Abcam, Cambridge, United Kingdom) and pSTAT3 antibodies (#9145; Cell Signaling, Danvers, USA). Double fluorescence immunostainings were performed as described before [314]. For quantitative analysis of pSTAT3-positive POMC neurons, a total of 2103 β-galactosidase-positive neurons were counted and digitally marked to prevent multiple counts. pSTAT3-positive POMC neurons were expressed as percentage of total POMC neurons.

For the staining of pAKT in POMC neurons, STAT3-C^{POMC} mice were crossed with ROSAArte26 reporter mice [312]. At the age of 10 to 14 weeks animals fasted for 48 h were anaesthetised and injected intravenously with either physiologic saline solution or 5 U of insulin for 10 min. Mice were transcardially perfused with physiologic saline solution and the dissected brains were postfixed in 4% (w/v) PFA at 4°C for 24 h, transferred to 20% (w/v) sucrose for 6 h, and frozen in tissue-freezing medium. The 25 μm coronal sections containing the ARC were stained with β-galactosidase (#9361; Abcam, Cambridge, United Kingdom) and pAKT antibodies (#4060; Cell Signaling, Danvers, USA). Double fluorescence immunostainings were performed as described before [314]. For quantitative analysis of pAKT-positive POMC neurons, a total of 2351 β-galactosidase-positive neurons were counted and digitally marked to prevent multiple counts. pAKT-positive POMC neurons were expressed as percentage of total POMC neurons.

Slides were viewed through a Zeiss Axioskop equipped with a Zeiss AxioCam (Göttingen, Germany) for acquisition of digital images using Zeiss AxioVision version 4.2 imaging software (Göttingen, Germany).

2.3.7.2 Analysis of *in situ* PIP$_3$ formation

For the quantitative analysis of PIP$_3$ levels in POMC neurons, STAT3-C^{POMC} mice were crossed with ROSAArte26 reporter mice [312]. At the age of 12 weeks animals fasted for 16 h were anaesthetised and injected intravenously with 5 U of insulin for 10 min. Mice were perfused transcardially with physiologic saline solution and the dissected brains were frozen in tissue-freezing medium. The 7 μm coronal sections containing the ARC were stained with β-Galactosidase (#555976; Cappel/Cosmobio, Cologne, Germany) and PIP$_3$ antibodies (#Z-G345; Echelon, Salt Lake City, USA). Double fluorescence immunostainings were performed as described before [314].

For quantitative analysis of PIP$_3$-levels in POMC neurons, a total of 1866 β-galactosidase-positive neurons were counted in ARC slices of control (n = 5; 842 POMC neurons) and STAT3-C^{POMC}ROSAArte26 (n = 5; 824 POMC neurons) mice and the amount of PIP$_3$ was classified as described previously [315] as low (less than 5 immunoreactive PIP$_3$-dots), moderate (5 to 10 immunoreactive PIP$_3$-dots) or high (more than 10 immunoreactive PIP$_3$-dots). Neurons positive for β-galactosidase were counted and marked digitally to prevent multiple counts, and PIP$_3$-immunoreactivity was rated as described above. Results were expressed as percentage of POMC neurons, showing the respective PIP$_3$-levels.

Slides were viewed through a Zeiss Axioskop equipped with a Zeiss AxioCam (Göttingen, Germany) for acquisition of digital images using Zeiss AxioVision version 4.2 imaging software (Göttingen, Germany).

2.3.7.3 Combined *in situ* hybridisation and immunohistochemistry

For SOCS3 and POMC probe synthesis, the plasmids pGEM-T SOCS3 and pGEM-T POMC described in paragraph 2.2.3.1 and 2.2.3.2 were transcribed *in vitro* into digoxigenin (DIG)-labelled RNA using 200 ng of *T7* promoter-containing plasmid pGEM-T SOCS3 or pGEM-T POMC and DIG RNA Labelling Kit (Roche, Basel, Switzerland) according to manufacturer´s guidelines. After incubation at 37°C for 2 h, the transcribed RNA was DNaseI-digested, ethanol-precipitated and the quality of RNA was assessed by electrophoresis on an agarose gel after quantification of RNA concentration (2.2.7).

For SOCS3 and POMC *in situ* hybridisation STAT3-C^{POMC} mice were mated with ROSAArte26 reporter mice [312] to generate STAT3-C^{POMC}ROSAArte26 and ROSAArte26^{POMC} mice. At the age of 10 to 14 weeks animals fasted for 16 h (for SOCS3 *in situ* hybridisation) or randomly fed animals (for POMC *in situ* hybridisation) were anaesthetised and perfused transcardially with saline followed by 4% (w/v) PFA. The brains were dissected, postfixed in 4% (w/v) PFA for 4 h, soaked in 20% (w/v) sucrose at 4°C for 24 h and frozen in tissue-freezing medium. For X-gal-combined SOCS3 or POMC *in situ* hybridisation, 8 μm thick coronal sections containing the ARC were X-gal-stained (2.3.7.1), washed with PBS, and treated with 0.25 μg/ml proteinase K for 10 min at 37°C. The sections were rinsed with 2 mg/ml glycine, placed into 4% (w/v) PFA, washed with PBS, and then washed with 2x SSC. Prehybridisation was carried out for 5 h at 56°C in prehybridisation buffer containing 50% (v/v) formamide, 5x SSC, 1x Denhardt´s solution, and 0.1% (v/v) Tween 20. Hybridisation was performed at 56°C overnight with 2 ng/μl digoxigenin-labelled RNA probe and 360 ng/μl competitor tRNA. After washing with 2x SSC, the sections were RNase digested for 1 h at 37°C and afterwards washed with 0.1x SSC for 1 h at 55°C, then cooled to RT. The sections were blocked for 1 h in Roti®-ImmunoBlock (Roth, Karlsruhe, Germany) and incubated with anti-DIG antibody coupled to alkaline phosphatase (Roche, Basel, Switzerland) for 1 h. After washing, SOCS3 and POMC *in situ* hybridisation were detected using Liquid Permanent Red (Dako North America, Carpinteria, USA) or BM Purple (Roche, Basel, Switzerland), respectively. After staining, the sections were embedded in Vectashield Mounting Medium containing DAPI (Vector Laboratories, Burlingame, USA).

For quantitative analysis of SOCS3-positive POMC neurons, a total of 3069 X-Gal-positive neurons were counted in ARC slides of control (n = 3; 1486 POMC neurons) and STAT3-C^{POMC}ROSAArte26 (n = 3; 1583 POMC neurons) mice and marked digitally to prevent multiple counts. SOCS3-positive POMC neurons were expressed as percentage of total POMC neurons.

For quantitative analysis of X-Gal-positive/POMC-mRNA-positive neurons, a total of 2214 POMC-mRNA-positive neurons were counted in ARC slides of control (n = 4; 1155 POMC-mRNA-positive neurons) and STAT3-C^{POMC}ROSAArte26 (n = 4; 1059 POMC-mRNA-positive neurons) mice and marked digitally to prevent multiple counts. X-Gal-positive/POMC-mRNA-positive neurons were expressed as percentage of total POMC-mRNA-positive neurons.

Slides were viewed through a Zeiss Axioskop equipped with a Zeiss AxioCam (Göttingen, Germany) for acquisition of digital images using Zeiss AxioVision version 4.6 imaging software (Göttingen, Germany).

2.3.7.4 Histomorphology

For general histology of embryonic brains, the complete head of E19.5 days old FOXO1ADA^{CNS} and control embryos were snap-frozen in tissue-freezing medium, and cut in 7 μm thick coronal sections using a freezing microtome (Leica, Solms, Germany). Specimens were collected on poly-L-lysine-coated glass slides (Menzel, Braunschweig, Germany), dried at RT overnight and used for hematoxylin and eosin (H&E). H&E (Sigma-Aldrich, Seelze, Germany) stainings was performed according to standard protocols [316, 317]. Slides were viewed through a Zeiss Axioskop equipped with a Zeiss AxioCam (Göttingen, Germany) for acquisition of digital images using Zeiss AxioVision version 4.6 imaging software (Göttingen, Germany).

2.3.7.5 TUNEL staining

The terminal deoxynucleotidyl transferase-mediated dUTP-biotin nick end labelling (TUNEL) method [318] was used to identify apoptotic cells in the embryonic brains by labelling fragmented DNA. The complete head of E19.5 days old FOXO1ADA^{CNS} and control embryos were snap-frozen in tissue-freezing medium, cut in 7 μm thick coronal sections using a freezing microtome (Leica, Solms, Germany) and stained by using the DeadEnd^{TM} Fluorometric TUNEL System (Promega, Madison, USA) according to manufacturer´s protocol.

2.4 Biochemistry

2.4.1 Enzyme-linked immunosorbent assay (ELISA)

Serum insulin, leptin, and corticosterone concentrations were measured by ELISA according to manufacturer's guidelines (Mouse Leptin ELISA, #90030, Crystal Chem, Downers Grove, USA; Mouse/Rat Insulin ELISA, #INSKR020, Crystal Chem, Downers Grove, USA; Corticosterone Enzyme Immunoassay Kit, #900-097, Assay Designs, Ann Arbor, USA).

2.4.2 Protein extraction

To prepare ES cell or MEF lysates, 1×10^6 cells were dissolved in 20 µl RIPA buffer (1x PBS, 1% NP-40, supplemented with complete mini protease inhibitor cocktail tablets). After centrifugation at 4°C, the supernatant was transferred into a new vial.

To prepare cytoplasmic and nuclear protein extracts, hypothalamic tissue, ES cells or MEFs were homogenised or suspended in hypotonic solution (10 mM HEPES [pH 7.6], 10 mM KCl, 2 mM $MgCl_2$, 0.1 mM EDTA, supplemented with complete mini protease inhibitor cocktail tablets) and incubated on ice for 10 min. 1% (v/v) NP-40 was added, incubated for 5 min and centrifuged 4°C. After removing the cytoplasmic fraction, the nuclear pellet was washed in hypotonic buffer and resuspended in high salt buffer (20 mM Hepes [pH 7.9], 420 mM NaCl, 1.5 mM $MgCl_2$, 0.5 mM DTT, 0.2 mM EDTA, 10 % (v/v) glycerol, completed with protease inhibitor cocktail). After incubation on ice and centrifugation at 4°C, the nuclear protein fraction was transferred into a new vial.

To generate hypothalamic lysates, snap-frozen tissues were thawed and homogenised in lysis buffer (20 mM Tris-HCl [pH 8.0], 1% (v/v) NP-40, 150 mM NaCl, 10 mM NaF, 1 mM Na_3VO_4, 1 mM $Na_4P_2O_7$, supplemented with 1x complete mini protease inhibitor cocktail) using 70 µm nylon cell strainers (Falcon, Belford, USA). After incubation on ice for 10 min and centrifugation at 4°C, protein lysates were transferred into new vials.

If necessary, mice, ES cells, or MEFs were fasted overnight and treated with leptin (5 mg/kg body weight), 30 U/ml LIF ESGRO® or 100 nM insulin, respectively, before protein extraction.

Protein concentrations were determined by measuring the sample absorption at 280 nm with a NanoDrop® ND-1000 UV-Vis Spectrophotometer (Peqlab, Erlangen, Germany). For electrophoretic mobility shift assay (EMSA), nuclear extracts were diluted to 4 µg/µl and stored at -80°C. For Western blot analysis, protein extracts were diluted to

10 mg/µl with lysis buffer and 4x SDS sample buffer (125 mM Tris-HCl [pH 6.8], 5% (w/v) SDS, 43.5% (v/v) glycerol, 100 mM DTT, and 0.02% (w/v) bromphenol blue), incubated at 95°C for 5 min and stored at -80°C.

2.4.3 Western blot analysis

Frozen protein extracts were thawed at 95°C for 5 min, separated on 10% to 12% (v/v) SDS polyacrylamide gels [319] and blotted onto polyvinylidene fluoride (PVDF) membranes (Bio-Rad, Munich, Germany). Membranes were incubated with 1% blocking reagent (Roche, Mannheim, Germany) for 1 h at RT or overnight at 4°C. Subsequently, primary antibodies (Table 10) diluted in 0.5% (v/v) blocking solution were applied for 1 h at RT or overnight at 4°C. PVDF membranes were then washed twice for 10 min with 1x TBS/Tween and incubated twice for 10 min with 0.5% (v/v) blocking solution. After 1 h incubation at RT with the respective secondary antibodies, membranes were washed 4 times for 5 min with 1x TBS/Tween, incubated for 1 min in Pierce ECL Western Blotting Substrate (Perbio Science, Bonn, Germany), sealed in a plastic bag and exposed to chemiluminescence films (Amersham, Braunschweig, Germany). Films were developed in an automatic developer (Agfa, Mortsel, Belgium).

Table 10: Primary antibodies used for Western blot analysis.

Antibody	Catalogue N°	Distributor	Dilution
α-Tubulin	#T6074	Sigma Aldrich, Seelze, Germany	1:5000
Bim	#2933	Cell Signaling, Danvers, USA	1:1000
Cleaved Caspase-3	#9661	Cell Signaling, Danvers, USA	1:1000
FKHR(N-18)	#sc-9809	Santa Cruz, Heidelberg, Germany	1:200
FOXO1	#2880	Cell Signaling, Danvers, USA	1:1000
LaminA/C	#sc-6215	Santa Cruz, Heidelberg, Germany	1:1000
pSTAT3	#9145	Cell Signaling, Danvers, USA	1:1000
STAT3	#4904	Cell Signaling, Danvers, USA	1:1000

2.4.4 Electrophoretic mobility shift assay (EMSA)

Mice were injected intraperitoneally with either saline or leptin (5 mg/kg body weight) after over night fasting and sacrificed 30 min after injection. Starved ES cells were stimulated with 30 U/ml LIF for 2 h. After isolation of nuclear extracts of hypothalamic tissue or ES cells (2.4.2), 4 µg of nuclear extracts were incubated at RT for 30 min with 2 µg poly(dI-dC) and 0.5 ng of ^{32}P-labelled probe (Table 11). The FOXO1 probe was

dimerised by boiling and cooling overnight of forward and reverse complimentary oligonucleotides. 100 ng of probe DNA (Table 11) were radioactively end-labelled in a 25 µl reaction mix containing 2.5 µCi γ^{32}P dATP and 25 U T4 polynucleotide kinase. Following 10 min incubation at 37°C the probe was purified from nonincorporated nucleotides with MicroSpin^{TM} G-20 columns (GE Healthcare, Munich, Germany) according to manufacturer's guidelines. For supershifting FOXO1, 1 µl of high-concentrated antibody (FKHR(N-18)X, #sc9809, Santa Cruz, Heidelberg, Germany or FOXO1, #2880, Cell Signaling) was added and incubated for 15 min at RT following by incubation on ice for 15 min. Samples were fractionated on a 5% (v/v) polyacrylamide gel overnight using 0.5x TBE as running buffer. The gel was incubated for 15 to 30 min in gelfix (20% MeOH, 10% acetic acid) and dried in a gel dryer (Bio-Rad, Munich, Germany). Dried gels were exposed to X-ray films (BioMAX MS, Eastman Kodak, Rochester, USA) at -80°C and films developed in an automatic developer (Agfa, Mortsel, Belgium).

Table 11: Probes used for EMSA.

Probe	Sequence (5´-3´)	Catalogue N°	Distributor
STAT3	GAT CCT TCT GGG AAT TCC TAG ATC	#sc-2571	Santa Cruz, Heidelberg, Germany
STAT3 mutant	GAT CCT TCT GGG CCG TCC TAG	#sc-2572	Santa Cruz, Heidelberg, Germany
SP1	ATT CGA TCG GGG CGG GGC GAG C	#sc-2502	Santa Cruz, Heidelberg, Germany
FOXO1	CTA TAA GTA GGG CCC TGT GAC TAG T	-	Eurogentec, Seraing, Belgium

2.5 Mouse experiments

General animal handling was performed as described by Hogan [297] and Silver [320].

2.5.1 Animal care

Care of animals was within institutional animal care committee guidelines and all animal procedures were conducted in compliance with protocols and approved by local government authorities (Bezirksregierung Köln) and were in accordance with National Institutes of Health guidelines. Mice were housed in groups of 3 to 5 or individually if required for an experiment as indicated. Mice were housed in a virus-free facility at 22 to 24°C on a 12 h light / 12 h dark cycle with the light on at 7 a.m. and were either fed a normal

chow diet (Teklad Global Rodent # T.2018.R12; Harlan, Borchen, Germany) containing 53.5% of carbohydrates, 18.5% of protein, and 5.5% of fat (12% of calories from fat) or a high fat diet (# C1057; Altromin, Lage, Germany) containing 32.7% of carbohydrates, 20% of protein, and 35.5% of fat (55.2% of calories from fat), respectively. All animals had access to water *ad libitum*. Food was only withdrawn if required for an experiment. Body weight was measured once a week. At the end of the study period, animals were sacrificed by lethal CO_2 anaesthesia. Body length (naso-anal length) was measured directly after sacrifice, and relevant organs were dissected and stored at -80°C until further preparation.

2.5.2 Mice

STAT3-C$^{floxstop/floxstop}$ mice [321] were mated with mice carrying the *pomc cre* transgene [322]. Breeding colonies were maintained by mating STAT3-C$^{floxstop/floxstop}$ with POMC-Cre, STAT3-C$^{floxstop/floxstop}$POMC-Cre (STAT3-C/C^{POMC}), and FOXO1DN$^{floxstop/+}$ mice [279, 281] to analyse STAT3-C$^{floxstop/+}$POMC-Cre (STAT3-C^{POMC}), STAT3-C/C^{POMC}, and STAT3-C$^{floxstop/}$FOXO1DN^{floxstop}POMC-Cre (STAT3-C/FOXO1DN^{POMC}) animals. Only animals from the same mixed background strain generation were compared. Mice were genotyped by PCR using genomic DNA isolated from tail tips (2.2.9). Germline deletion by the POMC-Cre was excluded using the NeoRT primer hybridising in the *lox*P-flanked stop cassette in tail biopsies (Table 5).

FOXO1ADA$^{floxstop/+}$ [280] were mated with mice carrying the *nestin cre* transgene [323] to analyse FOXO1ADA$^{floxstop/+}$Nestin-Cre (FOXO1ADA^{CNS}) animals. Only animals from the same mixed background strain generation were compared. Mice were genotyped by PCR using genomic DNA isolated from tail tips or liver (2.2.9). Germline deletion by the Nestin-Cre was excluded using primers (ΔFOXO1ADA) to detect deleted alleles in the liver (Table 5).

2.5.3 Collection of blood samples and determination of blood glucose levels

Tail bleeding of mice was performed according to Hogan [297] and Silver [320]. Blood glucose values were determined from whole venous blood using an automatic glucose monitor (GlucoMen® *GlycÓ*; A. Menarini Diagnostics, Florence, Italy). Determination of blood glucose levels and collection of blood samples were performed in the morning to avoid deviations due to circadian variations.

2.5.4 Food intake

Food intake was measured over a two-week period, during which mice were housed individually in regular cages using food racks. To minimise handling of the animals, food racks were weighed every second day and daily food intake was calculated as the average daily intake of chow within the time stated.

2.5.5 Analysis of body composition

Nuclear magnetic resonance (NMR) was employed to determine whole body composition of live animals using the NMR Analyzer minispec mq7.5 (Bruker Optik, Ettlingen, Germany).

2.5.6 Glucose and insulin tolerance test

Glucose tolerance tests (GTT) were performed on animals that had been fasted overnight for 16 h. Insulin tolerance tests (ITT) were performed on random fed mice. Animals were injected intraperitoneally with glucose (2 g/kg body weight) or with human regular insulin (0.75 U/kg body weight), respectively. Glucose levels were determined in blood collected from the tail tip immediately before and 15, 30, and 60 min after the injection, with an additional value determined after 120 min for the GTT.

2.5.7 Restraint stress

Mice were familiarised with gentle handling for approximately 8 weeks prior to the experiment. For determination of basal serum corticosterone levels, blood was drawn from the tail vein during the first 3 h of the light phase. Directly after that, mice were subjected to 1 h of restraint stress by enclosing the animals in a plastic tube with a diameter of 3 cm and openings for air supply. At the end of the experiment, blood samples were collected from the tail vein for determination of stressed plasma corticosterone levels.

2.5.8 Intraperitoneal leptin sensitivity test

Leptin sensitivity was examined by intraperitoneal injection of mice at the age of 15 weeks with saline twice a day for three consecutive days and subsequently with 2 mg/kg leptin twice a day for three consecutive days. Body weight and food intake were determined daily.

2.6 Computer analysis

2.6.1 Densitometrical analysis

Nuclear localisation of transcription factors was assessed by EMSA and protein expression by Western blot analysis. Bands were measured in intensity per mm^2 using the Quantity One Software (Bio-Rad, Munich, Germany). After background subtraction, each sample was normalised to an internal loading control. Average protein expression of control mice was set to 100% and compared to protein expression of transgenic animals unless stated otherwise.

2.6.2 Statistical methods

Data sets were analysed for statistical significance using a two-tailed unpaired student's t test. All *p* values below 0.05 were considered significant. All displayed values are means ± SEM. * $p \leq 0.05$; ** $p \leq 0.01$; *** $p \leq 0.001$ versus control.

3   Results

In the present study, the central role of the transcription factors STAT3 and FOXO1 has been elucidated by transgenic expression of mutant versions of these proteins. To this end, a constitutively active version of STAT3 (STAT3-C) that was inserted into the ubiquitously expressed *ROSA26* locus [324] preceded by a *lox*P-flanked stop cassette, was first characterised in ES cells and subsequently in proopiomelanocortin (POMC)-expressing neurons with respect to energy homeostasis and metabolism. Similarly, a dominant negative FOXO1 (FOXO1DN) as well as a constitutively active FOXO1 (FOXO1ADA) mutant was inserted into the *ROSA26* locus of ES cells, respectively. These constructs contained the strong *chicken β actin* promoter that was separated from the transgenic FOXO1 constructs by a *lox*P-flanked stop cassette, thus preventing its expression. The functionality of the FOXO1DN and FOXO1ADA constructs was first investigated *in vitro* and subsequently in POMC neurons and the whole brain of transgenic mice.

3.1   STAT3-C expression in POMC neurons provokes a negative feedback inhibition of leptin and insulin signalling in obesity

3.1.1   Verification of the constitutively active STAT3 construct in ES cells

The constitutively active variant of STAT3 dimerises spontaneously via disulfide bonds due to substitution of two residues to cysteins in the SH2-domain and activates transcription stimulus independent. STAT3-C ES cells contain a targeted STAT3-C cDNA preceded by a *lox*P-flanked transcriptional stop cassette within the ubiquitously expressed *ROSA26* locus [324]. The transfection of STAT3-C ES cells with a Cre-expressing plasmid causes Cre-mediated recombination of the *lox*P-flanked stop cassette leading to the composed expression of the *stat3-c* transgene and eGFP (Figure 8).

45
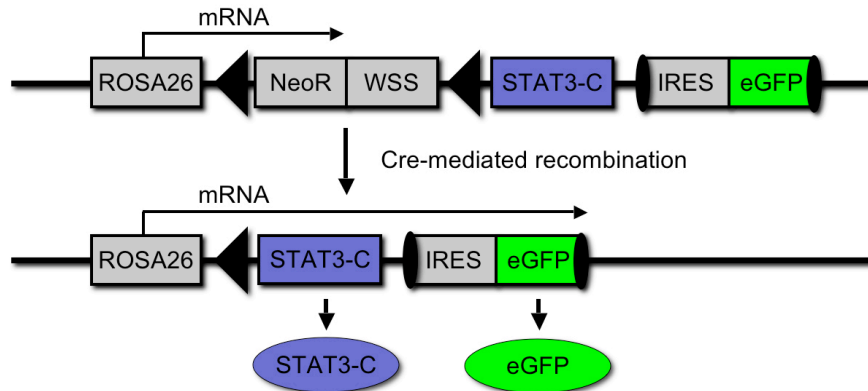
Figure 8: Cre-mediated expression of a constitutively active *stat3* transgene.
Scheme of the *stat3-c* transgene inserted into the *ROSA26* locus. Cre-mediated recombination eliminates the *lox*P-flanked NeoR and WSS only in cells expressing Cre thereby allowing transcription of the bicistronic STAT3-C eGFP mRNA. IRES, internal ribosome entry site; eGFP, enhanced *green fluorescent protein* gene; NeoR, *neomycine resistance* gene driven by the *TK* promoter; STAT3-C, constitutively active mutant of STAT3; WSS, Westphal stop sequence; filled triangles, *lox*P; closed ellipses, FRT sites.

To verify Cre-mediated recombination with accompanied eGFP expression, STAT3-C ES cells transfected with a control or Cre-expressing plasmid were analysed by fluorescence microscopy. eGFP-positive ES cells were visualised only upon Cre-mediated recombination and FACS analysis revealed that 0% of control and 88% of STAT3-C ES cells expressed eGFP (Figure 9).
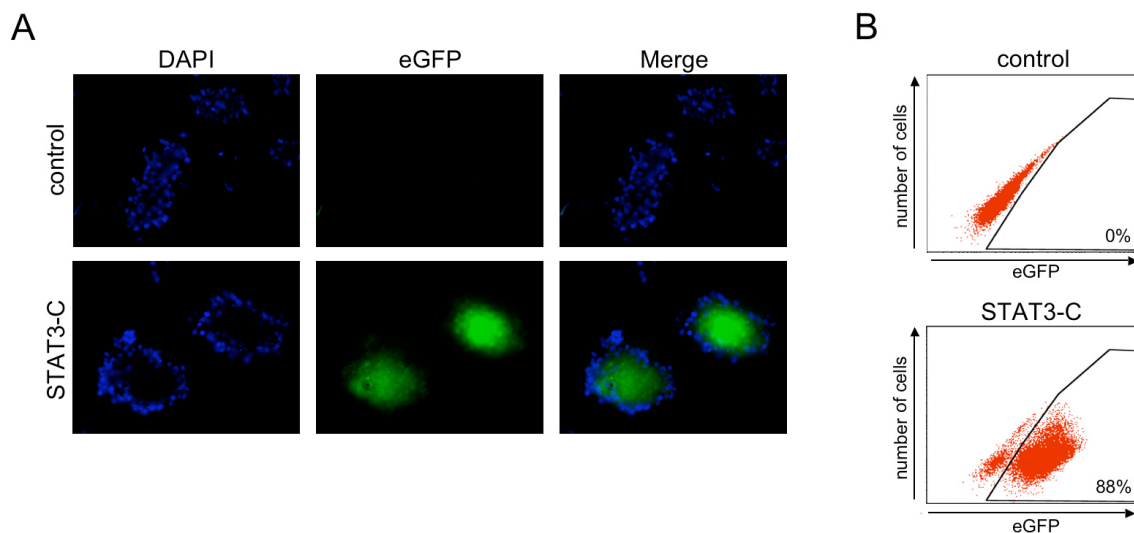
Figure 9: Verification of Cre-mediated expression of STAT3-C and eGFP in ES cells.
(A) Fluorescence microscopy of control and STAT3-C-expressing ES cell colonies. Magnification: 100x.
(B) FACS analysis of control and STAT3-C-expressing ES cells. Blue (DAPI), DNA; green, eGFP.

Moreover, Western blot analysis confirmed increased STAT3 expression in ES cells after Cre-mediated recombination (Figure 10A). While STAT3 in control cells translocated from the cytoplasm to the nucleus only upon stimulation with LIF, the STAT3-C mutant was detectable in the nucleus independent of LIF stimulation (Figure 10B, C).
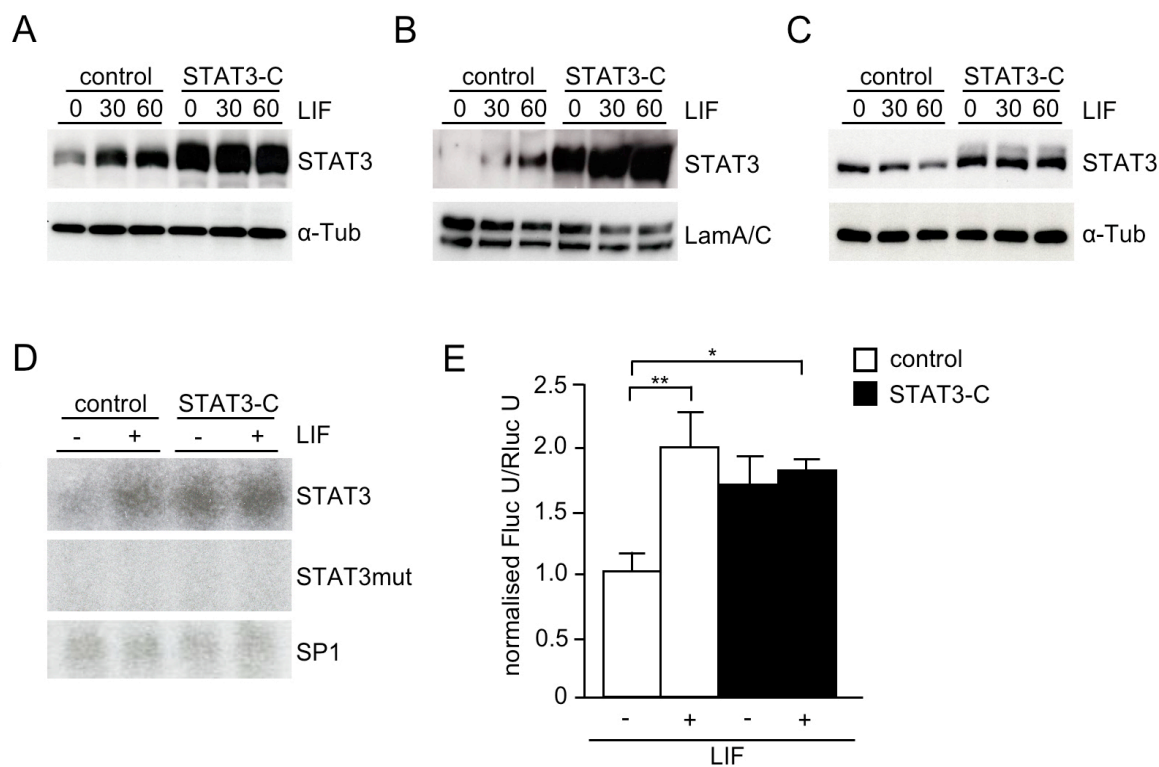
Figure 10: Functional validation of the constitutively active STAT3 construct in ES cells.
(A) Western blot analysis using STAT3 and α-Tubulin (α-Tub, loading control) antibodies of whole cell lysates from control and STAT3-C-expressing ES cells stimulated with leukemia inhibitory factor (LIF) for the indicated timepoints. **(B)** Western blot analysis using STAT3 and LaminA/C antibodies (LamA/C, loading control) of nuclear lysates from control and STAT3-C-expressing ES cells stimulated with LIF for the indicated timepoints. **(C)** Western blot analysis using STAT3 and α-Tubulin (loading control) antibodies of cytoplasmic lysates from control and STAT3-C-expressing ES cells stimulated with LIF for the indicated timepoints. **(D)** EMSA of nuclear extracts isolated from control and STAT3-C-expressing ES cells upon 2 h LIF stimulation using a radioactively labelled consensus sequence for STAT3, a mutant STAT3 consensus sequence and a specific protein (SP) 1 consensus sequence (loading control), respectively. **(E)** Transcriptional activity of STAT3 and STAT3-C in control and STAT3-C-expressing ES cells transfected with pSTAT3-TA-Luc and pRL-null. ES cells were incubated with or without LIF 24 h before measurement of firefly luciferase (Fluc) and renilla luciferase (Rluc) activity. Displayed values are means ± SEM. * $p \leq 0.05$ and ** $p \leq 0.01$ versus control.

To further functionally validate the STAT3-C construct, the DNA-binding capacity was assessed by an electrophoretic mobility shift assay (EMSA) using nuclear extracts from STAT3-C-expressing and control ES cells. LIF stimulation increased binding of STAT3, in contrast to the persistent binding of STAT3-C to its consensus DNA sequence (Figure 10D). The specificity of STAT3-C-binding was addressed using a mutated STAT3 consensus sequence with the same nuclear extracts demonstrating that mutation of three nucleotides within the STAT3 probe abrogates recognition by both endogenous STAT3 and STAT3-C.

A probe for specific protein (SP) 1 served as loading control (Figure 10D). Furthermore, transfection studies using a luciferase expression vector under the transcriptional control of STAT3-responsive elements substantiated LIF-independent activation of luciferase expression in STAT3-C-expressing ES cells compared to control ES cells (Figure 10E).

Taken together, Cre-mediated expression of the *stat3-c* transgene in ES cells leads to constitutive nuclear localisation of STAT3-C and target gene promoter occupancy, which implicates specific activation of STAT3 target gene expression.

3.1.2 Generation of POMC neuron-specific STAT3-C-expressing mice

To analyse the effect of excessive STAT3-dependent signalling in POMC-expressing neurons, STAT3-C$^{floxstop/floxstop}$ mice were intercrossed with mice carrying the *pomc cre* transgene (Figure 11A) [322] to obtain STAT3-C$^{floxstop/+}$POMC-Cre (STAT3-C^{POMC}) mice expressing STAT3-C selectively in POMC neurons, while Cre-negative mice of this breeding served as controls (Figure 11B). Furthermore, to investigate the dose-dependency of STAT3-controlled transcriptional regulation in POMC neurons, homozygous STAT3-C$^{floxstop/floxstop}$POMC-Cre (STAT3-C/C^{POMC}) mice were generated by intercrossing STAT3-C^{POMC} with STAT3-C$^{floxstop/floxstop}$ mice (Figure 11C).
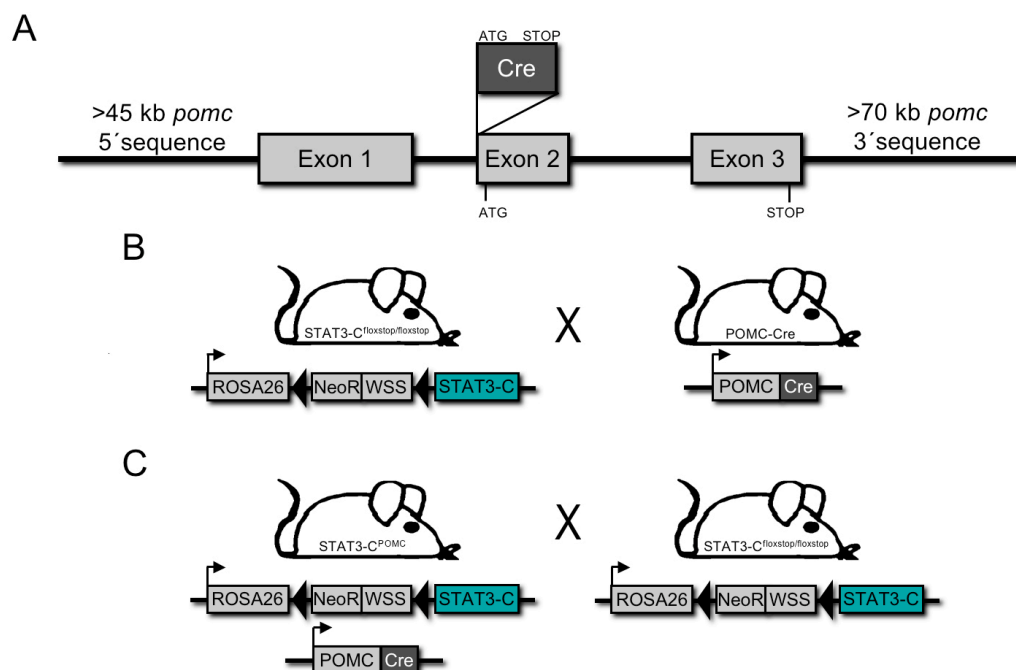
Figure 11: POMC neuron-restricted expression of STAT3-C.
(A) Scheme of *pomc cre* transgene. Mice expressing Cre recombinase (Cre) under control of the *pomc* promoter were generated by engineering a *pomc* bacterial artificial chromosome. The Cre translation initiation site (ATG) was inserted into the *pomc* ATG and deleted the first 30 bp of the *pomc* gene. **(B)** STAT3-C$^{floxstop/floxstop}$ mice were intercrossed with mice carrying the *pomc cre* transgene to obtain STAT3-C^{POMC} mice expressing STAT3-C selectively in POMC neurons. **(C)** To generate homozygous STAT3-C/C^{POMC} mice, STAT3-C^{POMC} mice were intercrossed with STAT3-C$^{floxstop/floxstop}$ mice.

The Cre-mediated recombination and POMC-specific expression of STAT3-C in the ARC was elucidated by immunohistochemistry detecting the eGFP expressed from the IRES inserted in the *stat3-c* transgene. eGFP-positive neurons were only detectable in hypothalami of mice carrying both the *stat3-c* and the *pomc cre* transgene, but not in controls. Consistently, the STAT3-C[POMC] mice showed a pattern of eGFP immunoreactivity in the ARC of the hypothalamus reflecting the described expression pattern of endogenously expressed POMC (Figure 12A) [322].
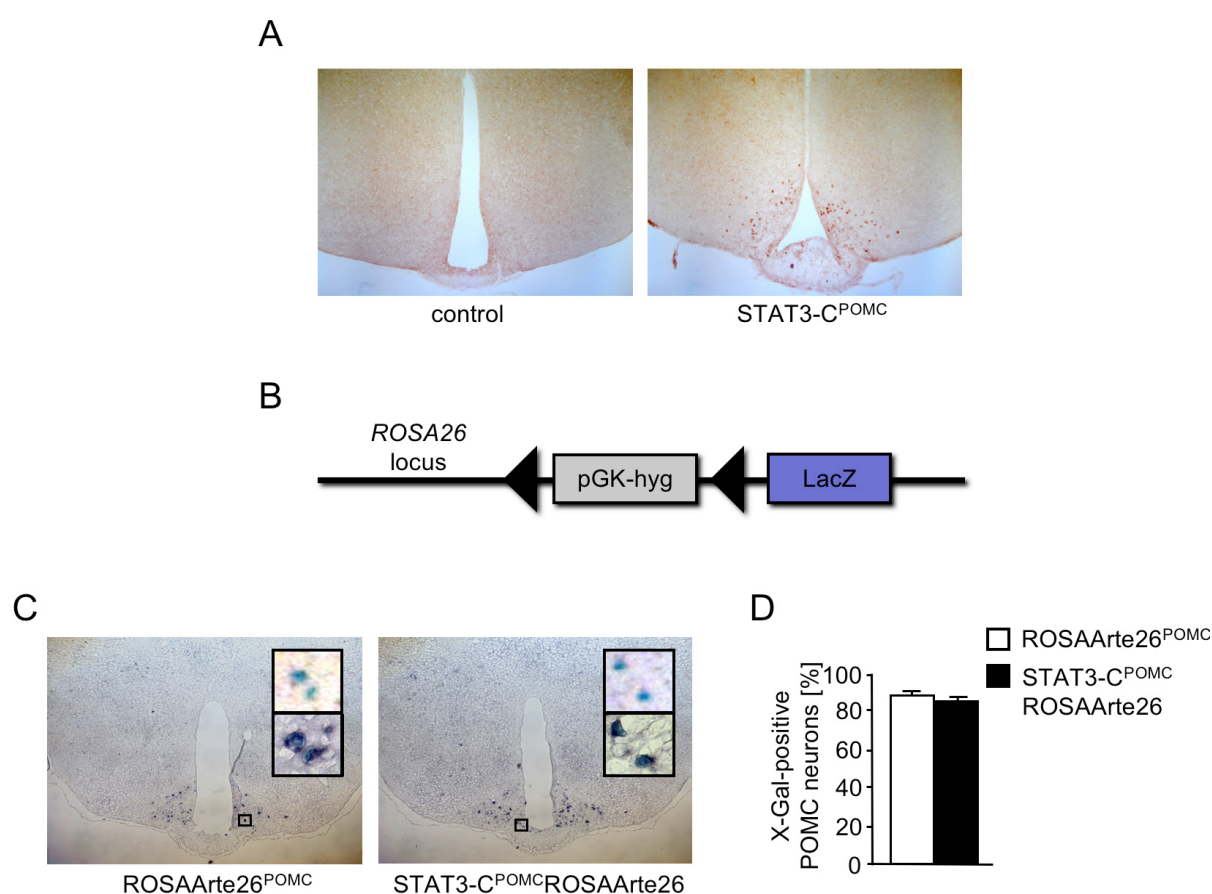
Figure 12: Verification of Cre-mediated recombination in POMC neurons of STAT3-C[POMC] mice.
(A) Immunohistochemistry for eGFP in brains of 12 weeks old control and STAT3-C[POMC] mice. Magnification: 80x. **(B)** Map of *LacZ* transgene for Cre-mediated expression from the *ROSA26* locus (ROSAArte26). pGK-hyg: *hygromycin resistance* gene driven by the *pGK (phosphoglycerate kinase)* promoter. In this configuration, Cre-mediated recombination removes the *lox*P-flanked *hygromycin resistance* gene only in cell types expressing Cre recombinase, resulting in transcription of *β-galactosidase*. **(C)** Representative *in situ* hybridisation using a POMC probe in hypothalamic neurons of ROSAArte26[POMC] and STAT3-C[POMC]ROSAArte26 mice at the age of 10 - 14 weeks. X-Gal-positive neurons before (small upper panel) and after *in situ* hybridisation (small lower panel). Blue, X-Gal; purple, POMC mRNA. Magnification: 50x, 400x. **(D)** Quantitation of X-Gal-positive/POMC mRNA-positive neurons in brain sections of ROSAArte26[POMC] and STAT3-C[POMC]ROSAArte26 mice at the age of 10 - 14 weeks (n = 4 per genotype). A total of 2214 POMC mRNA-positive neurons were analysed.

Additionally, to confirm POMC-restricted recombination, both STAT3-C/C[POMC] and POMC-Cre mice were crossed with a reporter mouse strain in which transcription of the *β-galactosidase* gene (*LacZ*) under control of the ubiquitously expressed *ROSA26* promoter is prevented by a *lox*P-flanked *hygromycin resistance* gene (ROSAArte26 mice) [312], thus leading to β-galactosidase expression only in cells expressing the Cre recombinase (Figure 12B). Subsequently, a hypothalamic X-Gal staining for Cre-dependent expression of β-galactosidase combined with *in situ* hybridisation for endogenous POMC mRNA was performed. In ROSAArte26[POMC] and STAT3-C[POMC]ROSAArte26 mice 88% and 85% of cells coexpressed POMC mRNA and β-galactosidase, respectively (Figure 12C, D).

Hypothalamic expression of STAT3-C was confirmed by quantitative RT-PCR using oligonucleotides located in exon 1 of the ROSA26 and in the STAT3-C transcript. Hypothalamic cDNA from STAT3-C/C[POMC] and STAT3-C[POMC] mice, but not from control mice led to a specific STAT3-C PCR product. Expression of endogenous STAT3 as well as glyceraldehyde-3-phosphate dehydrogenase (GAPDH) served as controls (Figure 13A).

To confirm the functionality of STAT3-C *in vivo*, the DNA-binding capacity was evaluated by EMSA using hypothalamic nuclear extracts from fasted STAT3-C/C[POMC] and control mice injected with saline or leptin, respectively. In contrast to endogenous STAT3, STAT3-C bound constitutively to its consensus sequence without dependence on the leptin-signal in mice (Figure 13B).

Taken together, these results validate the functionality of the *ROSA26 stat3-c* transgene in POMC cells of mice *in vivo*.
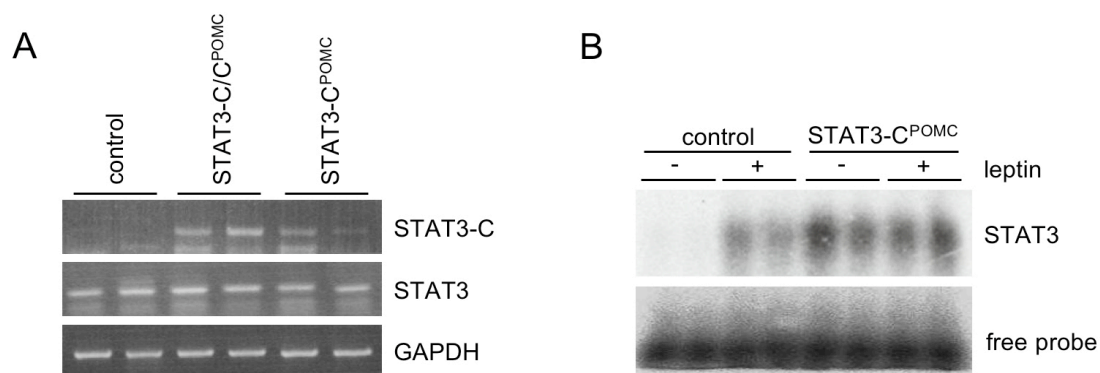
Figure 13: Functional validation of the constitutively active STAT3 construct in STAT3-C[POMC] mice.
(A) Hypothalamic expression of STAT3-C in STAT3-C[POMC] mice confirmed by RT-PCR of control, STAT3-C[POMC], and STAT3-C/C[POMC] mice using oligonucleotides detecting transgenic STAT3-C, endogenous STAT3, and glyceraldehyde-3-phosphate dehydrogenase (GAPDH). **(B)** EMSA of nuclear extracts isolated from fasted control and STAT3-C[POMC] mice after intraperitoneal injection with leptin or saline using a radioactively labelled STAT3 probe.

3.1.3 Mild obesity in STAT3-C^{POMC} mice

To determine the impact of constitutive STAT3 signalling in anorexigenic POMC-expressing neurons on the regulation of energy homeostasis, body weight of male control, STAT3-C^{POMC}, and STAT3-C/C^{POMC} mice was monitored from weaning until 20 weeks of age. STAT3-C^{POMC} mice exhibited an approximately 12% elevated body weight compared to control mice. This effect was mildly enhanced by expressing STAT3-C from two alleles although this effect did not reach statistical significance (Figure 14).

Figure 14: Increased body weight of STAT3-C^{POMC} mice.
Average body weight of male control, STAT3-C^{POMC}, and STAT3-C/C^{POMC} mice was determined weekly (n = 12 - 18 per genotype). Displayed values are means ± SEM. * $p \leq 0.05$, ** $p \leq 0.01$, and *** $p \leq 0.001$ versus control.

To examine whether the elevated body weight of STAT3-C^{POMC} mice was caused by an increase in body fat mass, the amount of epigonadal fat in male control, STAT3-C^{POMC}, and STAT3-C/C^{POMC} mice was analysed. Consistent with the body weight phenotype, STAT3-C/C^{POMC} mice exhibited significantly increased epigonadal fat pad mass at the age of 20 weeks compared to controls (Figure 15A, B). Moreover, enhanced adiposity in STAT3-C^{POMC} and STAT3-C/C^{POMC} mice was confirmed by determining body fat composition using *in vivo* magnetic resonance spectrometry. Mean body fat content was significantly increased by approximately 2 % in both STAT3-C^{POMC} and STAT3-C/C^{POMC} mice (Figure 15C). In addition, obesity in STAT3-C^{POMC} and STAT3-C/C^{POMC} mice was accompanied by significantly elevated plasma leptin concentrations in comparison to control mice (Figure 15D).
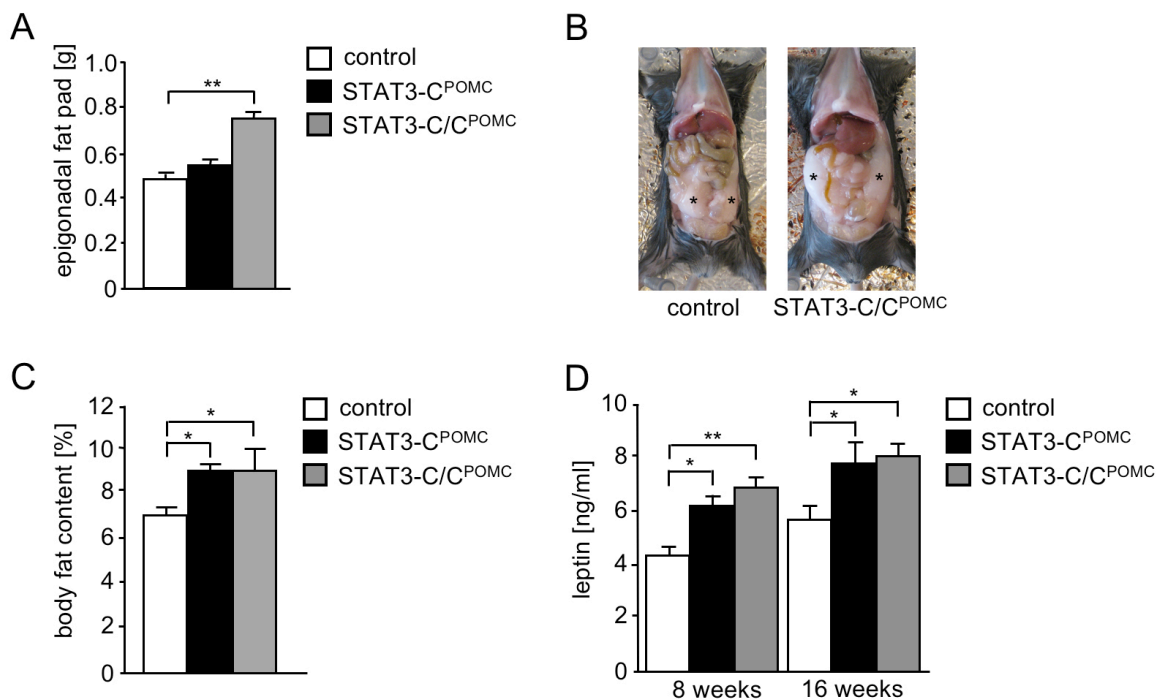
Figure 15: Increased adiposity of STAT3-C^{POMC} mice.
(A) Epigonadal fat pad weight of male control, STAT3-C^{POMC}, and STAT3-C/C^{POMC} mice at the age of 20 weeks (n = 12 – 18 per genotype). (B) *In situ* photographs of representative epigonadal fat pads of male control and STAT3-C/C^{POMC} mice of the same litter at the age of 20 weeks. Asterisks indicate epigonadal fat pads. (C) Whole body fat content of male control, STAT3-C^{POMC}, and STAT3-C/C^{POMC} mice at the age of 20 weeks was determined using *in vivo* nuclear magnetic resonance (n = 10 - 12 per genotype). (D) Serum leptin concentrations of male control, STAT3-C^{POMC}, and STAT3-C/C^{POMC} mice at the age of 8 and 16 weeks were investigated by ELISA (n = 12 - 20 per genotype). Displayed values are means ± SEM. * $p \leq 0.05$ and ** $p \leq 0.01$ versus control.

Since mice with impaired MC4R function show an increased body length [47], the body length of STAT3-C^{POMC} and STAT3-C/C^{POMC} mice was determined, revealing a significant increase in body length compared to control mice (Figure 16 A, B).

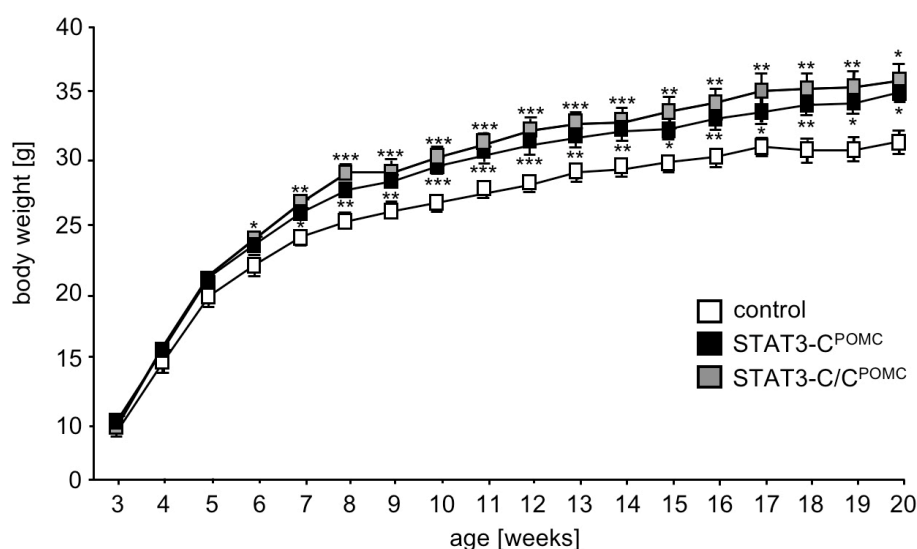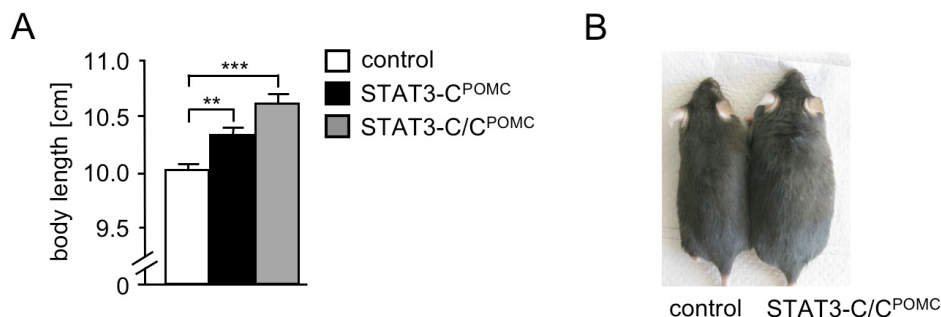**Figure 16: Increased body length of STAT3-C^{POMC} mice.**
(A) Body length of male control, STAT3-C^{POMC}, and STAT3-C/C^{POMC} mice at the age of 20 weeks (n = 10 – 12 per genotype). (B) Outward appearance of male control and STAT3-C/C^{POMC} mice of the same litter at the age of 20 weeks. Displayed values are means ± SEM. ** $p \leq 0.01$ and *** $p \leq 0.001$ versus control.

To investigate whether glucose homeostasis and insulin sensitivity were affected by expressing STAT3-C in POMC neurons, glucose and insulin tolerance tests were performed and serum insulin concentrations were determined. These analyses revealed no differences in whole body glucose homeostasis in STAT3-C^{POMC} mice compared to controls despite the mild obesity of the mutant mice (Figure 17A-C).
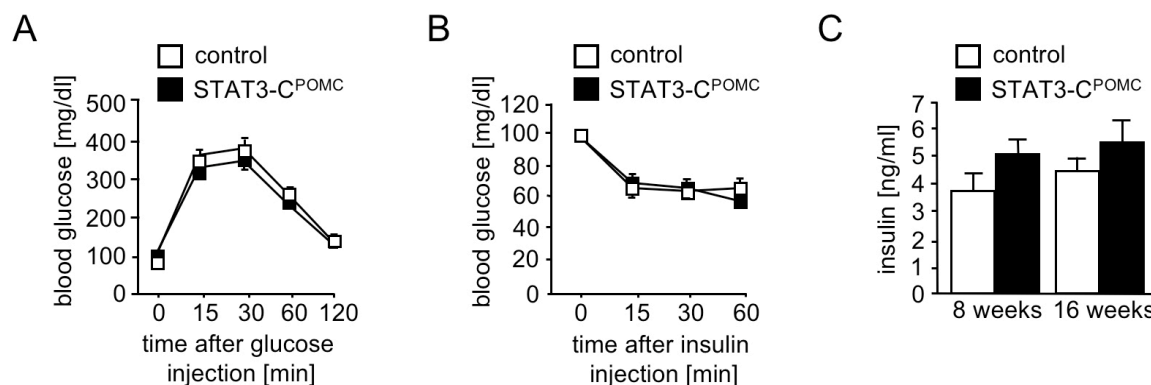
Figure 17: Unaltered glucose metabolism of STAT3-C^{POMC} mice.
(A) Glucose tolerance test of male control and STAT3-C^{POMC} mice at the age of 12 weeks (n = 12 - 15 per genotype). **(B)** Insulin tolerance test of male control and STAT3-C^{POMC} mice at the age of 13 weeks (n = 12 - 15 per genotype). **(C)** Serum insulin concentrations of male control and STAT3-C^{POMC} mice at the age of 8 and 16 weeks were investigated by ELISA (n = 13 - 15 per genotype).

POMC is not only expressed in the hypothalamus, but also detectable in the pituitary of POMC-Cre transgenic mice [281, 311]. Since the pituitary plays an important role in stress response, consequently, a stress test was conducted with STAT3-C^{POMC} mice to clarify the effects of STAT3 overactivation on the hypothalamic-pituitary-adrenal axis. However, basal as well as restraint-stress-induced corticosterone levels were comparable between controls and STAT3-C^{POMC} mice, thus revealing an unaltered stress response in these mice (Figure 18).
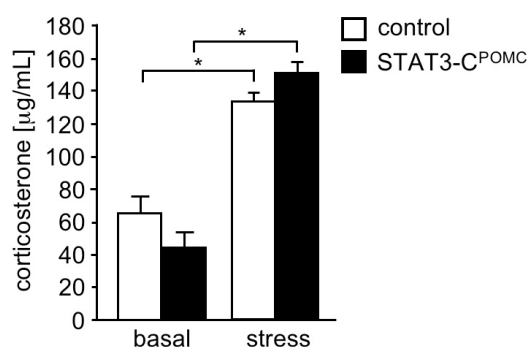
Figure 18: Unaltered stress response in STAT3-C^{POMC} mice.
Basal and restraint-stress-induced serum corticosterone levels of male control and STAT3-C^{POMC} mice at the age of 18 weeks (n = 12 per genotype). Displayed values are means ± SEM. * p ≤ 0.05 versus control.

Taken together, these results demonstrate that constitutive activation of STAT3-dependent signalling in POMC-expressing neurons causes mild obesity with increases in body weight, fat mass, circulating leptin concentrations, and gain of body length, without affecting whole body glucose homeostasis, insulin sensitivity, and the hypothalamic-pituitary-adrenal axis.

3.1.4 STAT3-C^{POMC} mice exhibit increased food intake and decreased POMC expression

An increase in body weight is a consequence of either a reduced energy expenditure, an elevated level of food intake, or a combination of both. As previously described, STAT3-C^{POMC} mice exhibit a tendency towards decreased energy expenditure compared to controls although this effect did not reach statistical significance [325]. To further investigate the mechanisms underlying the mild obesity detected in male STAT3-C^{POMC} mice, daily food intake and compensatory refeeding after a 24 h fasting period were measured in these mice. Assessment of food intake revealed a tendency for an increase in daily food intake in STAT3-C^{POMC} mice compared to controls, and a significant increase in STAT3-C/C^{POMC} mice (Figure 19A). Consistently, compensatory refeeding after fasting was significantly elevated in both STAT3-C^{POMC} and STAT3-C/C^{POMC} mice in comparison to controls (Figure 19B). Accordingly, constitutive STAT3 signalling in POMC neurons elevates steady state, as well as refeeding-associated food intake.
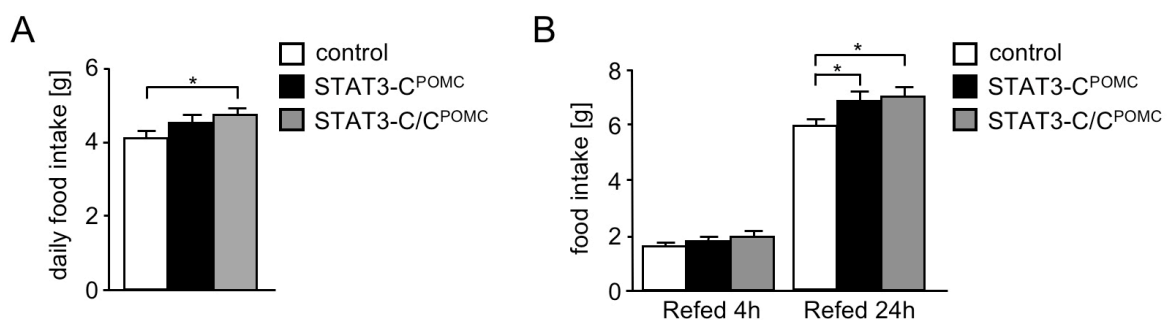
Figure 19: Increased food intake and compensatory refeeding in STAT3-C^{POMC} mice.
(A) Daily food intake of male control, STAT3-C^{POMC}, and STAT3-C/C^{POMC} mice at the age of 10 weeks (n = 8 - 18 per genotype). **(B)** Compensatory 4 h and 24 h refeeding after a 24 h fasting period of male control, STAT3-C^{POMC}, and STAT3-C/C^{POMC} mice at the age of 16 weeks (n = 7 - 9 per genotype). Displayed values are means ± SEM. * $p \leq 0.05$ versus control.

Next, hypothalamic mRNA expression levels of the neuropeptides agouti-related protein (AgRP), neuropeptide Y (NPY), and POMC, which are known to be involved in the regulation of food intake, were determined by quantitative RT-PCR. Unexpectedly, relative hypothalamic expression of anorexigenic POMC was reduced by 50% in both STAT3-C^{POMC} and STAT3-C/C^{POMC} mice compared to controls, in spite of the fact that STAT3 acts as transcriptional activator of POMC expression [73]. However, the hypothalamic expression levels of the orexigenic neuropeptides AgRP and NPY were unaltered in STAT3-C^{POMC} and STAT3-C/C^{POMC} mice (Figure 20).
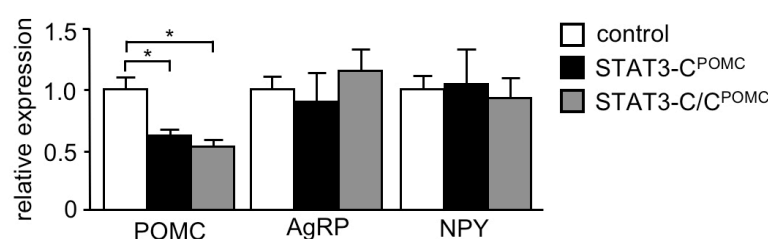
Figure 20: Hypothalamic neuropeptide expression in STAT3-C^{POMC} mice.
Relative hypothalamic expression of proopiomelanocortin (POMC), agouti-related protein (AgRP), and neuropeptide Y (NPY) under random fed conditions of male control, STAT3-C^{POMC}, and STAT3-C/C^{POMC} mice at the age of 20 weeks (n = 8 per genotype) using quantitative RT-PCR. Displayed values are means ± SEM. * p ≤ 0.05 versus control.

To investigate whether the decreased hypothalamic POMC mRNA expression in STAT3-C^{POMC} mice is a consequence of a reduced number of POMC-expressing neurons due to decreased POMC cell formation or increased POMC cell death, the number of POMC neurons in STAT3-C^{POMC} mice was calculated. To this end, brains of STAT3-C^{POMC}ROSAArte26 and ROSAArte26^{POMC} mice (3.1.2) were stained for β-galactosidase activity (Figure 21A).
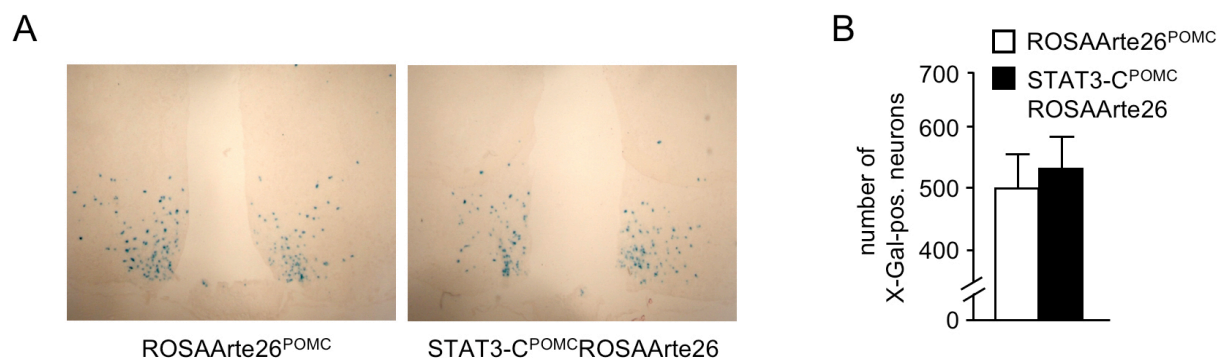
Figure 21: Unaltered number of POMC-expressing neurons in STAT3-C^{POMC} mice.
(A) X-Gal staining of brains isolated from ROSAArte26^{POMC} and STAT3-C^{POMC}ROSAArte26 mice at 12 weeks of age. Magnification: 100x. **(B)** Number of X-Gal-positive neurons in brains of ROSAArte26^{POMC} and STAT3-C^{POMC}ROSAArte26 mice at 12 weeks of age. X-Gal-positive neurons were counted in 4 coronal sections containing the ARC of 5 mice per genotype.

Counting X-Gal-positive neurons revealed indistinguishable POMC neuron numbers in STAT3-C^{POMC}ROSAArte26 and control mice since on average 495 POMC neurons in control and 546 POMC neurons in STAT3-C^{POMC}ROSAArte26 mice were identified in 4 coronal sections containing the ARC of 5 mice per genotype (Figure 21B).

Taken together, these results imply that the mild obesity observed in STAT3-C^{POMC} mice is the consequence of increased food intake caused by reduced hypothalamic POMC mRNA expression without alterations in hypothalamic POMC cell number.

3.1.5 STAT3-C^{POMC} mice are leptin-resistant and exhibit increased SOCS3 expression

To experimentally address whether the mild obesity of STAT3-C^{POMC} mice is the consequence of leptin resistance, leptin sensitivity was assessed by daily intraperitoneal injections of leptin over a 3-day-period and determination of food intake. Leptin treatment of control mice significantly reduced food intake by 20%, whereas leptin had no significant effect on food intake in both STAT3-C^{POMC} and STAT3-C/C^{POMC} mice (Figure 22).
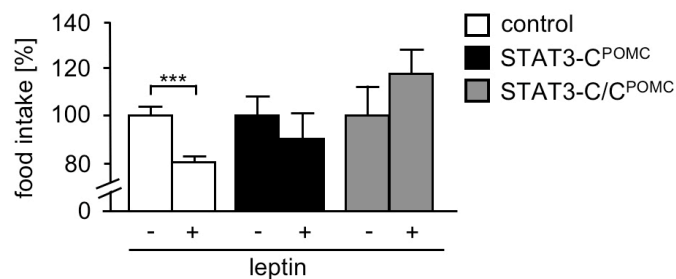
Figure 22: Leptin resistance in STAT3-C^{POMC} mice.
Leptin sensitivity test of male control, STAT3-C^{POMC}, and STAT3-C/C^{POMC} mice at the age of 17 weeks (n = 6 -10 per genotype). Mice were injected intraperitoneally for 3 consecutive days with saline twice a day and subsequently with leptin for 3 consecutive days twice a day. Food intake of saline-injected mice was set to 100%. Displayed values are means ± SEM. *** $p \leq 0.001$ versus control.

To investigate the cause of diminished leptin sensitivity of STAT3-C^{POMC} mice, the level of leptin-induced phosphorylation of STAT3 in the ARC was assessed by Western blot analysis. While leptin induced phosphorylation and thus activation of STAT3 in control mice, this response was clearly blunted in STAT3-C^{POMC} mice (Figure 23A).

Furthermore, brains of fasted and leptin- or saline-injected ROSAArte26^{POMC} and STAT3-C^{POMC}ROSAArte26 mice (3.1.2) were stained using antibodies specific for phosphorylated STAT3 and β-galactosidase to visualise leptin-induced STAT3 phosphorylation specifically in POMC neurons (Figure 23C). This experiment elucidated that 27% of POMC cells from control mice demonstrated nuclear accumulation of phosphorylated STAT3 after leptin injection, in contrast to only 4% of POMC neurons in STAT3-C^{POMC}ROSAArte26 mice (Figure 23B).
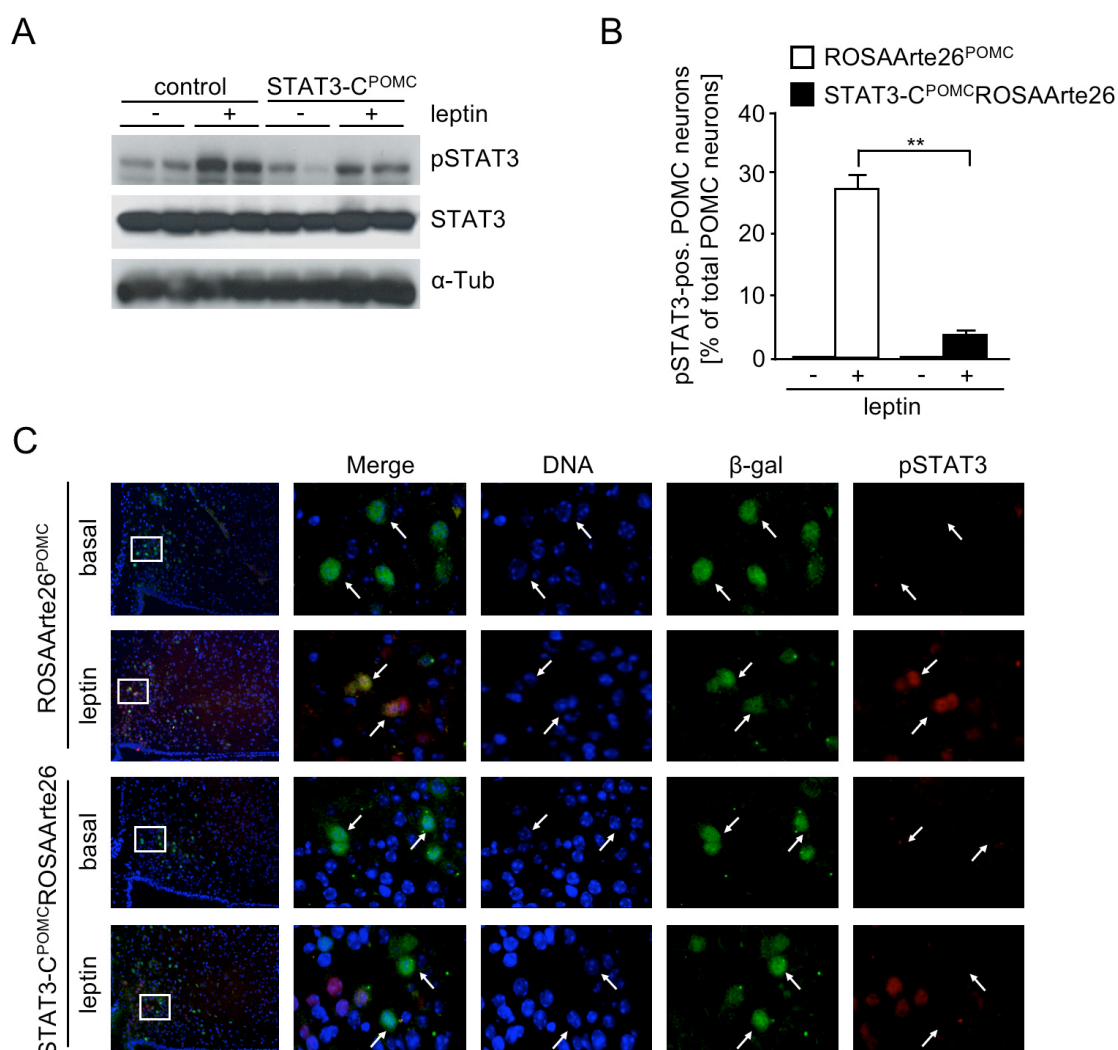
Figure 23: Inhibition of hypothalamic STAT3 signalling in STAT3-C^{POMC} mice.
(A) Western blot analysis of ARC extracts from fasted control and STAT3-C^{POMC} mice after intraperitoneal injection of leptin or saline using antibodies against phosphorylated STAT3 (pSTAT3), STAT3, and α-Tubulin (α-Tub, loading control). **(B)** Quantitation of pSTAT3-positive POMC neurons in hypothalamic sections of fasted ROSAArte26^{POMC} and STAT3-C^{POMC}ROSAArte26 mice after intraperitoneal injection of leptin or saline at the age of 10 - 12 weeks (n = 3 - 4 per genotype). A total of 2103 POMC neurons were analysed. **(C)** Representative immunohistochemistry of pSTAT3 and β-galactosidase (β-gal) in POMC neurons of fasted and saline- or leptin-injected ROSAArte26^{POMC} and STAT3-C^{POMC}ROSAArte26 mice at the age of 10 - 12 weeks. Blue (DAPI), DNA; green, β-gal (POMC neurons); red, pSTAT3. Magnification: 100x, 400x. Displayed values are means ± SEM. ** $p \leq 0.01$ versus control.

Leptin signalling is controlled by constitutively expressed proteins such as PIAS3, as well as by a negative feedback mechanism as the induction of SOCS3 expression; this leads to SOCS3-binding to phosphorylated leptin receptors and JAKs with subsequent silencing of the leptin signal [164, 165, 167]. To clarify whether chronic STAT3 signalling in POMC neurons leads to enhanced SOCS3 and PIAS3 expression, quantitative RT-PCR of hypothalamic RNA of control, STAT3-C[POMC], and STAT3-C/C[POMC] mice was performed. While PIAS expression was unaltered, expression of SOCS3 was significantly increased in hypothalami of both STAT3-C[POMC] and STAT3-C/C[POMC] mice compared to controls (Figure 24A) albeit approximately 5% of hypothalamic neurons express POMC and therefore also STAT3-C.
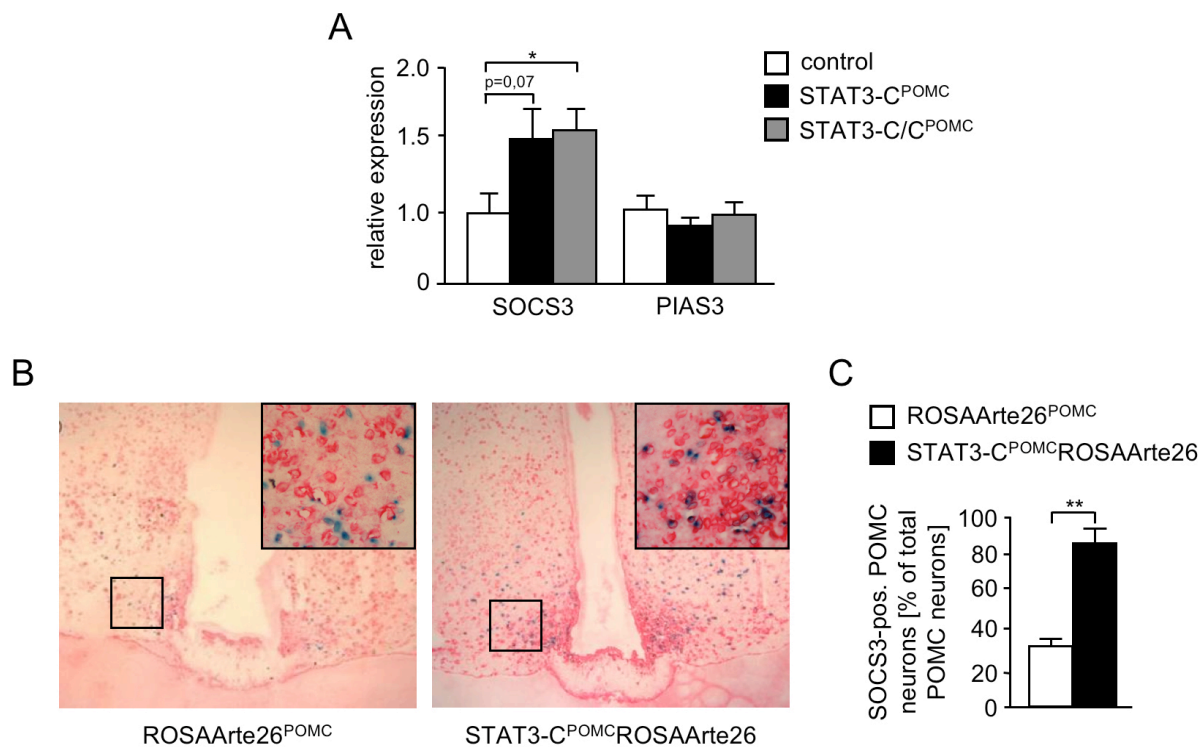
Figure 24: Increased hypothalamic SOCS3 expression in STAT3-C[POMC] mice.
(A) Relative hypothalamic expression of suppressor of cytokine signalling (SOCS) 3 and protein inhibitor of activated STAT (PIAS) 3 of male control, STAT3-C[POMC], and STAT3-C/C[POMC] mice under random fed conditions at the age of 20 weeks using a quantitative RT-PCR (n = 8 per genotype). **(B)** Representative *in situ* hybridisation using a SOCS3 probe in hypothalamic neurons of fasted ROSAArte26[POMC] and STAT3-C[POMC]ROSAArte26 mice at the age of 12 weeks. Blue, X-Gal (POMC neurons); red, SOCS3 mRNA. Magnification: 100x, 400x. **(C)** Quantitation of SOCS3-positive POMC neurons in hypothalamic sections of fasted ROSAArte26[POMC] and STAT3-C[POMC]ROSAArte26 mice at the age of 12 weeks (n = 3 per genotype). A total of 3069 X-Gal-positive neurons were analysed. Displayed values are means ± SEM. * $p \leq 0.05$ and ** $p \leq 0.01$ versus control.

To further directly address whether SOCS3 expression is primarily increased in POMC neurons, a combined *in situ* hybridisation/X-Gal staining using a SOCS3 probe on brain slices from food-deprived ROSAArte26[POMC] and STAT3-C[POMC]ROSAArte26 mice (3.1.2) (Figure 24B). This analysis visualised that in the fasted state, approximately 32% of POMC neurons from control mice expressed SOCS3, while 86% of STAT3-C-expressing POMC neurons were positive for SOCS3 mRNA (Figure 24C).

In summary, these data imply that chronic STAT3 signalling in POMC neurons diminishes whole body leptin sensitivity by an increased expression of the negative feedback regulator SOCS3.

3.1.6 Increased SOCS3 expression in POMC neurons leads to central insulin resistance

Since SOCS3 was also shown to inhibit not only leptin but also insulin signalling via binding to the IR as well as by ubiquitin-mediated degradation of IRS [326, 327], it was investigated whether STAT3-induced SOCS3 expression, besides provoking leptin resistance, also affects insulin action in POMC neurons. To this end, fasted ROSAArte26[POMC] and STAT3-C[POMC]ROSAArte26 mice (3.1.2) were injected with insulin and their brains were used for double immunohistochemical analysis for phosphatidylinositol-3,4,5-trisphosphate (PIP$_3$) and β-galactosidase. Upon insulin stimulation control mice exhibited ratios of low:moderate:high PIP$_3$-immunoreactive POMC neurons comparable to those previously described in response to insulin treatment [315]. In contrast, STAT3-C[POMC]ROSAArte26 mice showed a significantly increased number of low PIP$_3$-immunoreactive POMC neurons accompanied by a significantly decreased number of high PIP$_3$-immunoreactive POMC neurons. This analysis implies that STAT3-C expression inhibits insulin-stimulated PI3K activation in POMC neurons (Figure 25).
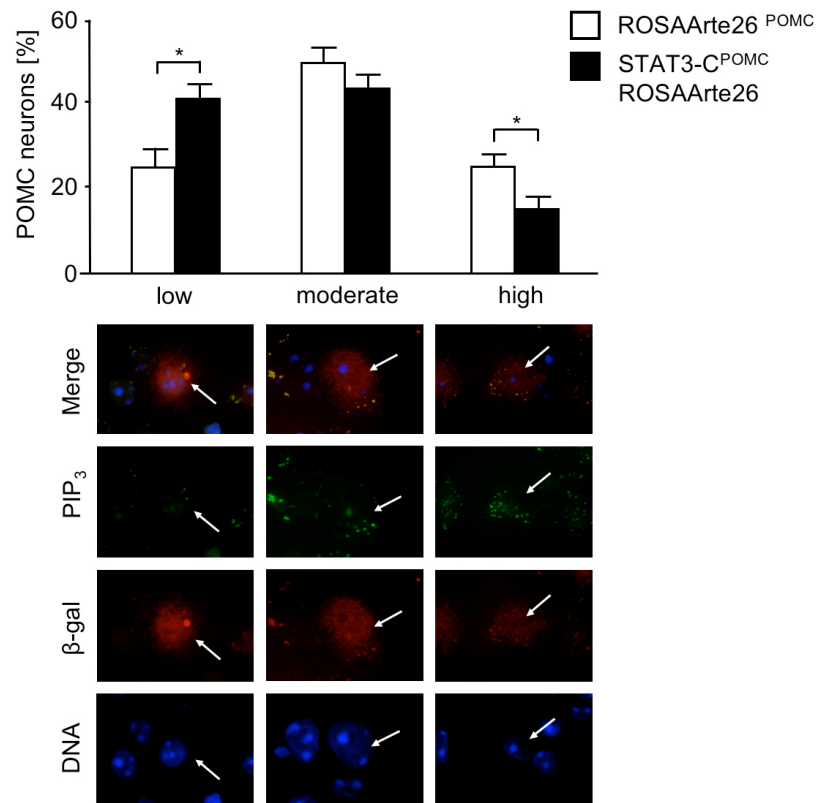
Figure 25: Reduced insulin-induced PIP$_3$ formation in STAT3-C-expressing POMC neurons.
Representative stainings and quantitation of phosphatidylinositol-3,4,5-trisphosphate (PIP$_3$) levels in fasted ROSAArte26^{POMC} and STAT3-C^{POMC}ROSAArte26 mice after intravenous injection of insulin (n = 5 per genotype). A total of 1866 POMC neurons were analysed. PIP$_3$ immunoreactivity was classified in low (less than 5 dots), moderate (5 – 10 dots), and high (more than 10 dots). Blue (DAPI), DNA; red, β-gal (POMC neurons); green, PIP$_3$. Magnification: 630x. Displayed values are means ± SEM. * p ≤ 0.05 versus control.

To confirm this result, hypothalamic insulin signalling of STAT3-C^{POMC} mice was assessed by double immunohistochemistry for phosphorylated protein kinase B (pAKT) and β-galactosidase in fasted and insulin- or saline-injected STAT3-C^{POMC}ROSAArte26 and ROSAArte26^{POMC} mice (3.1.2). While no activation of AKT was detectable in POMC neurons of fasted animals, 23% of POMC neurons of control mice exhibited insulin-stimulated AKT phosphorylation, an effect that was significantly reduced to 10% in STAT3-C-expressing POMC neurons (Figure 26).
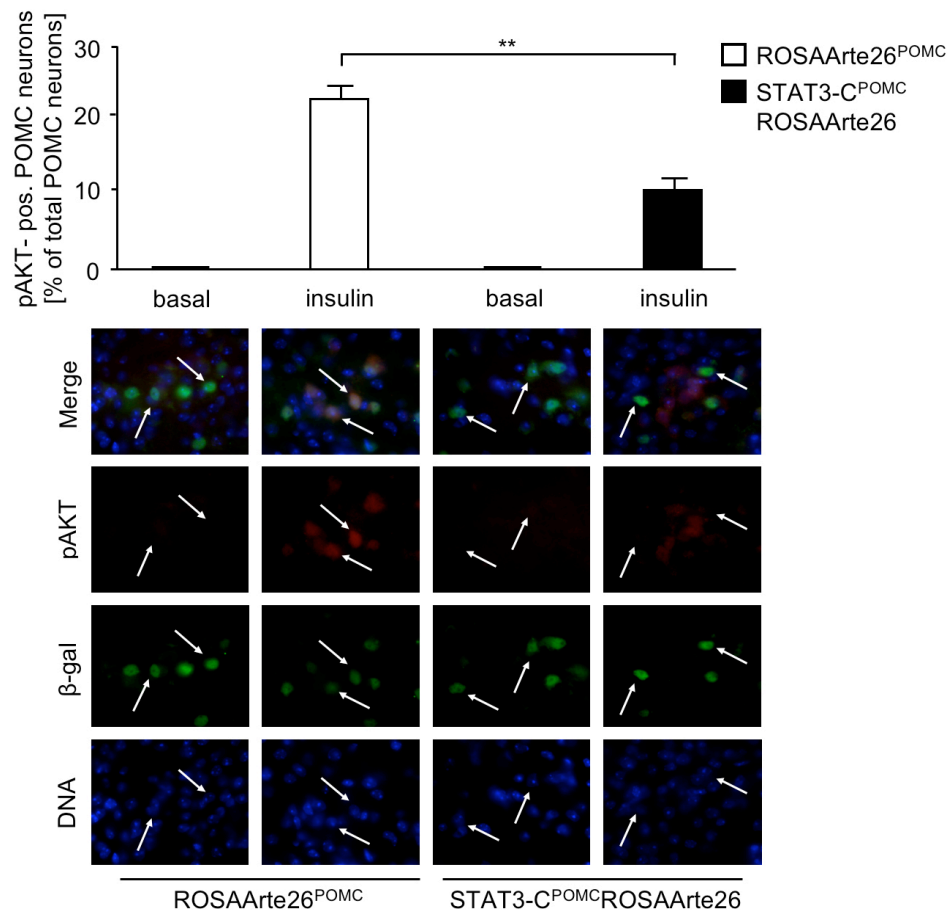
Figure 26: Reduced insulin-induced phosphorylation of AKT in STAT3-C-expressing POMC neurons.
Representative stainings and quantitation of pAKT-positive POMC neurons in hypothalamic sections of fasted ROSAArte26[POMC] and STAT3-C[POMC]ROSAArte26 mice after intravenous injection of insulin or saline at the age of 10 - 14 weeks (n = 5 per genotype). A total of 2351 POMC neurons were analysed. Blue (DAPI), DNA; green, β-gal (POMC neurons); red, pAKT. Magnification: 400x. Displayed values are means ± SEM. ** $p \leq 0.01$ versus control.

Next, control and STAT3-C[POMC] mice were intercrossed with POMC-EGFP reporter mice [62] and perforated patch clamp recordings of eGFP-expressing POMC neurons were performed to analyse their electrophysiological response to insulin. Representative recordings of insulin-responsive and noninsulin-responsive POMC neurons as well as the reversion of insulin's effect by application of the K_{ATP} channel blocker tolbutamide are shown in figure 27. In line with previous experiments, 50% (5 of 10 neurons) of control POMC neurons responded to insulin by hyperpolarisation and silencing, whereas this was significantly reduced to 15% (2 of 13 neurons) in STAT3-C[POMC] mice.

Taken together, these experiments clearly provide evidence that expression of STAT3-C in POMC neurons causes POMC cell-specific insulin resistance in STAT3-C[POMC] mice.

A

control   insulin   tolbutamide

insulin-responsive

0 mV

20 mV

noninsulin-responsive

0 mV

1 s   20 mV

20 min   60 min   75 min

B

■ insulin-responsive
☐ noninsulin-responsive

100

50

0

POMC-EGFP   STAT3-C^{POMC}
                        POMC-EGFP
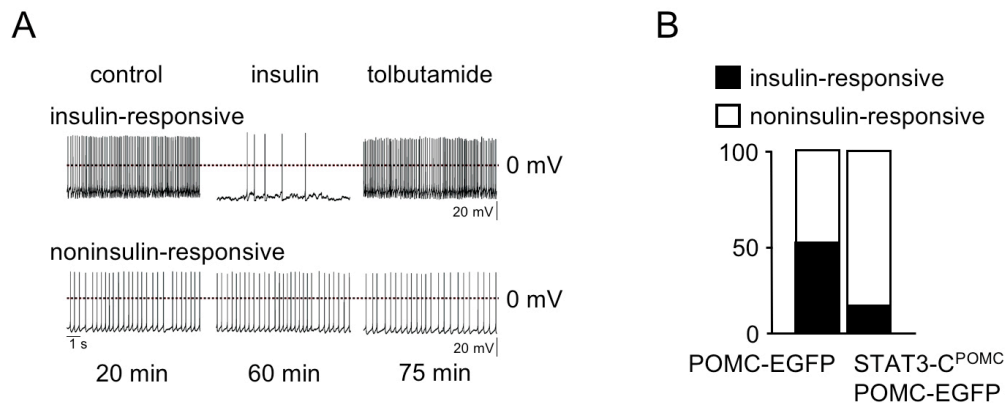
Figure 27: Reduced insulin responsiveness in STAT3-C-expressing POMC neurons.
(A) Representative perforated patch recordings of an insulin-responsive and a noninsulin-responsive POMC-EGFP neuron. The traces represent sections of the recordings before and during bath application of 200 nM insulin (~35 min after application start). In the insulin-responsive neurons bath application of 200 μM tolbutamide reversed the insulin effect. The times below the traces indicate the duration after establishing the recording. **(B)** The percentage of POMC-EGFP (5 of 10) and STAT3-C^{POMC}POMC-EGFP neurons (2 of 13) that responded to bath application of 200 nM insulin with a significant hyperpolarisation. A neuron was determined to be insulin-responsive when the magnitude of hyperpolarisation was greater than 3 times the standard deviation.

3.1.7 Chronic STAT3 signalling in POMC neurons has no effect under leptin-resistant conditions

In order to address whether chronic STAT3 activation affects mice under leptin-resistant conditions, STAT3-C^{POMC}, STAT3-C/C^{POMC}, and control mice were exposed to high fat diet (HFD) upon weaning. However, body weight of STAT3-C^{POMC} and STAT3-C/C^{POMC} mice was indistinguishable from controls under HFD conditions (Figure 28).

Furthermore, STAT3-C^{POMC}, STAT3-C/C^{POMC}, and control mice exhibited similar daily food intake (Figure 29A). Consistently, epigonadal fat pad weight and body fat content were unaltered in STAT3-C^{POMC} and STAT3-C/C^{POMC} mice in comparison to controls (Figure 29B, C).
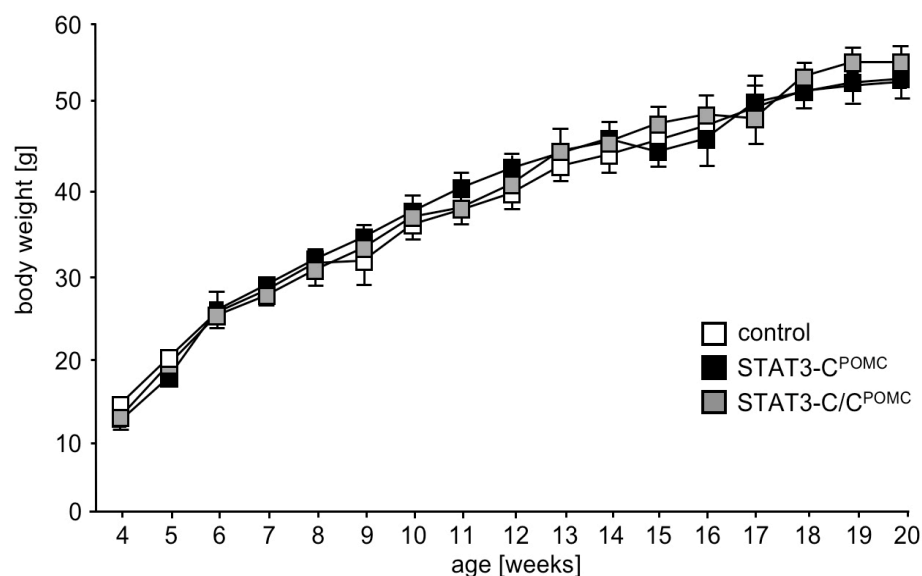
Figure 28: Indistinguishable body weight of control and STAT3-C^POMC mice under HFD conditions.
Average body weight of male control, STAT3-C^POMC, and STAT3-C/C^POMC mice on high fat diet was determined weekly (n = 8 - 14 per genotype).
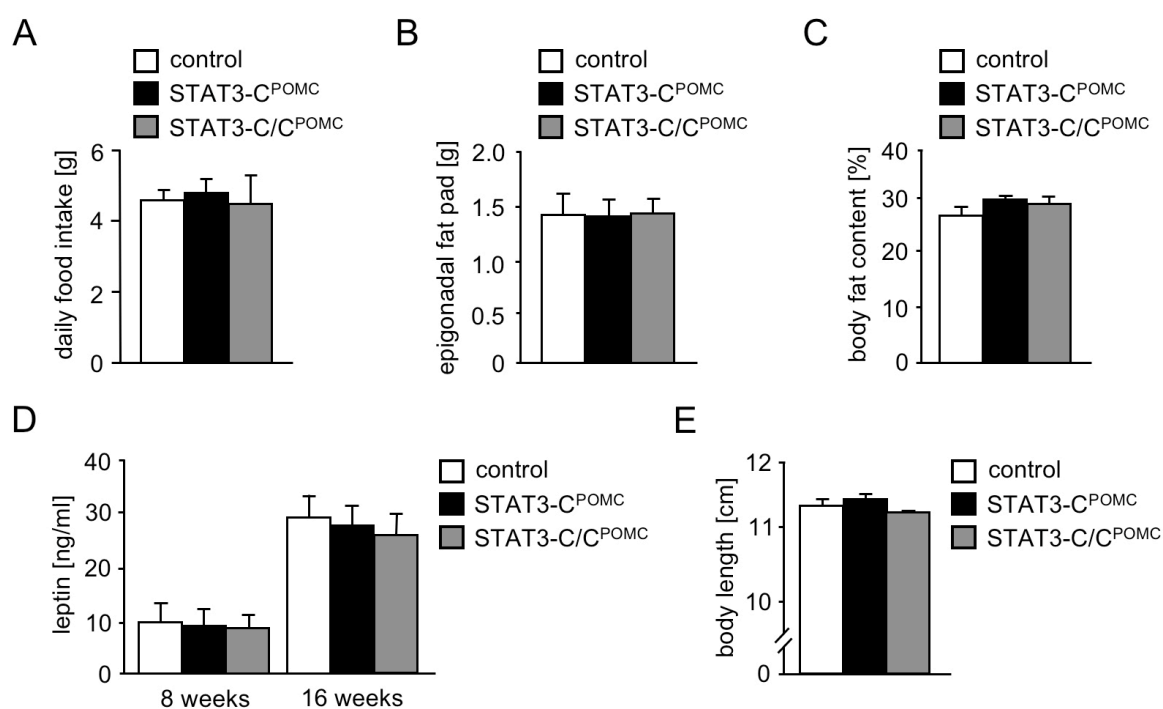
Figure 29: Indistinguishable food intake, body fat content, leptin level, and body length of control and STAT3-C^POMC mice under HFD conditions.
(A) Daily food intake of male control, STAT3-C^POMC, and STAT3-C/C^POMC mice at the age of 10 weeks under high fat diet (HFD) conditions (n = 8 - 14 per genotype). (B) Epigonadal fat pad weight of male control, STAT3-C^POMC, and STAT3-C/C^POMC mice on HFD at the age of 20 weeks (n = 10 - 13 per genotype). (C) Body fat content of male control, STAT3-C^POMC, and STAT3-C/C^POMC mice on HFD at the age of 20 weeks was determined using *in vivo* nuclear magnetic resonance (n = 10 - 13 per genotype). (D) Serum leptin concentrations of male control, STAT3-C^POMC, and STAT3-C/C^POMC mice on HFD at the age of 8 and 16 weeks was determined by ELISA (n = 12 - 16 per genotype). (E) Body length of male control, STAT3-C^POMC, and STAT3-C/C^POMC mice on HFD at the age of 20 weeks (n = 8 - 13 per genotype).

In addition, serum leptin levels were significantly increased under HFD conditions compared to mice exposed to normal chow diet (NCD), but remained unchanged in STAT3-C^{POMC} and STAT3-C/C^{POMC} mice compared to controls, both at 8 and 16 weeks of age (Figure 29D). Moreover, no differences in body length were observed between STAT3-C^{POMC}, STAT3-C/C^{POMC}, and control mice (Figure 29E).

To analyse the impact of HFD feeding on hypothalamic SOCS3 and POMC expression, quantitative RT-PCR was performed using total mRNA isolated from hypothalami of control, STAT3-C^{POMC}, and STAT3-C/C^{POMC} mice exposed to NCD and HFD. This analysis revealed significantly increased mRNA expression of SOCS3 in control mice under HFD conditions compared to NCD fed controls, but HFD feeding attenuated the effect of STAT3-C on hypothalamic SOCS3 expression. Similarly, POMC expression was consistently reduced in all groups of mice when exposed to HFD to an extent similar to that observed in mice expressing STAT3-C in POMC neurons under NCD conditions (Figure 30).
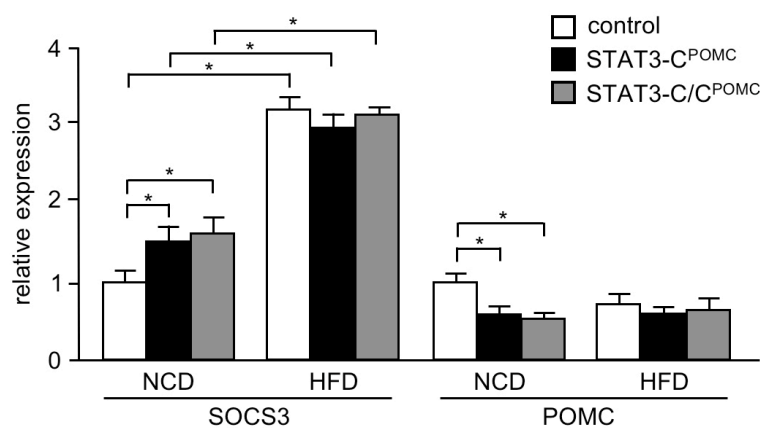
Figure 30: Hypothalamic expression of SOCS3 and POMC in STAT3-C^{POMC} mice under HFD conditions. Relative hypothalamic expression of suppressor of cytokine signalling (SOCS) 3 and proopiomelanocortin (POMC) of male control, STAT3-C^{POMC}, and STAT3-C/C^{POMC} mice under normal chow diet (NCD) (n = 12 per genotype) and high fat diet (HFD) (n = 4 per genotype) condition at the age of 20 weeks using quantitative RT-PCR. Displayed values are means ± SEM. * p ≤ 0.05 versus control.

To investigate whether elevated leptin levels in obesity translates into enhanced basal STAT3 activation in the ARC of control mice, EMSA of random fed C57BL/6 mice on NCD and HFD was performed (Figure 31A). Strikingly, HFD feeding-induced obesity led to significantly enhanced basal STAT3-binding to its consensus sequence in the ARC compared to NCD feeding, similarly as observed in STAT3-C^{POMC} mice (Figure 31B).
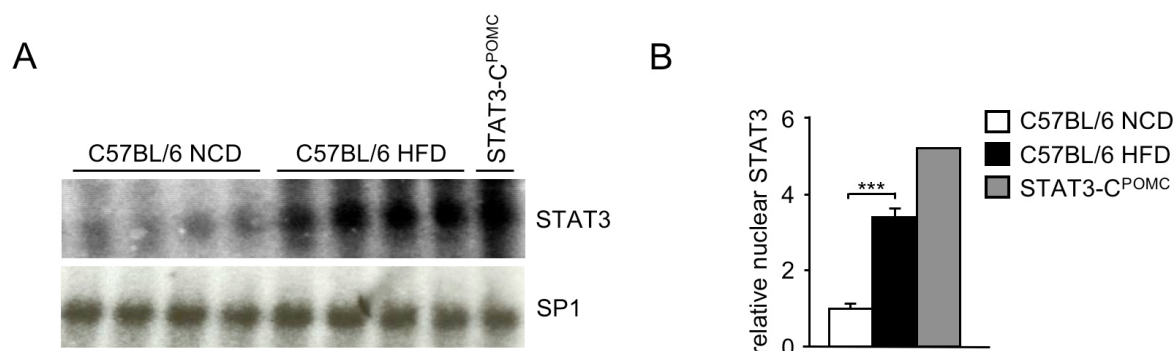
Figure 31: Increase of nuclear STAT3 under HFD condition in C57BL/6 mice.
(A) EMSA of nuclear extracts isolated from arcuate nuclei of 4 individual C57BL/6 mice exposed to normal chow diet (NCD) and high fat diet (HFD) and from one STAT3-C^{POMC} mouse on NCD using radioactively labelled STAT3 and specific protein 1 (SP1, loading control) probes, respectively. **(B)** Densitometrical analysis of nuclear STAT3 in ARC of 4 individual C57BL/6 mice exposed to NCD and HFD and from one STAT3-C^{POMC} mouse on NCD. Displayed values are means ± SEM. *** $p \leq 0.001$ versus control.

These experiments clearly demonstrate that chronic activation of STAT3 signalling in POMC neurons has no additional effect on body weight, body fat content, serum leptin concentration, body length, and hypothalamic gene expression under conditions of hyperleptinemia induced by HFD feeding. Therefore, these results indicate that during the course of HFD-induced central leptin and insulin resistance, STAT3 overactivation in POMC neurons is a pathophysiologically relevant component.

3.2 POMC neuron-specific expression of a dominant negative variant of FOXO1 partially attenuates mild obesity of STAT3-C^{POMC} mice

Not only STAT3, but also the transcription factor FOXO1 is known to regulate POMC expression. FOXO1, which is negatively regulated by insulin signalling and STAT3 have overlapping binding sites within the *pomc* promoter, thus leading to a competition of binding. In contrast to STAT3, FOXO1 acts as transcriptional repressor of POMC [73, 152]. To further elucidate the role of FOXO1 in this context, a Cre-inducible FOXO1DN mouse strain was generated and intercrossed with STAT3-C^{POMC} mice. FOXO1DN is a C-terminal truncated variant of FOXO1 that blocks binding of endogenous FOXO1 and presumably other FOXO proteins by occupying the consensus sequence of the DNA without dependence on insulin or other growth factor signals.

3.2.1 Generation of a Cre-inducible FOXO1DN mouse strain

To analyse the role of FOXO1 in the regulation of energy homeostasis, a transgenic mouse strain containing a Cre-inducible FOXO1DN construct in the *ROSA26* locus preceded by a transcriptional stop cassette was generated. For this a targeting vector was designed that contains homology arms to the *ROSA26* locus and the *CAGGS* promoter followed by the *lox*P-flanked WSS stop cassette. Subsequently, the FOXO1DN cDNA was inserted upstream of the IRES eGFP cassette (Figure 32A). Afterwards, the FOXO1DN ROSA26 targeting vector was electroporated into V6.5 ES cells and selected with G418. 10 days after electroporation 96 ES cell clones were isolated as single clones and subjected to Southern blot analysis. Homologous recombinant ES cell clones were identified by Southern blot analysis using an external ROSA26 probe and an internal Neo probe (Figure 32B, C). Southern blot analysis of *Eco*RI digested genomic DNA using the ROSA26 probe resulted in a 7.1 kb targeted band besides the 16 kb wild-type band (Figure 32D). To demonstrate single integration of the construct, Southern blot analysis of *Nsi*I digested genomic DNA and usage of the Neo probe resulted in a single 17.7 kb band (Figure 32E).
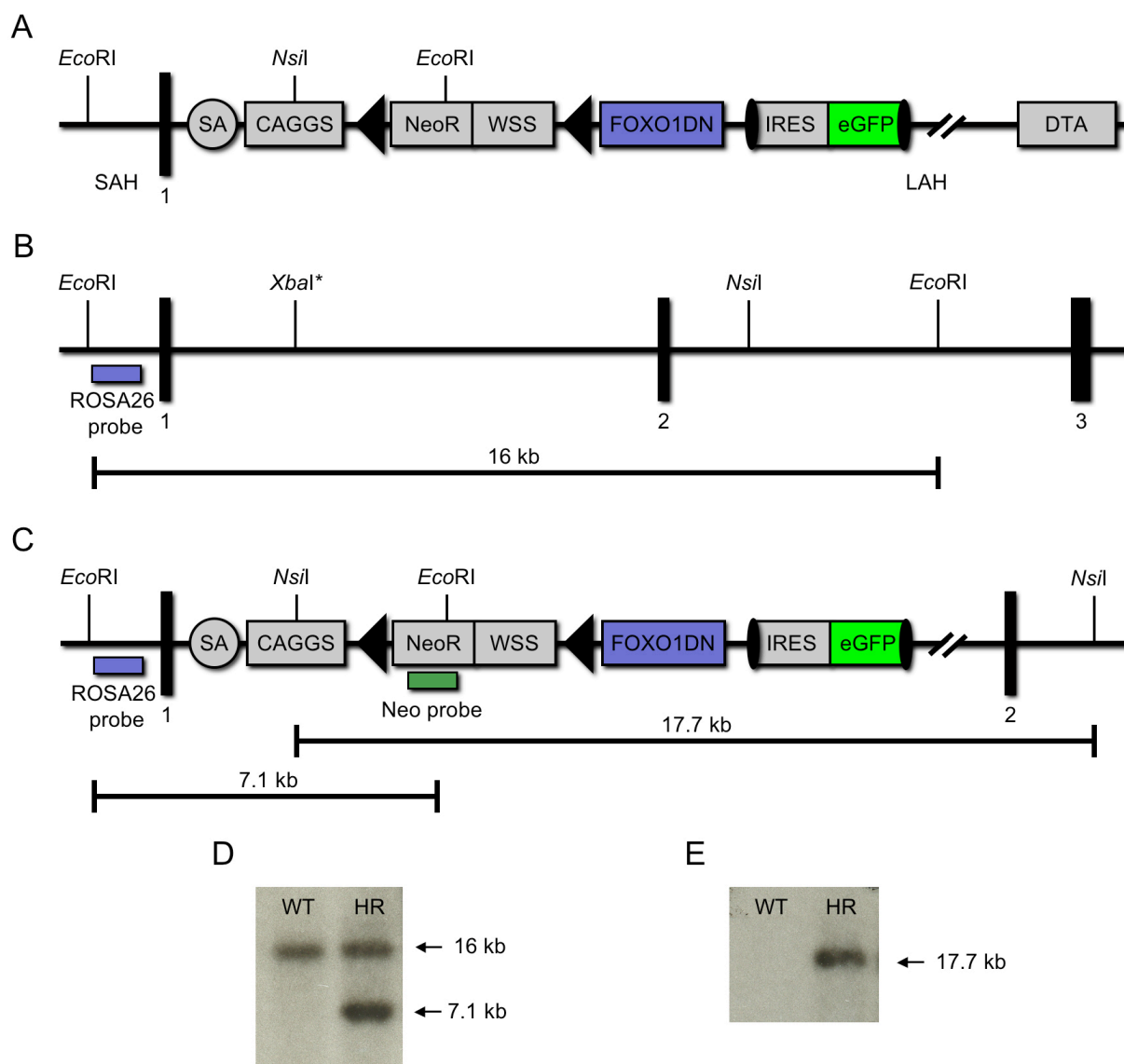
Figure 32: Targeting of FOXO1DN into the *ROSA26* locus.
(A) Scheme of the FOXO1DN ROSA26 targeting vector with *Eco*RI and *Nsi*I restriction sites. **(B)** Scheme of the *ROSA26* genomic locus with *Eco*RI, *Nsi*I and *Xba*I restriction sites. **(C)** Scheme of the *ROSA26* genomic locus after homologous recombination with *Eco*RI and *Nsi*I restriction sites. **(D)** Southern blot analysis of *Eco*RI digested genomic DNA with external probe ROSA26 resulted in a 7.1 kb targeted band besides the 16 kb wild-type band. **(E)** Southern blot analysis of *Nsi*I digested genomic DNA with probe Neo resulted in a 17.7 kb band indicating single integration of the construct. CAGGS, *chicken β actin* promoter with upstream *CMV* enhancer; DTA, *diphtheria toxin A* gene driven by *pGK* promoter; eGFP, enhanced *green fluorescent protein* gene; FOXO1DN, dominant negative mutant of forkhead box-containing protein class O 1; HR, homologous recombinant; IRES, internal ribosome entry site; LAH, 4.2 kb long arm of homology; NeoR, *neomycine resistance* gene driven by *TK* promoter; SA, adenoviral splice acceptor; SAH, 1.0 kb short arm of homology; WSS, Westphal stop sequence; WT, wild-type; filled triangles, *lox*P; filled rectangles, exons; closed ellipses, FRT sites.

Finally, four ES cell clones were identified as homologous recombinants and injected into CB20 blastocysts. Chimeric mice from clone G6, G12, and H11 were unable to transmit the transgene germline, while the chimeras of clone G9 transmitted the transgene to their

offspring. To test the FOXO1DN construct *in vivo,* FOXO1DN$^{floxstop/+}$ mice were intercrossed with both C57BL/6 and FOXO1DN$^{floxstop/+}$ mice.

3.2.2 Verification of the dominant negative FOXO1 construct in MEFs

To functionally validate the FOXO1DN construct *in vitro*, MEFs were isolated from FOXO1DN$^{floxstop/+}$ and FOXO1DN$^{floxstop/floxstop}$ embryos. Subsequently, these MEFs were treated with His-TAT-NLS-Cre (HTNC) to cause Cre-mediated recombination of the *lox*P-flanked stop cassette leading to composed expression of the *foxo1dn* transgene and eGFP (Figure 33).
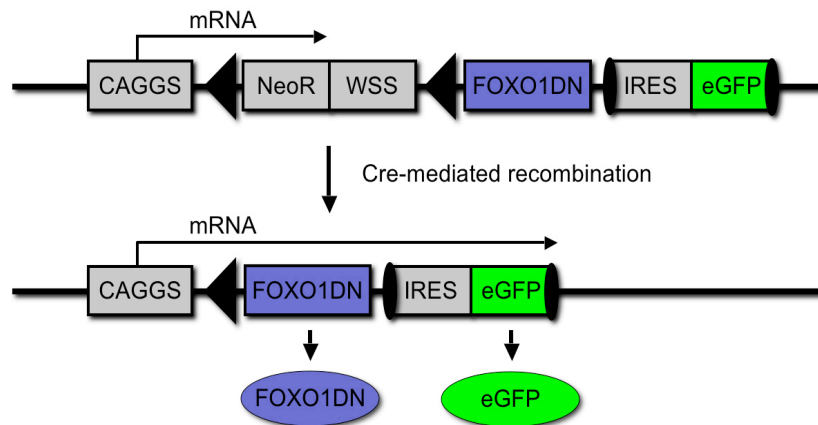
Figure 33: Cre-mediated expression of the dominant negative *foxo1* transgene.
Scheme of the *foxo1dn* transgene inserted into the *ROSA26* locus. Cre-mediated recombination eliminates the *lox*P-flanked NeoR and WSS only in cells expressing Cre and thereby allowing transcription of the bicistronic FOXO1DN eGFP mRNA. CAGGS, *chicken β actin* promoter with upstream *CMV* enhancer; IRES, internal ribosome entry site; eGFP, enhanced *green fluorescent protein* gene; FOXO1DN, dominant negative mutant of forkhead box-containing protein class O 1; NeoR, *neomycine resistance* gene driven by the *TK* promoter; WSS, Westphal stop sequence; filled triangles, *lox*P; closed ellipses, FRT sites.

To verify Cre-mediated recombination with accompanied eGFP expression, FOXO1DN$^{floxstop/floxstop}$ (control) and HTNC-treated FOXO1DN$^{floxstop/+}$ (FOXO1DN/+) and FOXO1DN$^{floxstop/floxstop}$ (FOXO1DN/DN) MEFs were analysed by fluorescence microscopy. eGFP-positive MEFs were detectable only after Cre-mediated recombination by HTNC-treatment. As expected, eGFP expression from two alleles in FOXO1DN/DN MEFs was more intense than in FOXO1DN/+ MEFs (Figure 34A). FACS analysis revealed that 0% of control, 94% of FOXO1DN/+, and 98% of FOXO1DN/DN MEFs expressed eGFP (Figure 34B).
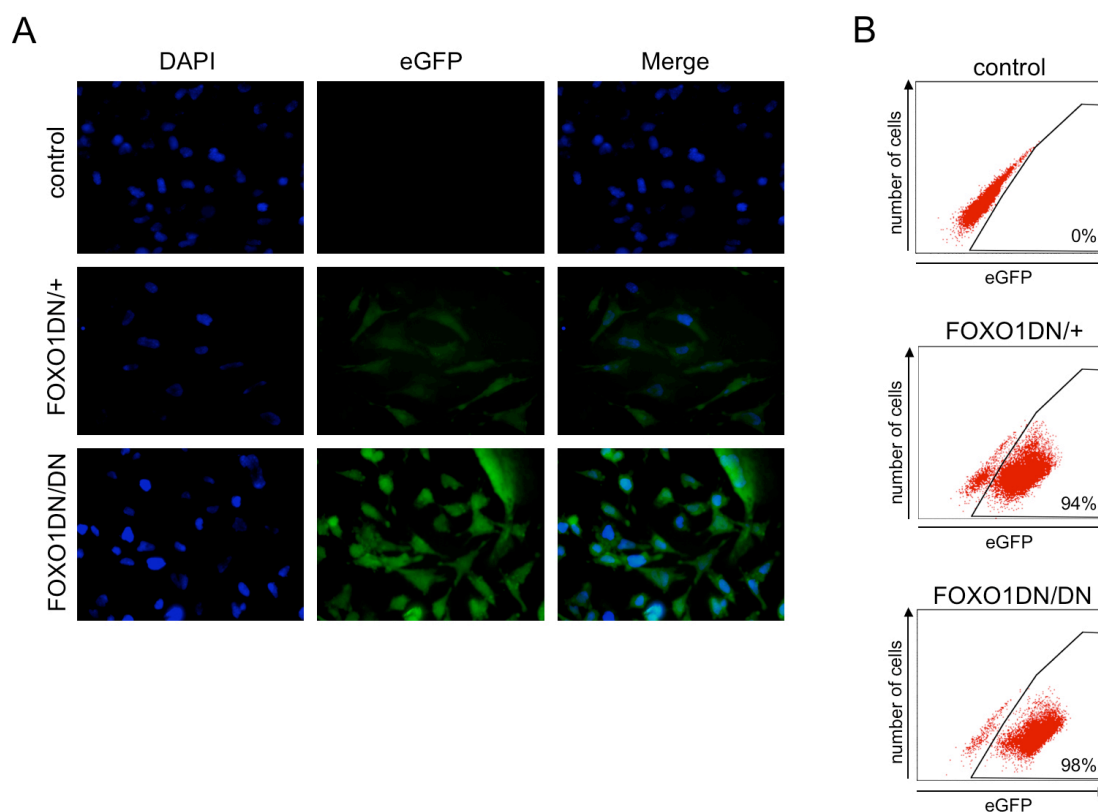
Figure 34: Verification of Cre-mediated recombination in FOXO1DN MEFs.
(A) Fluorescence microscopy of control, FOXO1DN/+-, and FOXO1DN/DN-expressing MEFs. Blue (DAPI), DNA; green, eGFP. Magnification: 200x. **(B)** FACS analysis of control, FOXO1DN/+-, and FOXO1DN/DN-expressing MEFs.

Western blot analysis indicated expression of FOXO1DN in MEFs after Cre-mediated recombination. Due to the fact that FOXO1DN is a truncated variant of FOXO1, they can be easily discriminated by size (Figure 35A). Since FOXO1DN contains a DBD, but lacks TAD including residues essential for nuclear export, FOXO1DN binds permanently to recognition sequences without transcriptional activity [279]. Consistently, endogenous FOXO1 translocated from the nucleus to the cytoplasm upon stimulation with insulin, while FOXO1DN localisation was not affected by insulin stimulation (Figure 35B, C).
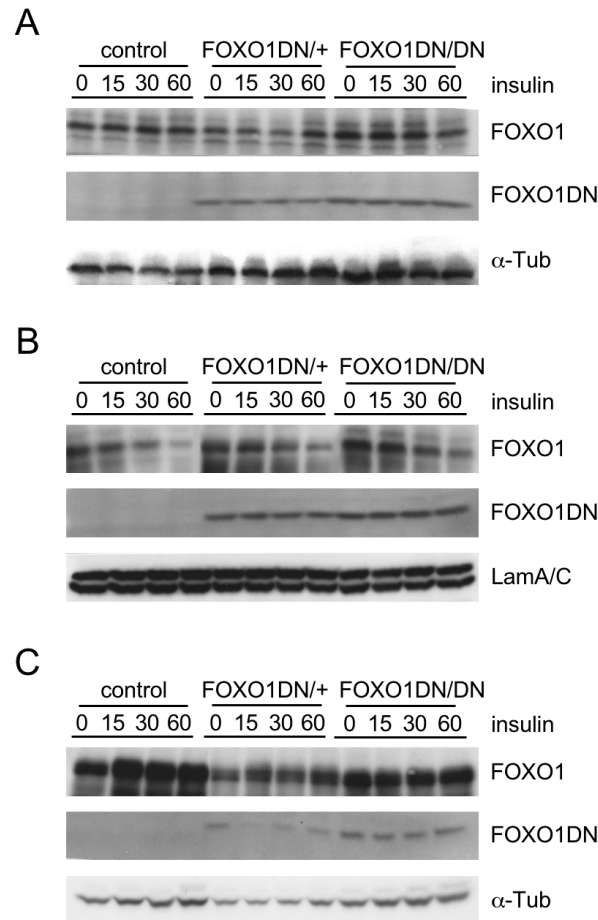
Figure 35: Functional validation of the dominant negative FOXO1 construct in MEFs.
(A) Western blot analysis using FOXO1 and α-Tubulin (α-Tub, loading control) antibodies of whole cell lysates from control, FOXO1DN/+-, and FOXO1DN/DN-expressing MEFs stimulated with insulin for the indicated timepoints. **(B)** Western blot analysis using FOXO1 and LaminA/C (LamA/C, loading control) antibodies of nuclear lysates from control, FOXO1DN/+-, and FOXO1DN/DN-expressing MEFs stimulated with insulin for the indicated timepoints. **(C)** Western blot analysis using FOXO1 and α-Tub (loading control) antibodies of cytoplasmic lysates from control, FOXO1DN/+-, and FOXO1DN/DN-expressing MEFs stimulated with insulin for the indicated timepoints.

To further validate FOXO1DN function, the DNA-binding capacity was assessed by EMSA using nuclear extracts from control, FOXO1DN/+, and FOXO1DN/DN MEFs. Insulin stimulation decreased the binding capacity of FOXO1, in contrast to the persistent binding of FOXO1DN to its consensus DNA sequence. The specificity of FOXO1- and FOXO1DN-binding was addressed by supershift using antibodies recognising FOXO1 and FOXO1DN, respectively (Figure 36).

Taken together, Cre-mediated expression of the FOXO1DN transgene in MEFs leads to constitutive nuclear localisation of FOXO1DN and target gene promoter occupancy independent of insulin stimulation.
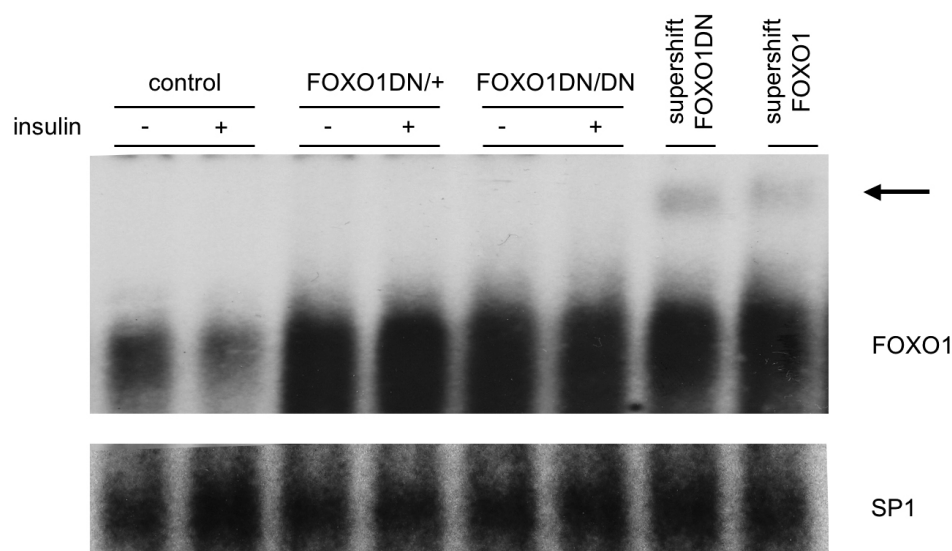
Figure 36: FOXO1 DNA-binding capacity of FOXO1DN in MEFs.
EMSA of nuclear extracts isolated from control, FOXO1DN/+-, and FOXO1DN/DN-expressing MEFs upon 2 h insulin stimulation using a radioactively labelled consensus sequence for FOXO1 and specific protein 1 (SP1, loading control), respectively. For supershift, two FOXO1 antibodies were used for detecting either FOXO1 or FOXO1DN. Arrow indicates supershift of FOXO1 or FOXO1DN.

3.2.3 POMC neuron-specific FOXO1DN expression partially attenuates mild obesity of STAT3-C^{POMC} mice

In order to analyse whether expression of FOXO1DN can rescue the mild obesity observed in STAT3-C^{POMC} mice, FOXO1DN$^{floxstop/+}$ mice were intercrossed with STAT3-C/C^{POMC} mice (3.1.2) to obtain STAT3-C^{floxstop}/FOXO1DN^{floxstop}POMC-Cre (STAT3-C/FOXO1DN^{POMC}) mice expressing STAT3-C and FOXO1DN selectively in POMC neurons, while Cre-negative mice of this breeding served as controls (Figure 37).
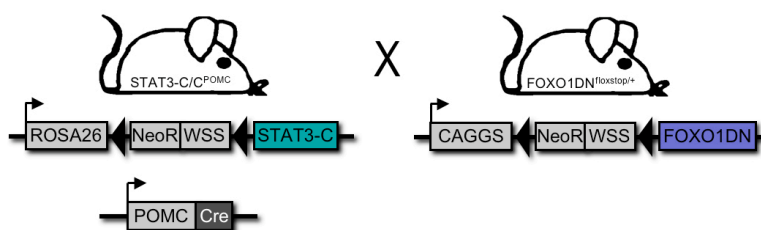
Figure 37: POMC neuron-restricted expression of STAT3-C and FOXO1DN.
STAT3-C/C^{POMC} mice were intercrossed with FOXO1DN$^{floxstop/+}$ mice to obtain STAT3-C/FOXO1DN^{POMC} mice expressing STAT3-C and FOXO1DN selectively in POMC neurons.

To confirm Cre-mediated recombination and FOXO1DN expression in POMC neurons of STAT3-C/FOXO1DN^{POMC} mice, ARC protein lysates of control, STAT3-C^{POMC}, and STAT3-C/FOXO1DN^{POMC} mice were analysed by Western blot. FOXO1DN was only

detected in STAT3-C/FOXO1DN^{POMC} mice, but not in control and in STAT3-C^{POMC} mice (Figure 38).
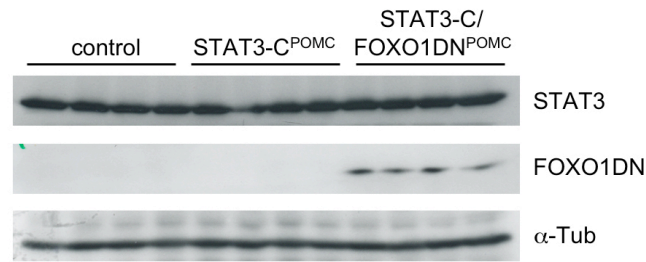
Figure 38: Verification of Cre-mediated expression of FOXO1DN in STAT3-C/FOXO1DN^{POMC} mice.
Western blot analysis of ARC extracts from control, STAT3-C^{POMC}, and STAT3-C/FOXO1DN^{POMC} mice using antibodies against STAT3, FOXO1DN, and α-Tubulin (α-Tub, loading control).

To determine the impact of FOXO1DN signalling on the regulation of energy homeostasis, body weight of male control, STAT3-C^{POMC}, and STAT3-C/FOXO1DN^{POMC} mice was monitored from weaning until 16 weeks of age (Figure 39). As demonstrated in paragraph 3.1.3, STAT3-C^{POMC} mice exhibit a significantly increased body weight compared to controls. However, STAT3-C/FOXO1DN^{POMC} mice exhibited an up to 6%, but not significantly reduced body weight compared to STAT3-C^{POMC} mice, while body weight of STAT3-C/FOXO1DN^{POMC} was significantly increased compared to control mice (Figure 39).
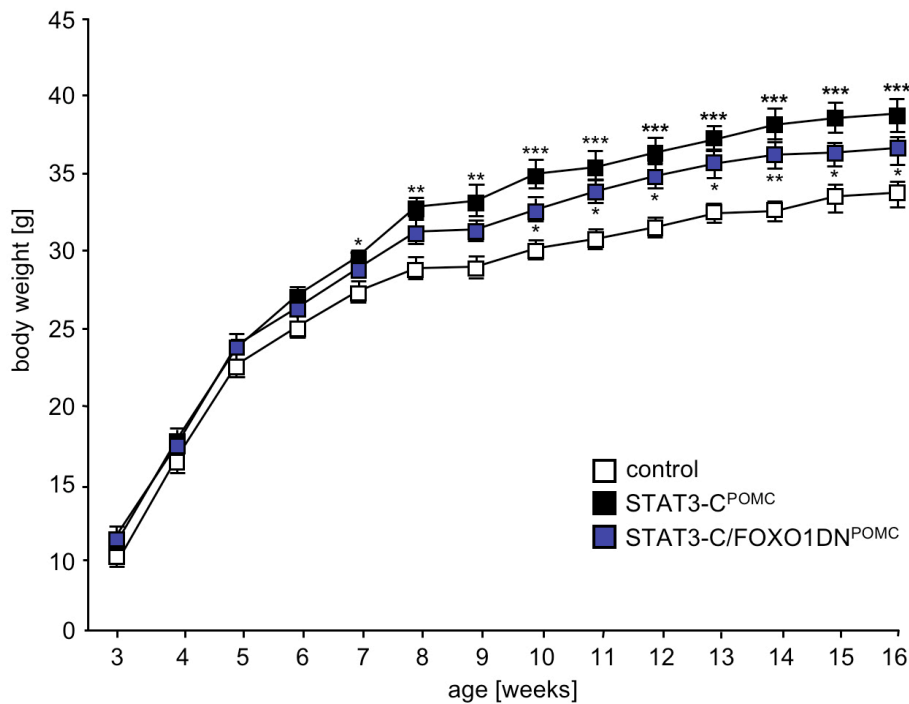
Figure 39: FOXO1DN expression decreased body weight of STAT3-C^{POMC} mice.
Average body weight of male control, STAT3-C^{POMC}, and STAT3-C/FOXO1DN^{POMC} mice was determined weekly (n = 18 - 21 per genotype). Displayed values are means ± SEM. * $p \leq 0.05$, ** $p \leq 0.01$, and *** $p \leq 0.001$ versus control.

To examine whether the partially diminished mild obesity in STAT3-C/FOXO1DN^{POMC} mice is accompanied by reduced body fat mass, the amount of epigonadal fat in male control, STAT3-C^{POMC}, and STAT3-C/FOXO1DN^{POMC} mice was analysed. Consistently, STAT3-C/FOXO1DN^{POMC} mice exhibited a reduced epigonadal fat pad mass at the age of 18 weeks compared to STAT3-C^{POMC} mice, while in comparison to controls it was still increased (Figure 40A). Furthermore, *in vivo* magnetic resonance spectrometry analysis confirmed the reduced adiposity in STAT3-C/FOXO1DN^{POMC} mice (Figure 40B). Moreover, the significantly increased body length observed in STAT3-C^{POMC} mice was partly rescued by POMC cell-specific expression of FOXO1DN (Figure 40C).
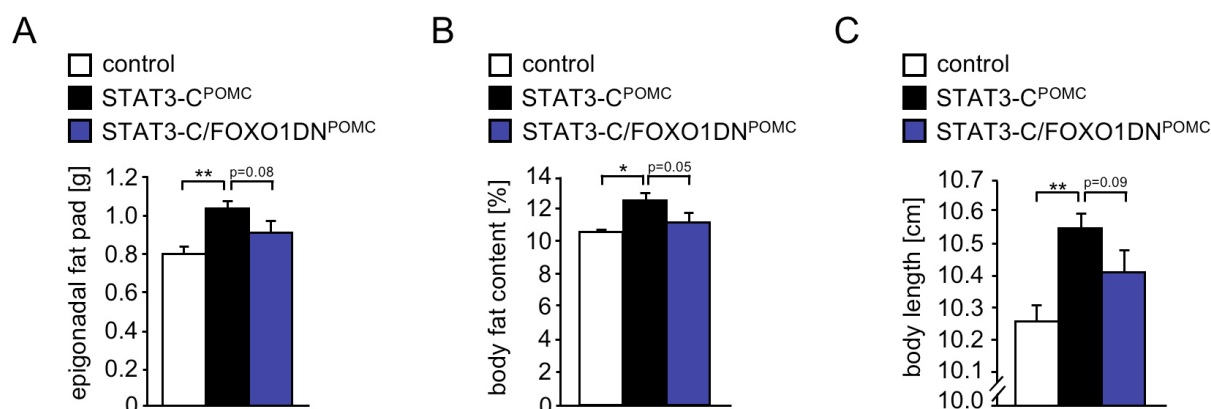
Figure 40: FOXO1DN expression decreased body fat content and body length of STAT3-C^{POMC} mice.
(A) Epigonadal fat pad weight of male control, STAT3-C^{POMC}, and STAT3-C/FOXO1DN^{POMC} mice at the age of 18 weeks (n = 18 - 21 per genotype). **(B)** Body fat content of male control, STAT3-C^{POMC}, and STAT3-C/FOXO1DN^{POMC} mice at the age of 18 weeks was determined using *in vivo* nuclear magnetic resonance (n = 18 - 21 per genotype). **(C)** Body length of male control, STAT3-C^{POMC}, and STAT3-C/FOXO1DN^{POMC} mice at the age of 18 weeks (n = 18 - 21 per genotype). Displayed values are means ± SEM. * $p \leq 0.05$ and ** $p \leq 0.01$ versus control.

To investigate whether POMC cell-specific expression of FOXO1DN in STAT3-C^{POMC} mice also normalises POMC, quantitative RT-PCR was performed using total mRNA isolated from ARC of control, STAT3-C^{POMC}, and STAT3-C/FOXO1DN^{POMC} mice. This analysis revealed slightly elevated POMC mRNA levels in STAT3-C/FOXO1DN^{POMC} mice compared to STAT3-C^{POMC} mice, however, POMC mRNA was still decreased compared to control mice (Figure 41).
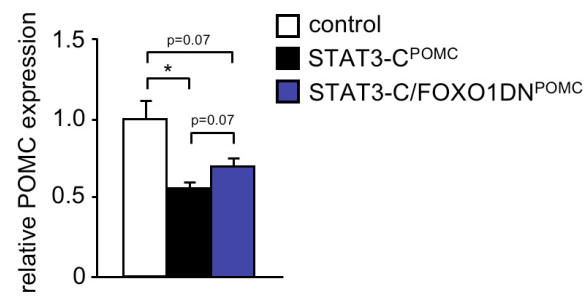
Figure 41: Hypothalamic expression of POMC in STAT3-C/FOXO1DN^POMC mice.
Relative hypothalamic expression of proopiomelanocortin (POMC) of male control, STAT3-C^POMC, and STAT3-C/C^POMC mice at the age of 18 weeks (n = 14 - 15 per genotype) using quantitative RT-PCR. Displayed values are means ± SEM. * $p \leq 0.05$ versus control.

Taken together, these results reveal that dominant inhibition of FOXO1 in POMC-expressing neurons of STAT3-C^POMC mice ameliorates the mild obesity caused by enhanced activation of STAT3 in these neurons.

3.3 Constitutive FOXO1 activation in the central nervous system causes postnatal lethality induced by neuronal apoptosis

FOXO proteins are involved in a variety of cellular processes such as differentiation, cell cycle, detoxification, and survival [328]. To investigate the impact of persistent FOXO1 activation, a mouse strain expressing a Cre-inducible constitutively active version of FOXO1 (FOXO1ADA) was generated. Since the three AKT/SGK phosphorylation sites of FOXO1 were exchanged by site-directed mutagenesis to nonphosphorylatable amino acids (T24A, S256D, S319A), FOXO1ADA acts as a constitutive activator of transcription independent of insulin signalling.

3.3.1 Generation of a Cre-inducible FOXO1ADA mouse strain

To analyse the role of FOXO1 in metabolism, a transgenic mouse strain containing a Cre-inducible FOXO1ADA construct in the *ROSA26* locus preceded by a transcriptional stop cassette was generated. To this end, a targeting vector was designed that contains homology arms to the *ROSA26* locus and the *CAGGS* promoter followed by the *lox*P-flanked WSS stop cassette. Subsequently, the FOXO1ADA cDNA was inserted upstream of the IRES eGFP cassette (Figure 42A). Afterwards, the FOXO1ADA ROSA26 targeting vector was electroporated into V6.5 ES cells and selected with G418. 10 days after electroporation 96 ES cell clones were isolated as single clones and subjected to Southern blot analysis. Homologous recombinant ES cell clones were identified by Southern blot analysis using an external ROSA26 probe and an internal Neo probe (Figure 42B, C). Southern blot analysis of *Eco*RI digested genomic DNA using the ROSA26 probe resulted in a 7.1 kb targeted band besides the 16 kb wild-type band (Figure 42D). To demonstrate the single integration of the construct, Southern blot analysis of *Nsi*I digested genomic DNA and usage of the Neo probe resulted in a single 17.7 kb band (Figure 42E).

Ultimately, 33 of 96 ES cell clones were identified as homologous recombinants, while 8 positive FOXO1ADA clones were injected into CB20 blastocysts. Chimeric mice of clones D3 and D9 resulted in germline transmission of the FOXO1ADA construct. To test the FOXO1ADA construct *in vivo,* FOXO1ADA$^{floxstop/+}$ mice were intercrossed with both C57BL/6 and FOXO1ADA$^{floxstop/+}$ mice.
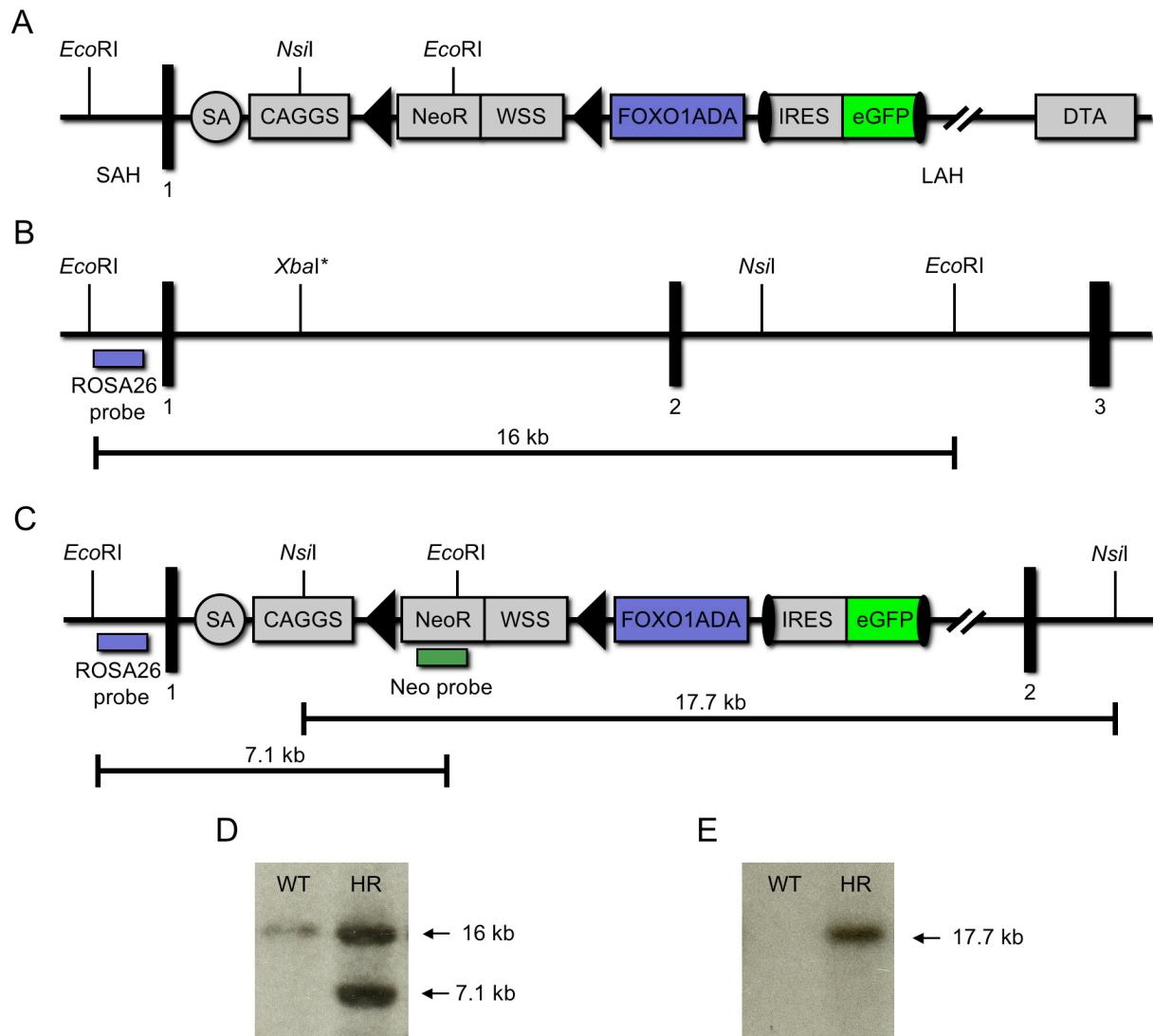
Figure 42: Targeting of FOXO1ADA into the *ROSA26* locus.
(A) Scheme of the FOXO1ADA ROSA26 targeting vector with *Eco*RI and *Nsi*I restriction sites. **(B)** Scheme of the *ROSA26* genomic locus with *Eco*RI, *Nsi*I and *Xba*I restriction sites. **(C)** Scheme of the *ROSA26* genomic locus after homologous recombination with *Eco*RI and *Nsi*I restriction sites. **(D)** Southern blot analysis of *Eco*RI digested genomic DNA with external probe ROSA26 resulted in a 7.1 kb targeted band besides the 16 kb wild-type band. **(E)** Southern blot analysis of *Nsi*I digested genomic DNA with probe Neo resulted in a 17.7 kb band indicating single integration of the construct. CAGGS, *chicken β actin* promoter with upstream *CMV* enhancer; DTA, *diphtheria toxin A* gene driven by *pGK* promoter; eGFP, enhanced *green fluorescent protein* gene; FOXO1ADA, constitutively active mutant of forkhead box-containing protein class O 1; HR, homologous recombinant; IRES, internal ribosome entry site; LAH, 4.2 kb long arm of homology; NeoR, *neomycine resistance* gene driven by *TK* promoter; SA, adenoviral splice acceptor; SAH, 1.0 kb short arm of homology; WSS, Westphal stop sequence; WT, wild-type; filled triangles, *lox*P; filled rectangles, exons; closed ellipses, FRT sites.

3.3.2 Verification of the constitutively active FOXO1 construct in MEFs

To test constitutive activation of FOXO1ADA, MEFs were isolated from FOXO1ADA^floxstop/+ and FOXO1ADA^floxstop/floxstop embryos. These MEFs were incubated with HTNC leading to Cre-mediated recombination of the *lox*P-flanked stop cassette, thus resulting in the composed expression of the *foxo1ada* transgene and eGFP (Figure 43).
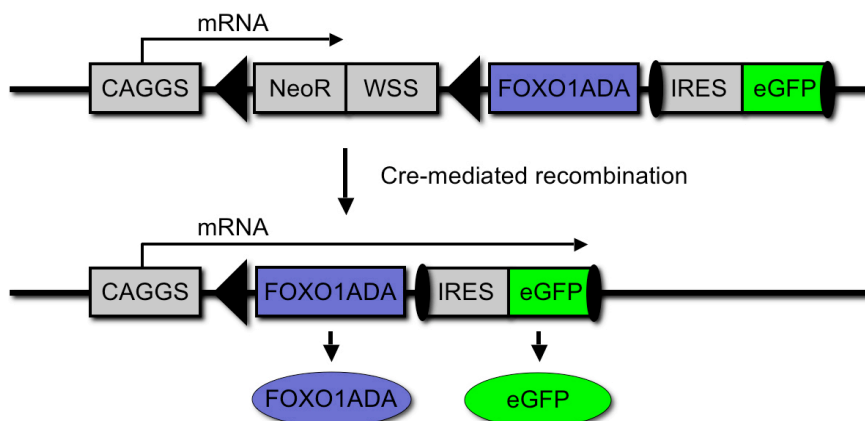
Figure 43: Cre-mediated expression of a constitutively active *foxo1* transgene.
Scheme of the *foxo1ada* transgene inserted into the *ROSA26* locus. Cre-mediated recombination eliminates the *lox*P-flanked NeoR and WSS only in cells expressing Cre and thereby allowing transcription of the bicistronic FOXO1ADA eGFP mRNA. CAGGS, *chicken β actin* promoter with upstream *CMV* enhancer; IRES, internal ribosome entry site; eGFP, enhanced *green fluorescent protein* gene; FOXO1ADA, constitutively active mutant of forkhead box-containing protein class O 1; NeoR, *neomycine resistance* gene driven by the *TK* promoter; WSS, Westphal stop sequence; filled triangles, *lox*P; closed ellipses, FRT sites.

The Cre-mediated recombination efficiency was assessed by FACS analysis of FOXO1ADA$^{\text{floxstop/floxstop}}$ (control) and HTNC-treated FOXO1ADA$^{\text{floxstop/+}}$ (FOXO1ADA/+) and FOXO1ADA$^{\text{floxstop/floxstop}}$ (FOXO1ADA/ADA) MEFs. While 50% of FOXO1ADA/+ and 52% of FOXO1ADA/ADA MEFs expressed eGFP, 0% of control MEFs were identified as eGFP-positive (Figure 44).
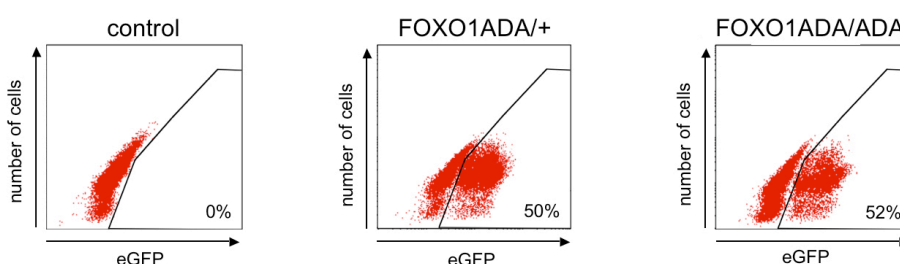
Figure 44: Verification of Cre-mediated recombination in FOXO1ADA MEFs.
FACS analysis of control, FOXO1ADA/+-, and FOXO1ADA/ADA-expressing MEFs.

Furthermore, expression of FOXO1ADA in MEFs upon Cre-mediated recombination was confirmed by Western blot analysis. This experiment revealed increased total FOXO1 protein levels in FOXO1ADA/+ and FOXO1ADA/ADA MEFs compared to controls, while FOXO1ADA expression from two alleles in FOXOADA/ADA MEFs was clearly enhanced in comparison to FOXO1ADA expression from one allele in FOXO1ADA/+ MEFs (Figure 45). As a result of the substitution of the AKT/SGK phosphorylation sites to nonphosphorylatable amino acids (T24A, S256D, S319A) in FOXO1ADA, insulin-stimulated

phosphorylation of FOXO1ADA is expected to be blocked [280]. Consistently, the increase of insulin-stimulated Ser[256] phosphorylation of FOXO1 in FOXO1ADA/+ and FOXO1ADA/ADA MEFs was comparable to control MEFs (Figure 45).

In summary, Cre-mediated recombination of the *lox*P-flanked stop cassette leads to the expression of the *foxo1ada* transgene in MEFs and insulin stimulation failed to phosphorylate FOXO1ADA.
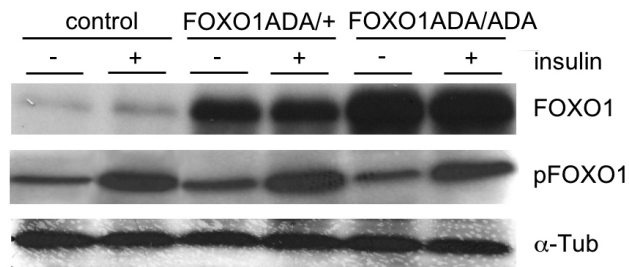
Figure 45: Functional validation of the constitutively active FOXO1 construct in MEFs.
Western blot analysis using FOXO1, phosphorylated Ser[256] FOXO1 (pFOXO1), and α-Tubulin (α-Tub, loading control) antibodies of whole cell lysates from fasted and 1 h insulin-stimulated control, FOXO1ADA/+-, and FOXO1ADA/ADA-expressing MEFs.

3.3.3 Constitutively active FOXO1 expression causes apoptosis in MEFs

Recently, it was demonstrated that in the absence of insulin and other growth factors FOXO proteins are able to induce apoptosis [259, 329]. Therefore, the cleavage of caspase-3 in FOXO1ADA/+ and FOXO1ADA/ADA MEFs was assessed by Western blot analysis. This analysis revealed that the apoptotic cleaved caspase-3 fragments were detectable in FOXO1ADA-expressing MEFs in a dose-dependent manner, while control MEFs showed no sign of apoptosis (Figure 46). Furthermore, all three isoforms of the proapoptotic protein Bim, which is a known FOXO target gene [233, 329, 330], were clearly increased in FOXO1ADA/+ and FOXO1ADA/ADA MEFs compared to the controls (Figure 46).

In summary, expression of FOXO1ADA in MEFs induces apoptosis indicated by caspase-3 cleavage due to enhanced expression of Bim.
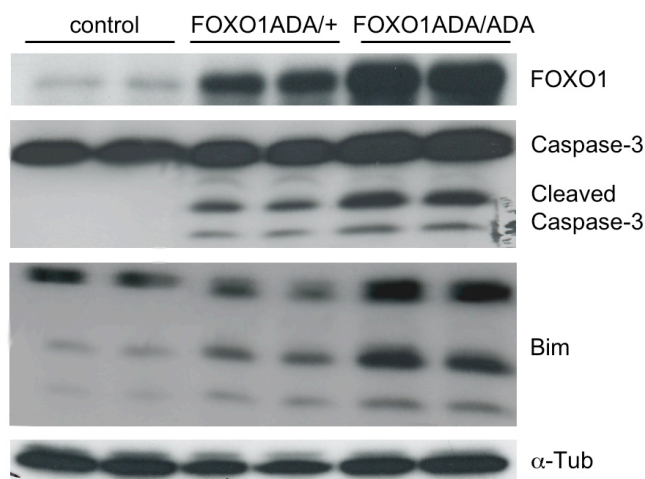
Figure 46: Expression of FOXO1ADA induces apoptosis in MEFs.
Western blot analysis using FOXO1, Caspase-3, Bim, and α-Tubulin (α-Tub, loading control) antibodies of whole cell lysates from control, FOXO1ADA/+-, and FOXO1ADA/ADA-expressing MEFs.

3.3.4 Generation of central nervous system-specific FOXO1ADA-expressing mice

To investigate the effect of excessive FOXO1 signalling in neurons, FOXO1ADA$^{floxstop/floxstop}$ mice were intercrossed with mice carrying the *nestin cre* transgene (Figure 47A) [323] to obtain FOXO1ADA$^{floxstop/+}$Nestin-Cre (FOXO1ADA^{CNS}) mice expressing FOXO1ADA selectively in the central nervous system (CNS). Cre-negative mice of this breeding served as controls. (Figure 47B). In contrast to Synapsin-Cre mice, which express Cre recombinase in mature neurons [331], Nestin-Cre mice are wildly used for pan-neuronal expression of genes of interest [323].
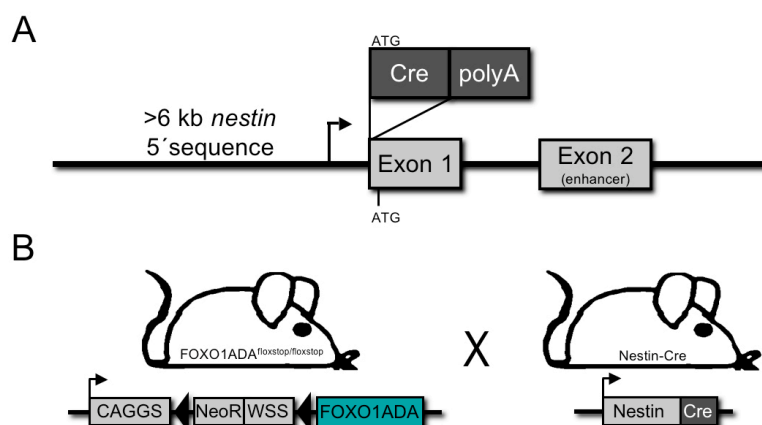
Figure 47: Central nervous system-restricted expression of FOXO1ADA.
(A) In *nestin cre* transgenic mice the Cre recombinase (Cre) expression cassette was inserted into the translation initiation site (ATG) of *nestin* exon 1. Exon 2 of the *nestin* gene contains a known enhancer of Nestin expression. **(B)** FOXO1ADA$^{floxstop/floxstop}$ mice were intercrossed with mice carrying the *nestin cre* transgene to obtain FOXO1ADA^{CNS} mice expressing FOXO1ADA selectively in the central nervous system.

Surprisingly, expression of FOXO1ADA in the CNS led to the death of pups within two days after birth (Figure 48A, C). FOXO1ADA^{CNS} embryos were still alive at E19.5 (Figure 48B), despite the fact that Cre recombinase expression is initiated at E10.5 [332].
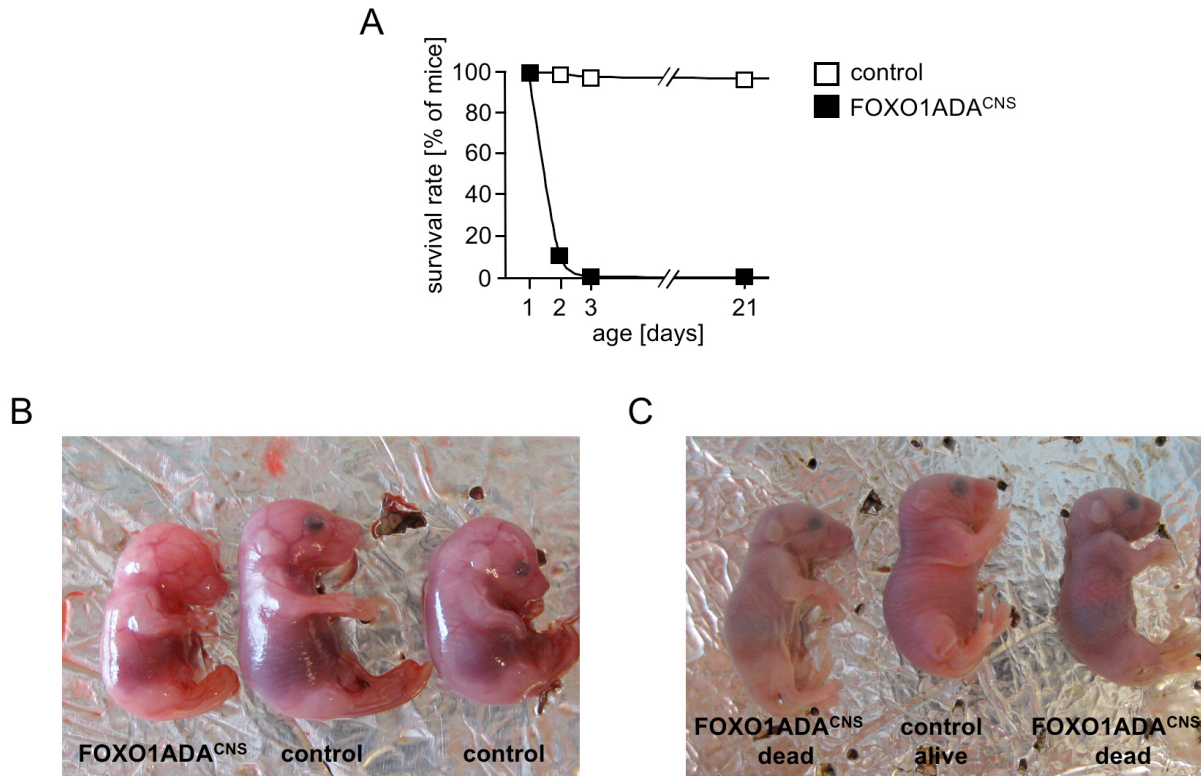
Figure 48: FOXO1ADA^{CNS} mice die within two days after birth.
(A) Survival rate of control and FOXO1ADA^{CNS} mice from day 1 to day 21 after birth (n = 22 – 56 per genotype). **(B)** Photographs of representative control and FOXO1ADA^{CNS} embryos at E19.5. **(C)** Photographs of representative control and FOXO1ADA^{CNS} pups at day 2.

To assess whether expression of FOXO1ADA leads to alterations in brain morphology of FOXO1ADA^{CNS} embryos at E19.5, histological analyses were performed. However, H&E stainings of control and FOXO1ADA^{CNS} embryonic brains revealed no obvious alterations in brain morphology (Figure 49).

To address whether the lethality of FOXO1ADA^{CNS} mice is a consequence of postnatal neuronal apoptosis, fragmented DNA in neurons was visualised by the TUNEL method in control and FOXO1ADA^{CNS} embryonic brains at E19.5. While in control brains apoptotic cells were hardly detectable, in the brain of FOXO1ADA^{CNS} embryos excessive amounts of TUNEL-positive cells could be visualised in ARC, cortex, thalamus, and midbrain (Figure 50).

Taken together, the expression of FOXO1ADA in the CNS results in lethality within two days after birth, presumably mediated by neuronal apoptosis.

control   FOXO1ADA^{CNS}
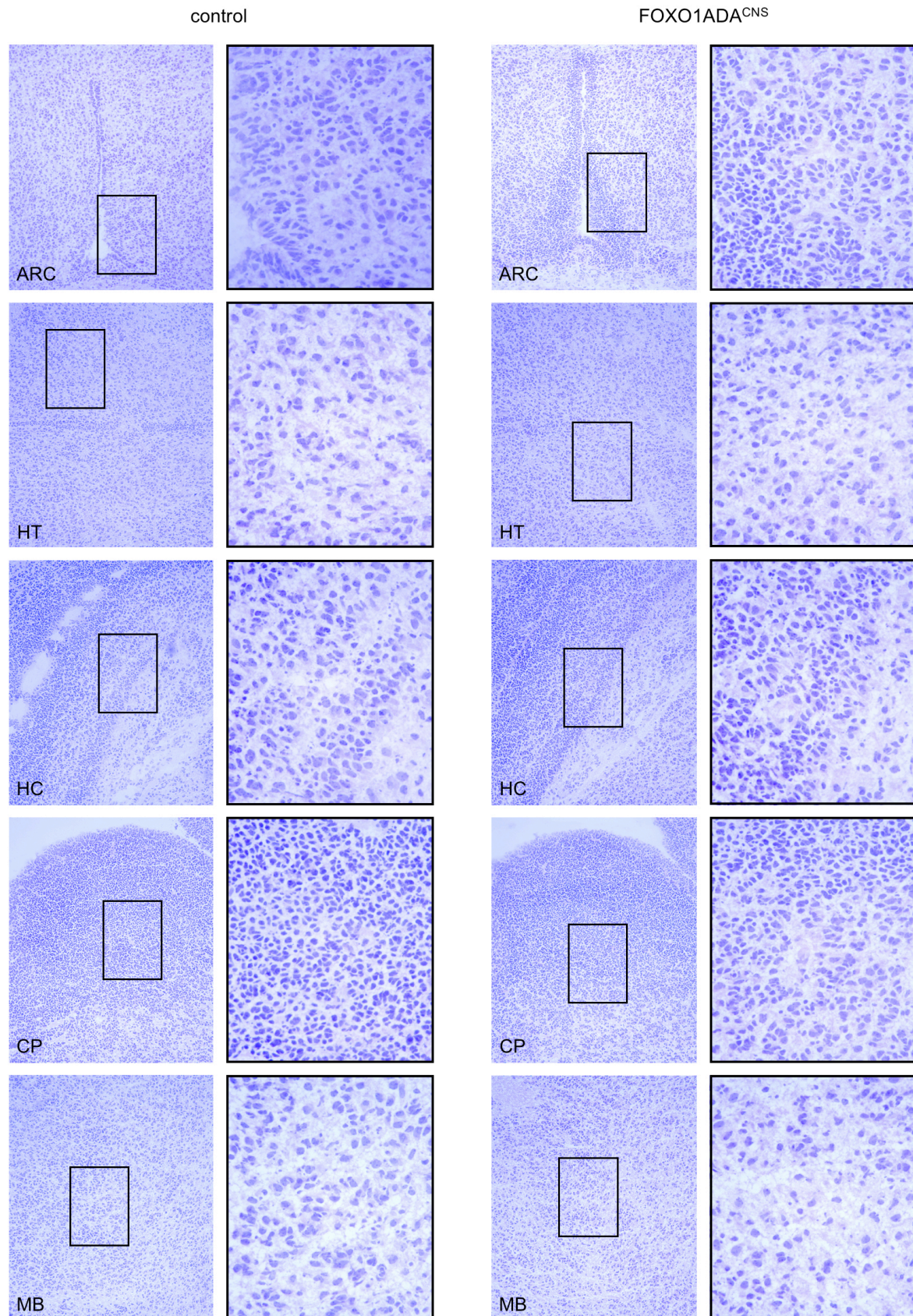
Figure 49: Unaltered brain morphology in FOXO1ADA^{CNS} embryos.
Representative hematoxylin/eosin staining of arcuate nucleus (ARC), hypothalamus (HT), hippocampus (HC), caudate putamen (CP), and midbrain (MB) from control and FOXO1ADA^{CNS} embryos at E19.5. Magnification: 100x, 400x.
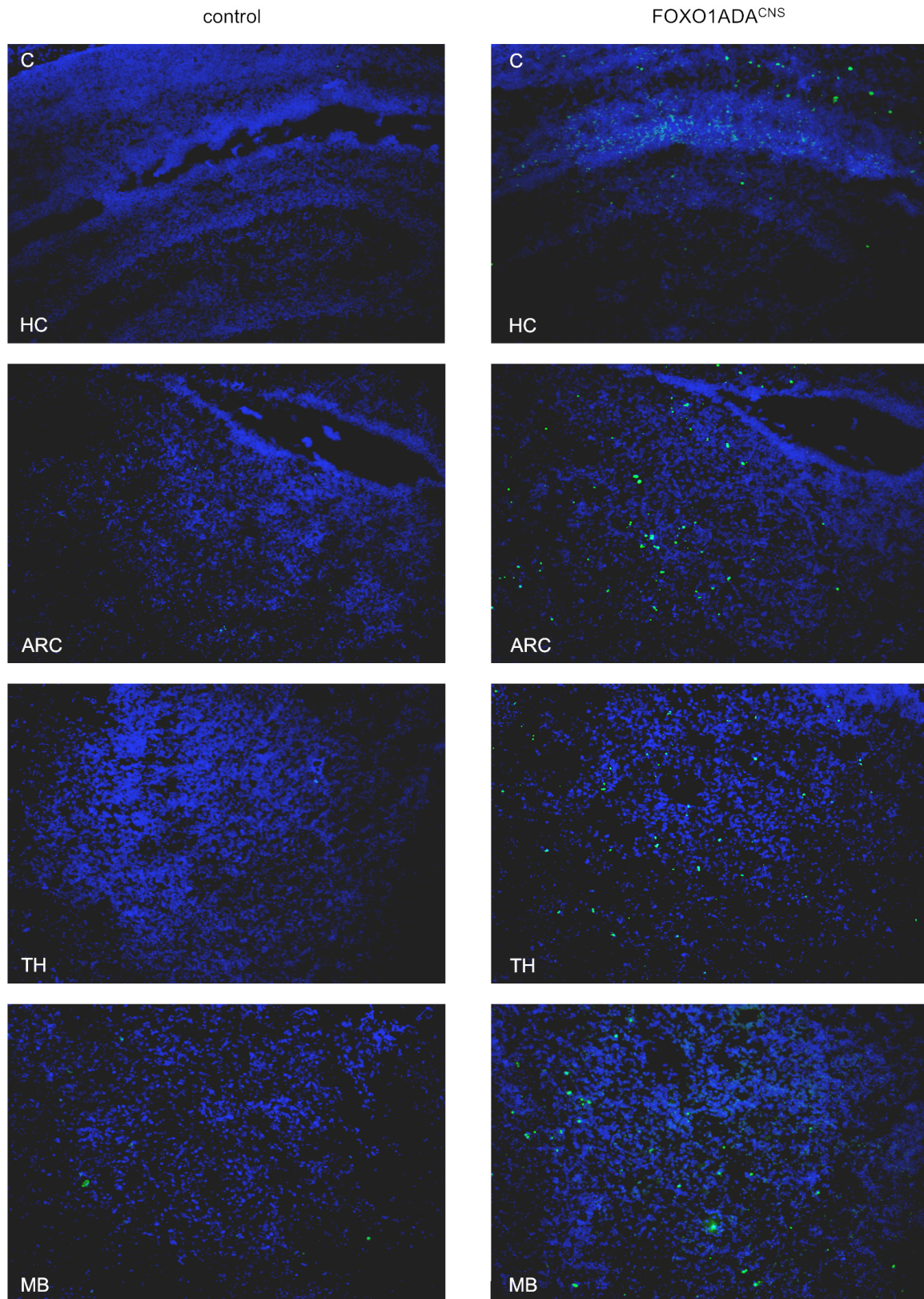
Figure 50: Apoptotic neurons in FOXO1ADA^{CNS} embryos.
Representative TUNEL staining of cortex (C), hippocampus (HC), arcuate nucleus (ARC), thalamus (TH), and midbrain (MB) from control and FOXO1ADA^{CNS} embryos at E19.5. Blue (DAPI), DNA; green, TUNEL-positive cells. Magnification: 200x.

4 Discussion

The incidence of obesity and type 2 diabetes are intimately connected and represent a steadily growing worldwide health problem [2, 6]. For the development of new therapeutic strategies to prevent and treat these diseases, a detailed understanding of energy homeostasis and elucidation of involved signalling cascades are essential. Numerous studies over the last decade have highlighted the crucial role of central leptin and insulin signalling to control body weight and glucose homeostasis [97, 192, 333, 334].

The aim of this study was to investigate the central function of leptin- and insulin-regulated transcription factors STAT3 (signal transducer and activator of transcription) and FOXO1 (forkhead box-containing protein class O 1) by cell type-specific transgenic expression of mutant versions of these proteins. Cell type-specific expression of mutant gene variants is a powerful tool in modern mouse genetics to gain mechanistic insights into the physiological function of signalling pathways. Since it was shown that the *ROSA26* locus is expressed in all cells of adult mice, this locus is widely used for the ubiquitous expression of transgenes [312, 335, 336]. The usage of a *lox*P-flanked stop cassette in such *ROSA26* insertion strategies allows for Cre-inducible activation of transgenes [296, 337]. Therefore, intercrossing of *ROSA26* transgenic mice with Cre-expressing mouse lines, *e.g.* POMC-Cre and Nestin-Cre mice [322, 323], results in specific expression of the respective transgene in cell types, which express the Cre recombinase. However, the transgenes expressed from the *ROSA26* locus seem to be expressed at low to intermediate levels [335]. While the STAT3 mutant was generated using the conventional reliable strategy in which the endogenous *ROSA26* promoter drives expression of the STAT3 mutant upon Cre-mediated excision of the stop cassette, both FOXO1 constructs contain the strong *chicken β actin* promoter [288] to enhance their expression upon Cre-mediated recombination.

4.1 Functional validation of the transcription factor mutants

In the present study, the central role of the transcription factors STAT3 and FOXO1 was elucidated by transgenic expression of a constitutively active version of STAT3 (STAT3-C), a dominant negative version of FOXO1 (FOXO1DN), and a constitutively active version of FOXO1 (FOXO1ADA).

The STAT3-C mutant dimerises spontaneously via disulfide bonds due to substitution of two residues to cysteins in the SH2-domain, and thus activates transcription independent of any stimulation [172]. The functional validation of the STAT3-C construct in ES cells was performed using Western blot analysis, EMSA (electrophoretic mobility shift assay), and luciferase assay and confirmed the constitutive nuclear localisation of STAT3-C and target gene promoter occupancy, which implicates specific activation of STAT3 target gene expression. Consistently, constitutive binding of STAT3-C to its consensus sequence could also be validated *in vivo* in STAT3-C[POMC] mice.

The FOXO1DN construct is a C-terminal truncated variant of FOXO1 that blocks binding of endogenous FOXO1 and presumably other endogenous FOXO proteins by occupying the consensus sequence of the DNA independent of insulin or other growth factor signals [279]. In contrast, FOXO1ADA acts as a constitutive activator of transcription due to the amino acid substitutions T24A, S256D, and S319A of FOXO1. Thus, FOXO1ADA is unable to be phosphorylated by AKT/SGK that would lead to nuclear exclusion of FOXO1 [280]. To test the function of the mutant FOXO1DN construct, EMSA and Western blot analysis of FOXO1DN-expressing MEFs confirmed both the constitutive nuclear localisation of FOXO1DN and target gene promoter occupancy. Moreover, Western blot analysis of FOXO1ADA-expressing MEFs indicated that insulin stimulation failed to phosphorylate FOXO1ADA.

4.2 STAT3-C expression in POMC neurons provokes a negative feedback inhibition of leptin and insulin signalling

Numerous studies over the last decade have demonstrated the crucial role of central leptin and insulin signalling to control body weight and glucose homeostasis [97, 192, 333, 334]. The primary sites of both leptin and insulin action are first order neurons in the ARC of the hypothalamus that express either anorexigenic proopiomelanocortin (POMC) or orexigenic agouti-related peptide (AgRP) and neuropeptide Y (NPY) neuropeptides [68, 72].

Cell type-specific disruptions of key players in POMC neurons using POMC-Cre mice gained new insights into the signalling pathways regulated by leptin and insulin [153, 193, 322]. These studies revealed that inactivation of the leptin receptor and the downstream transcription factor STAT3 lead to mild obesity indicating a crucial role of leptin-regulated STAT3 in the control of POMC expression, energy expenditure, and food intake [153, 322].

However, despite the new insights provided by these studies, more than 95% of obesity are not caused by genetic alterations but rather by environmental factors and lifestyle changes accounting for a yet unsolved mechanism, termed leptin resistance, in which leptin levels are high and STAT3 signalling is increasingly activated in the basal state [21, 338-340].

To investigate the effect of increased basal STAT3 signalling specifically in POMC neurons as present in obesity, mice expressing a constitutively active mutant of STAT3 [172] exclusively in POMC neurons were generated (STAT3-C[POMC] mice). Besides the POMC neuron-specific Cre-mediated expression of STAT3-C, the constitutively DNA-binding capacity of the STAT3-C protein was also demonstrated *in vivo*. Although persistently activated STAT3 was identified in a variety of clinical cancer samples [151] and STAT3-C has been described to hold an oncogenic potential [172], no obvious tumour genesis was detected in STAT3-C[POMC] mice, probably because the level of STAT3 activity is too low to cause tumour genesis. This observation is in line with the description that AgRP neuron-specific expression of STAT3-C neither affects cell size nor induces proliferation/transformation of AgRP neurons in mice [325]. Taken together, mice expressing a constitutively active STAT3 mutant specifically in POMC neurons provide an adequate tool to study the role of STAT3 signalling in these cells *in vivo*.

Since POMC neurons have been identified as the primary cell type for mediating leptin's anorexigenic effect [45, 61, 62, 341], consistently, POMC neuron-restricted STAT3-deficient mice as well as POMC cell-specific ObRb-knockout mice are mildly obese [153, 322]. Surprisingly, STAT3 overactivation in STAT3-C[POMC] mice also mirrors this phenotype. The mild obesity accompanied by hyperleptinemia in these mice is a consequence of increased food intake, whereas locomotor activity is not significantly reduced as described previously [325]. It has been demonstrated that POMC transcription is positively regulated by STAT3 in a leptin-dependent manner [73, 153, 342]. As the constitutively active STAT3 mimics elevated leptin signalling in POMC neurons, an increase of POMC expression was expected instead of decreased POMC expression as observed. A leptin sensitivity test as well as Western blot and immunohistochemical analysis of leptin-mediated phosphorylation of STAT3 clearly elucidated that STAT3-C[POMC] mice develop obesity as a consequence of leptin resistance.

The failure of elevated leptin levels to reduce food intake and to increase energy expenditure is defined as leptin resistance [343] and is likely caused by multiple mechanisms including defects in leptin transport into the brain as well as reduced leptin signalling in hypothalamic neurons [107]. The cellular leptin resistance is caused by a block of

leptin-mediated STAT3 signalling as shown in *db/db* mice [98], in mice carrying mutated ObRb (T1138S) with abolished STAT3-binding sites [131], and in neuron-specific STAT3-deficient mice [133] as well as by increased action of negative regulators of STAT3 signalling. Besides constitutively expressed proteins such as PIAS, SHP2, and PTP1B, cytokine-induced proteins as SOCS3 and CIS negatively control STAT3 activation [162, 163]. While PIAS expression was unchanged, significantly increased SOCS3 mRNA levels were detected in the hypothalamus of STAT3-C^{POMC} mice albeit only approximately 5% of hypothalamic neurons express POMC. Moreover, SOCS3 *in situ* hybridisation analysis confirmed the POMC-specific elevated SOCS3 level due to STAT3-C expression. The STAT3-activated SOCS3 interacts with phosphorylated ObRb and JAK proteins and functions as a classical feedback loop of cytokine signalling [164, 165, 344]. Specific interaction of SOCS3 with tyrosine residues 985 and 1138 of the ObRb inhibits phosphorylation of STAT3, thus suppressing expression of SOCS3 [165, 345]. Besides affecting leptin signalling, SOCS3 functions also as a negative regulator of insulin signalling by inhibiting tyrosine phosphorylation of IRS as well as promoting ubiquitin-mediated degradation of IRS [326, 327, 346]. Consistently, both SOCS3-haploinsufficient mice and POMC neuron-specific SOCS3-deficient mice exhibit enhanced leptin sensitivity accompanied by improved glucose homeostasis [347, 348]. Ultimately, POMC neuron-specific overexpression of SOCS3 impairs STAT3 and mTOR signalling and subsequently leads to obesity, leptin resistance, and glucose intolerance [349]. In line with these observations, analysis of insulin-induced PIP$_3$ formation and AKT phosphorylation as well as perforated patch recordings of STAT3-C-expressing POMC neurons clearly provide evidence that these neurons are not only leptin-, but also insulin-resistant due to increased STAT3-mediated SOCS3 expression.

4.3 STAT3-C expression has no effect in diet-induced obesity

Although various genetic factors have been identified accounting for the development of human obesity such as mutations in *leptin*, *lepr*, *pomc*, and *mc4r* genes [18], the worldwide prevalence of obesity is more likely caused by environmental and behavioural changes such as lack of physical activity and high caloric diet [21]. Consistently, wild-type mice fed with high fat diet (HFD) develop a diet-induced obesity (DIO) [338]. After increase of fat mass, peripheral leptin sensitivity is reduced in turn leading to central leptin resistance [338, 339]. Indeed, both DIO and accompanied leptin resistance are reversible by replacing HFD with

normal chow diet (NCD) [350]. Two independent mechanisms are proposed to cause DIO-mediated central leptin resistance: (i) circulating leptin is unable to reach central targets and (ii) intracellular signalling is impaired in leptin-responsive neurons [31, 339, 351]. Peripheral leptin administration to DIO mice revealed that prominently neurons located in the ARC, in comparison with neurons in other hypothalamic and extrahypothalamic sites, show a dramatic decrease of phosphorylated STAT3 [351]. However, DIO mice retain the capacity to respond to centrally applied leptin, but with a substantially reduced magnitude of STAT3 activation [339]. In contrast, recently it was reported that the effect of centrally applied leptin to phosphorylate STAT3 is attenuated in DIO mice due to an elevated basal STAT3 phosphorylation level compared to NCD mice [340]. In line with this finding, the experiments in this study demonstrated that DIO significantly enhances basal STAT3-binding capacity in the ARC of wild-type mice. Moreover, POMC neuron-restricted STAT3-C expression has no effect on regulation of energy homeostasis under HFD-conditions. The central leptin resistance during DIO, concomitantly increasing STAT3 signalling, blunts the effect of STAT3-C-mediated POMC neuron-specific leptin and insulin resistance. This was confirmed by similar increases of SOCS3 expression levels in the ARC of STAT3-C[POMC] and control mice under HFD conditions accompanied by comparable decreases in POMC expression.

However, there is some discrepancy about the observed decreased POMC expression levels in DIO mice. Enriori *et al*. demonstrated that neither baseline nor leptin-induced POMC transcription were affected in DIO mice, while leptin-induced α-MSH secretion was significantly reduced. Indeed, the impaired leptin-induced α-MSH secretion is restored by replacing HFD to NCD [352]. In contrast, Gout *et al*. reported that basal POMC mRNA levels were significantly decreased in DIO mice and additionally that leptin-induced transcription of POMC was blocked in these mice [353]. Furthermore, Lin *et al.* illustrated that the effect during DIO in inhibiting leptin-induced POMC expression was positively correlated with the exposure time of HFD feeding [354]. Consistently, HFD fed wild-type mice as well as mice expressing STAT3-C in POMC neurons exposed to HFD, exhibit a similar reduction of basal POMC expression equally to extents observed in STAT3-C[POMC] mice under NCD conditions.

Concordant with the observation that constitutive STAT3 activation in POMC neurons increases SOCS3 expression and thus is a reasonable explanation for the development of leptin and insulin resistance in POMC neurons, this phenomenon has also been demonstrated in the ARC of DIO mice [351, 352]. Similar to DIO mice, seasonally obese rodents such as the field vole and the siberian hamster also exhibit an increased SOCS3 expression in the ARC [355, 356]. Likewise to POMC, SOCS3 is a direct target gene of STAT3 and acts as a

negative feedback regulator of leptin signalling [129, 130, 344]. However, while baseline SOCS3 expression is increased in DIO mice, the leptin-induced upregulation of SOCS3 expression is impaired in these mice [351, 352]. Consistently, studies of heterozygous SOCS3-deficient and central nervous system (CNS)-restricted SOCS3-knockout mice demonstrated that SOCS3 is a key regulator of diet-induced leptin and insulin resistance as such mice failed to develop DIO [347, 357]. In line with these findings, HFD feeding causes a significant increase of hypothalamic SOCS3 expression in control mice as well as in STAT3-C^{POMC}mice; however, STAT3-C expression did not further increase SOCS3 expression. Accordingly, POMC-restricted SOCS3-deficient mice illustrate attenuation of DIO due to substantial improvements in leptin and insulin sensitivity under HFD feeding [348]. In contrast, POMC-restricted overexpression of SOCS3 resulted in impaired STAT3 and mTOR signalling subsequently leading to obesity, leptin resistance, and glucose intolerance [349].

Taken together, the observation that enhanced STAT3 signalling in obesity can initiate a vicious negative regulatory feedback circle to inhibit not only leptin, but also insulin action in the CNS explains how initial weight loss restores leptin sensitivity by reducing circulating leptin concentrations as a driving force of elevated basal STAT3 activation and subsequent SOCS3-mediated leptin and insulin resistance [358]. Furthermore, these data also offer the conclusion that chronically elevated leptin levels, as seen in overweight and/or obese patients, is not able to reduce body weight due to chronic activation of the SOCS3 negative feedback loop, leading to leptin and insulin resistance. This is in line with the hypothesis that leptin and the hypothalamic control circuit were evolutionary necessary to protect against weight loss instead of weight gain [359, 360].

4.4 Simultaneous POMC neuron-specific dominant FOXO1 inhibition in STAT3-C^{POMC} mice partially attenuates obesity

Although STAT3 is the main regulator of POMC expression, as predicted from the STAT responsive element in the *pomc* promoter [73], POMC expression in STAT3-C^{POMC}mice would not be expected to be downregulated even in the presence of increased SOCS3, since STAT3-C should still bind to and activate the *pomc* promoter [73, 153, 342]. The experiments in this study clearly indicate the existence of another, SOCS3-sensitive, leptin- and/or insulin-induced signalling molecule required for POMC expression, even in the presence of fully activated STAT3. In line with this proposal, it was

demonstrated that hypothalamic administration of FOXO1 siRNA decreases food intake, whereas hypothalamic injection of a constitutively active FOXO1 adenovirus increases food intake and suppresses POMC expression [152]. Furthermore, a FOXO responsive element was recently identified within the POMC promoter [73]. However, the transcription factors FOXO1 and STAT3 have opposing effects on POMC expression through transcriptional squelching [73]. While leptin signalling causes STAT3 activation and translocation in the nucleus [127], both leptin and insulin administration mediate nuclear exclusion of FOXO1 as shown in mice expressing a FOXO1GFP fusion protein selectively in POMC neurons [361].

To study the impact of FOXO1 on POMC expression *in vivo*, a Cre-inducible dominant negative FOXO1 mouse strain was generated. Intercrossing of FOXO1DN with STAT3-C^{POMC} mice resulted in mice expressing both a constitutively active STAT3 and a dominant negative FOXO1 mutant specifically in POMC neurons (STAT3-C/FOXO1DN^{POMC} mice). These mice provide an adequate tool for studying interactions of STAT3 and FOXO1 at the *pomc* promoter *in vivo*.

The impact of FOXO1DN to block FOXO1-mediated inhibition of POMC expression is controversially discussed. Belgardt *et al.* demonstrated that in POMC neuron-specific PDK1-knockout mice (PDK1$^{\Delta POMC}$ mice) the reduced POMC expression, initial hyperphagia, and mild obesity can be restored by POMC cell-restricted expression of FOXO1DN (FOXO1DN:PDK1$^{\Delta POMC}$ mice) [281]. In contrast, Iskandar *et al.* showed that POMC neuron-restricted expression of FOXO1DN has no effect on POMC expression in PDK1$^{\Delta POMC}$ and wild-type mice albeit in the hypothalamus of FOXO1DN:PDK1$^{\Delta POMC}$ mice, FOXO1DN, instead of phosphorylated STAT3, interacts with the *pomc* promoter [362]. Indeed, Iskandar *et al.* analysed the effect of *ROSA26* promoter-driven expression of a FLAG-tagged version of FOXO1DN, while Belgardt *et al.* used the strong *chicken β actin* promoter [288] to express non-modified FOXO1DN as described in this study. Moreover, Iskandar *et al.* also demonstrated that POMC neuron-specific expression of a constitutively active FOXO1 version in PDK1$^{\Delta POMC}$ mice even more decreases POMC expression [362].

Indeed, a crucial role for insulin signalling to inhibit FOXO1-mediated repression of POMC expression could be confirmed in this study, though elucidated by other means. While STAT3-C^{POMC} mice display mild obesity due to inhibited POMC expression as a consequence of SOCS3-mediated POMC neuron-specific leptin and insulin resistance, the POMC cell-restricted expression of FOXO1DN partially attenuates this effect of STAT3-C. In contrast to these findings, Plum *et al.* demonstrated that adult mice with a POMC neuron-specific ablation of FOXO1 showed unchanged POMC expression [255]. On the

contrary to the ablation of FOXO1, the FOXO1DN construct used in this study blocks binding of endogenous FOXO1 but presumably also that of redundant FOXO3a, FOXO4, and FOXO6 by occupying the consensus sequences in the DNA and regulating POMC expression.

Beside the hypothesis that FOXO1 inhibits POMC expression by binding to the FOXO1 responsive element [73, 152], Yang *et al.* demonstrated that FOXO1 binds directly to STAT3 and thus interrupts the interaction of STAT3 with the *pomc* promoter-bound transcription factor SP1 thereby inhibiting transcription of POMC [363]. Moreover, as an additional mechanism, mice with a POMC neuron-specific ablation of FOXO1 exhibit an increase of carboxypeptidase E expression and selective α-MSH secretion, which decrease food intake and body weight [255].
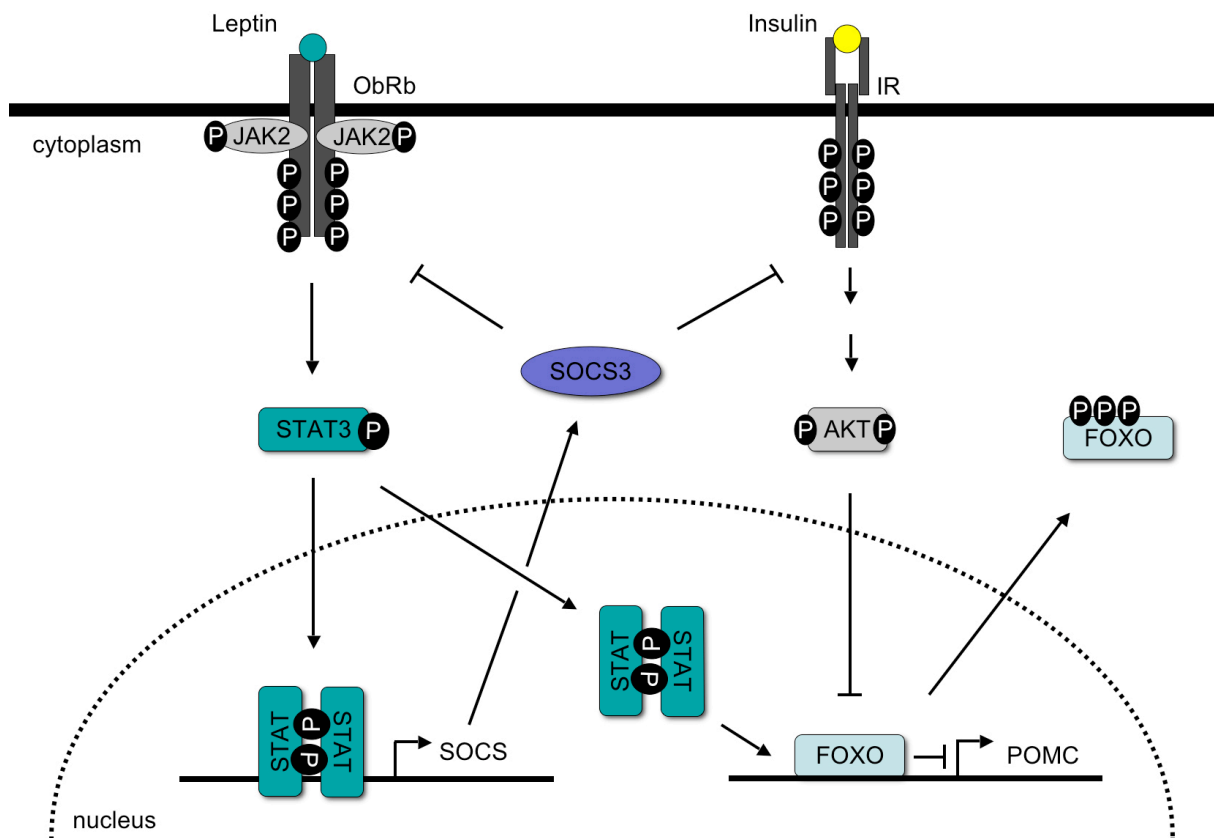
Figure 51: Model of SOCS3-mediated leptin and insulin resistance in POMC neurons.
Increased STAT3-mediated SOCS3 expression as present in early hyperleptinemia leads to the combined feedback inhibition of leptin and insulin signalling. Decreased insulin signalling leads to inefficient FOXO phosphorylation, thereby occupying the *pomc* promoter and thus inhibiting binding of STAT3, which serves as a transcriptional activator of POMC expression. AKT, protein kinase B; FOXO, forkhead box-containing protein class O; IR, insulin receptor; JAK2, Janus kinase 2; ObRb, long form of leptin receptor; P, phosphorylation; STAT3, signal transducer and activator of transcription 3; SOCS 3, suppressor of cytokine signalling 3.

The findings in this study indicate that in obesity the negative effects of increased SOCS3 levels on leptin and insulin signalling not only result in impaired STAT3 activation,

but also in decreased POMC expression as a consequence of impaired FOXO1 nuclear exclusion; the STAT3-binding sites in the *pomc* promoter are occupied by FOXO1 leading to the inaccessibility of STAT3 to activate POMC expression (Figure 51). Moreover, this study elucidates that FOXO1 removal is a prerequisite for functional STAT3-binding, even when expressed as a constitutively active mutant.

4.5 Enhanced FOXO1 activation in neurons results in apoptosis

Although our understanding about how FOXO1 is involved in the regulation of cellular processes such as differentiation, cell cycle, detoxification, and survival has improved significantly over the last years [328], the specific role of FOXO1 in neurons remains controversial. Therefore, to study the impact of neuronal FOXO1 signalling *in vivo*, a Cre-inducible constitutively active FOXO1 mouse strain was generated and intercrossed with the Nestin-Cre mouse line. Consistently with the finding that in the absence of insulin or other growth factors FOXO proteins are associated with the induction of apoptosis [240], *in vitro* analysis revealed that expression of FOXO1ADA induces apoptosis. Identification of FOXO target genes involved in cell survival and apoptosis has led to the conclusion that activated FOXO1 proteins can induce apoptosis through mitochondria-dependent and -independent pathways [240]. FOXO1-mediated expression of Fas ligand (FasL) or tumour necrosis factor-related apoptosis-inducing ligand (TRAIL) causes activation of death receptors [259, 364], while transcriptional activation of proapoptotic Bcl-2 family members, such as Bim and bNIP3 lead to mitochondrial permeability [233, 329, 365]. Consistently, FOXO1ADA expression in MEFs causes prominent increased protein levels of all Bim isoforms.

To investigate the role of enhanced FOXO1 activation in neurons, mice expressing FOXO1ADA exclusively in the CNS were generated (FOXO1ADA^{CNS} mice). While FOXO proteins have been implied in playing a role also in neuronal survival by transcriptional regulation of FasL and Bim [233, 366, 367], the pan-neuronal FOXO1ADA expression in neurons induces apoptosis, ultimately leading to premature death of mice within two days after birth. Consistently, the ischemia-induced neuronal death in gerbil and mouse brains is associated with dephosphorylation and nuclear localisation of FOXO proteins and concomitant enhanced FasL and Bim expression [368, 369]. Furthermore, it was demonstrated that oxidative stress, which has been linked to the development of neurodegenerative diseases such as Alzheimer and Parkinson disease [370], leads to FOXO

nuclear localisation due to JNK- and MST1-mediated phosphorylation of FOXO in neurons [366, 367, 371]. However, besides the expression of apoptosis-initiating proteins, stress-induced nuclear localisation of FOXO proteins can also result in upregulation of proteins involved in detoxification such as catalase and manganese superoxide dismutase [372].

In contrast to the pan-neuronal FOXO1ADA expression in this study, the expression of FOXO1ADA in mature neurons of an Alzheimer disease mouse model led to a life-span of at least 60 weeks, which was nonetheless shorter than the life-time of control mice [373]. Consequently, the effect of FOXO1 to induce neuronal apoptosis seems to depend on the developmental stage of the neuron.

The findings in this study clearly demonstrate that nuclear localisation of FOXO1 as present in FOXO1ADA^{CNS} mice and caused by oxidative stress and/or by the absence of growth factors in wild-type mice is crucial for the induction of neuronal apoptosis (Figure 52).
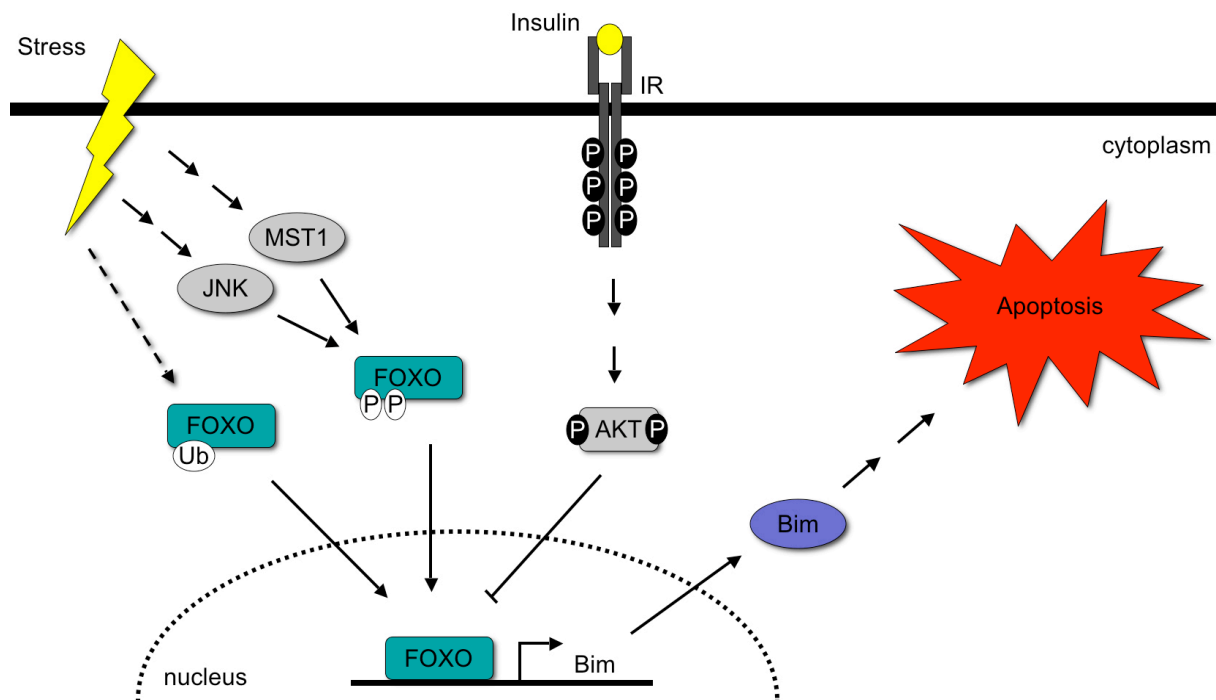
Figure 52: Model of FOXO-induced neuronal apoptosis.
Cellular stress and the absence of insulin cause nuclear localisation of FOXO, which activates transcription of the proapoptotic Bim, thus leading to apoptosis. AKT, protein kinase B; Bim, Bcl-2 interacting mediator of cell death; FOXO, forkhead box-containing protein class O; IR, insulin receptor; JNK, c-jun-N-terminal kinase; MST1, mammalian sterile 20-like protein kinase 1; P, phosphorylation; Ub, ubiquitination.

4.6 Perspectives

The POMC neuron-restricted expression of a constitutively active STAT3 mutant provides important novel insights into the molecular consequences of HFD-induced SOCS3 expression. However, the findings presented in this thesis support the importance of other leptin-resistant neurons besides POMC cells in the development of DIO [309, 374]. Therefore, further studies will be necessary to identify and characterise these neuronal populations.

Furthermore, the coexpression of a constitutively active STAT3 and a dominant negative FOXO1 mutant exclusively in POMC neurons expanded the knowledge of the coordinated STAT3 and FOXO1 transcriptional activation of the *pomc* promoter and the consequential effects on body weight and fat mass. Future experiments are necessary to detect and investigate additional potential factors involved in regulating energy homeostasis. An additional study could focus on the impact of AKT-mediated effects on maintaining energy balance by coexpressing a constitutively active STAT3 with a constitutively active AKT mutant selectively in POMC neurons.

Nevertheless, new insights of HFD-induced SOCS3 expression as well as STAT3- and FOXO1-dependent regulation of POMC expression may provide promising new targets for the development of novel therapeutic approaches to treat obesity and type 2 diabetes.

5 Summary

The central nervous system (CNS) has been identified as a major site mediating leptin's and insulin's effects on energy and glucose homeostasis. Cell type-specific disruption of key molecules in the CNS has delivered new insights into the signalling pathways influenced by leptin and insulin. Such studies revealed that inactivation of leptin or its receptor leads to massive obesity, closely resembling the situation in patients deficient for these genes. However, more than 95% of obesity account for another yet unsolved mechanism, termed leptin resistance, in which leptin levels are high and signalling components are increasingly activated.

In this study the effect of increased basal STAT (signal transducer and activator of transcription) 3 signalling specifically in the anorexigenic proopiomelanocortin (POMC)-expressing neurons, as present in obesity, was investigated. Therefore, mice expressing a constitutively active version of STAT3 (STAT3-C) in POMC neurons were characterised (STAT3-C^{POMC} mice). On normal chow diet, these animals develop obesity as a result of hyperphagia and decreased POMC expression accompanied by central leptin and insulin resistance. This finding coincides with POMC cell-specific, STAT3-mediated upregulation of SOCS3 expression inhibiting both, leptin and insulin signalling. In contrast, upon exposure to high fat diet, food intake and body weight were unaltered in STAT3-C^{POMC} mice compared to control mice. These experiments directly demonstrate that enhanced basal STAT3 activation in POMC neurons, as present in control mice upon high fat feeding, contributes to the development of hypothalamic leptin and insulin resistance. Moreover, these data also indicate that constitutive STAT3 activation is not sufficient to promote POMC expression, but instead requires simultaneous PI3K-dependent release of forkhead box protein O (FOXO) 1 repression. This assumption was verified by a partial rescue of POMC expression and the mild obesity observed in STAT3-C^{POMC} mice when a dominant negative version of FOXO1 was coexpressed in POMC neurons of these mice.

Furthermore, the generation and characterisation of mice expressing a constitutively active version of FOXO1 (FOXO1ADA) selectively in the CNS (FOXO1ADA^{CNS} mice) indicated a crucial role for FOXO1 in neuronal survival, since FOXO1ADA^{CNS} mice die within two days after birth due to FOXO1ADA-mediated apoptosis of neurons.

Taken together, this study highlights the importance of the transcription factors STAT3 and FOXO1 to centrally regulate energy homeostasis and neuronal survival using state of the art techniques.

6 Zusammenfassung

Leptin und Insulin regulieren die Glukose- und Energiehomöostase hauptsächlich über ihren Effekt auf das Zentrale Nervensystem (ZNS). Durch zelltypspezifische Inaktivierung von Schlüsselmolekülen im ZNS konnten zahlreiche neue Erkenntnisse über die durch Leptin und Insulin regulierten Signaltransduktionsprozesse gewonnen werden. Solche Studien zeigten, dass die Inaktivierung von Leptin oder seinem Rezeptor zu massiver Adipositas führt, was die Situation von Patienten widerspiegelt, die Mutationen in diesen Genen tragen. Allerdings werden 95% der Adipositasfälle durch einen anderen, bisher unzureichend untersuchten Prozess, genannt Leptin-resistenz, verursacht, bei dem der Leptinspiegel hoch und die Signalmoleküle überaktiviert sind.

In dieser Studie wurde der Effekt von erhöhter basaler STAT (signal transducer and activator of transcription) 3 Aktivität in den Proopiomelanocortin (POMC) produzierenden Neuronen untersucht, der auch bei einer Adipositas vorliegt. Daher wurden Mäuse generiert, die eine konstitutiv aktive STAT3 Variante (STAT3-C) spezifisch in POMC Neuronen exprimieren. Diese Mäuse entwickeln unter Standard-Diät-Bedingungen eine leichte Adipositas in Folge erhöhter Nahrungsaufnahme und verringerter POMC Expression kombiniert mit zentraler Leptin- und Insulinresistenz. Dieser Phänotyp resultiert aus der POMC-spezifisch erhöhten SOCS3 Expression, welche über STAT3 vermittelt wird und Leptin- wie auch Insulin-Signaltransduktion inhibiert. Im Gegensatz dazu zeigen STAT3-C^{POMC} Mäuse bei fettreicher Diät im Vergleich zu Kontrolltieren keinen Unterschied in Nahrungsaufnahme und Körpergewicht. Somit bewirkt eine erhöhte Basalaktivität von STAT3 in POMC Neuronen eine hypothalamische Leptin- und Insulin-resistenz, wie es auch bei mit fettreicher Diät gefütterten Kontrollen der Fall ist. Außerdem weisen diese Beobachtungen darauf hin, dass konstitutiv aktiviertes STAT3 nicht alleine die POMC Expression reguliert, sondern eine simultane PI3K-abhängige Freigabe von FOXO (forkhead box protein O) 1 erforderlich ist. Diese Annahme wurde durch die zusätzliche POMC-selektive Expression einer dominant negativen FOXO1 Variante in STAT3-C^{POMC} Mäusen bestätigt, die zur partiellen Verbesserung der inhibierten POMC Expression und auch Adipositas führte.

Die Charakterisierung von Mäusen, die ZNS-spezifisch eine konstitutiv aktive FOXO1 Variante (FOXO1ADA) exprimieren, zeigte eine entscheidende Rolle von FOXO1 für das Überleben von Neuronen, da FOXO1ADA^{CNS} Mäuse innerhalb von zwei Tagen nach der Geburt an neuronaler Apoptose sterben.

Zusammenfassend zeigen diese Ergebnisse, dass STAT3 und FOXO1 eine entscheidende Rolle in der Regulation der Energiehomöostase und im Überleben von Neuronen spielen.

7 References

1. Haslam, D.W. and W.P. James, *Obesity*. Lancet, 2005. 366(9492): p. 1197-209.
2. Seidell, J.C., *Obesity, insulin resistance and diabetes--a worldwide epidemic*. Br J Nutr, 2000. 83 Suppl 1: p. S5-8.
3. Mei, Z., et al., *Validity of body mass index compared with other body-composition screening indexes for the assessment of body fatness in children and adolescents*. Am J Clin Nutr, 2002. 75(6): p. 978-85.
4. WHO, *Obesity and overweight*. Fact sheet, 2006. N° 311.
5. Haslam, D., N. Sattar, and M. Lean, *ABC of obesity. Obesity--time to wake up*. BMJ, 2006. 333(7569): p. 640-2.
6. Dixon, J.B., *The effect of obesity on health outcomes*. Mol Cell Endocrinol, 2009.
7. Mokdad, A.H., et al., *Prevalence of obesity, diabetes, and obesity-related health risk factors, 2001*. JAMA, 2003. 289(1): p. 76-9.
8. Calle, E.E., et al., *Body-mass index and mortality in a prospective cohort of U.S. adults*. N Engl J Med, 1999. 341(15): p. 1097-105.
9. Manson, J.E., et al., *Body weight and mortality among women*. N Engl J Med, 1995. 333(11): p. 677-85.
10. Hogan, P., T. Dall, and P. Nikolov, *Economic costs of diabetes in the US in 2002*. Diabetes Care, 2003. 26(3): p. 917-32.
11. Wild, S., et al., *Global prevalence of diabetes: estimates for the year 2000 and projections for 2030*. Diabetes Care, 2004. 27(5): p. 1047-53.
12. Scheen, A.J. and P.J. Lefebvre, *Insulin action in man*. Diabetes Metab, 1996. 22(2): p. 105-10.
13. Leahy, J.L., *Pathogenesis of type 2 diabetes mellitus*. Arch Med Res, 2005. 36(3): p. 197-209.
14. Campbell, R.K., *Type 2 diabetes: where we are today: an overview of disease burden, current treatments, and treatment strategies*. J Am Pharm Assoc (2003), 2009. 49 Suppl 1: p. S3-9.
15. WHO, *Definiton and diagnosis of diabetes mellitus and intermediate hyperglycemia*. Report of a WHO/IDF consultation, 2006.
16. WHO, *The leading causes of death by broad income group, 2004*. Fact sheet, 2008. 310.
17. WHO, *Diabetes*. Fact sheet, 2009. 312.
18. Barsh, G.S., I.S. Farooqi, and S. O'Rahilly, *Genetics of body-weight regulation*. Nature, 2000. 404(6778): p. 644-51.
19. Fischer, J., et al., *Inactivation of the Fto gene protects from obesity*. Nature, 2009. 458(7240): p. 894-8.
20. Freathy, R.M., et al., *Common variation in the FTO gene alters diabetes-related metabolic traits to the extent expected given its effect on BMI*. Diabetes, 2008. 57(5): p. 1419-26.
21. Jequier, E., *Pathways to obesity*. Int J Obes Relat Metab Disord, 2002. 26 Suppl 2: p. S12-7.
22. Schwartz, M.W. and D. Porte, Jr., *Diabetes, obesity, and the brain*. Science, 2005. 307(5708): p. 375-9.
23. Woods, S.C., et al., *Signals that regulate food intake and energy homeostasis*. Science, 1998. 280(5368): p. 1378-83.

24.   Hill, J.O. and J.C. Peters, *Environmental contributions to the obesity epidemic.* Science, 1998. 280(5368): p. 1371-4.

25.   Hetherington, A.W., and Ranson, S.W. , *Hypothalalmic lesions and adipocyty in the rat.* Anat Record, 1940. 78: p. 149.

26.   Anand, B.K. and J.R. Brobeck, *Localization of a "feeding center" in the hypothalamus of the rat.* Proc Soc Exp Biol Med, 1951. 77(2): p. 323-4.

27.   Williams, G., J.A. Harrold, and D.J. Cutler, *The hypothalamus and the regulation of energy homeostasis: lifting the lid on a black box.* Proc Nutr Soc, 2000. 59(3): p. 385-96.

28.   Gao, Q. and T.L. Horvath, *Neurobiology of feeding and energy expenditure.* Annu Rev Neurosci, 2007. 30: p. 367-98.

29.   Wynne, K., et al., *Appetite control.* J Endocrinol, 2005. 184(2): p. 291-318.

30.   Broadwell, R.D. and M.W. Brightman, *Entry of peroxidase into neurons of the central and peripheral nervous systems from extracerebral and cerebral blood.* J Comp Neurol, 1976. 166(3): p. 257-83.

31.   Banks, W.A., et al., *Leptin enters the brain by a saturable system independent of insulin.* Peptides, 1996. 17(2): p. 305-11.

32.   Banks, W.A., *The source of cerebral insulin.* Eur J Pharmacol, 2004. 490(1-3): p. 5-12.

33.   McMinn, J.E., et al., *Effect of intracerebroventricular alpha-MSH on food intake, adiposity, c-Fos induction, and neuropeptide expression.* Am J Physiol Regul Integr Comp Physiol, 2000. 279(2): p. R695-703.

34.   Rossi, M., et al., *A C-terminal fragment of Agouti-related protein increases feeding and antagonizes the effect of alpha-melanocyte stimulating hormone in vivo.* Endocrinology, 1998. 139(10): p. 4428-31.

35.   Larhammar, D., *Evolution of neuropeptide Y, peptide YY and pancreatic polypeptide.* Regul Pept, 1996. 62(1): p. 1-11.

36.   Harris, J.I., *Studies on pituitary polypeptide hormones. III. The structure of alpha-melanocyte-stimulating hormone from pig pituitary glands.* Biochem J, 1959. 71(3): p. 451-9.

37.   Joseph, S.A., W.H. Pilcher, and C. Bennett-Clarke, *Immunocytochemical localization of ACTH perikarya in nucleus tractus solitarius: evidence for a second opiocortin neuronal system.* Neurosci Lett, 1983. 38(3): p. 221-5.

38.   Lacaze-Masmonteil, T., et al., *Characterization of proopiomelanocortin transcripts in human nonpituitary tissues.* Proc Natl Acad Sci U S A, 1987. 84(20): p. 72-5.

39.   Zhou, A., B.T. Bloomquist, and R.E. Mains, *The prohormone convertases PC1 and PC2 mediate distinct endoproteolytic cleavages in a strict temporal order during proopiomelanocortin biosynthetic processing.* J Biol Chem, 1993. 268(3): p. 1763-9.

40.   Shimizu, H., et al., *Effects of MSH on food intake, body weight and coat color of the yellow obese mouse.* Life Sci, 1989. 45(6): p. 543-52.

41.   Adan, R.A., et al., *Differential effects of melanocortin peptides on neural melanocortin receptors.* Mol Pharmacol, 1994. 46(6): p. 1182-90.

42.   Mountjoy, K.G., et al., *Localization of the melanocortin-4 receptor (MC4-R) in neuroendocrine and autonomic control circuits in the brain.* Mol Endocrinol, 1994. 8(10): p. 1298-308.

43.   Jegou, S., I. Boutelet, and H. Vaudry, *Melanocortin-3 receptor mRNA expression in pro-opiomelanocortin neurones of the rat arcuate nucleus.* J Neuroendocrinol, 2000. 12(6): p. 501-5.

44.   Krude, H., et al., *Severe early-onset obesity, adrenal insufficiency and red hair pigmentation caused by POMC mutations in humans.* Nat Genet, 1998. 19(2): p. 155-7.

45.   Yaswen, L., et al., *Obesity in the mouse model of pro-opiomelanocortin deficiency responds to peripheral melanocortin.* Nat Med, 1999. 5(9): p. 1066-70.

46.   Swart, I., et al., *Hypothalamic NPY, AGRP, and POMC mRNA responses to leptin and refeeding in mice.* Am J Physiol Regul Integr Comp Physiol, 2002. 283(5): p. R1020-6.

47.   Huszar, D., et al., *Targeted disruption of the melanocortin-4 receptor results in obesity in mice.* Cell, 1997. 88(1): p. 131-41.

48.   Chen, A.S., et al., *Inactivation of the mouse melanocortin-3 receptor results in increased fat mass and reduced lean body mass.* Nat Genet, 2000. 26(1): p. 97-102.

49.   Butler, A.A., et al., *A unique metabolic syndrome causes obesity in the melanocortin-3 receptor-deficient mouse.* Endocrinology, 2000. 141(9): p. 3518-21.

50.   Ollmann, M.M., et al., *Antagonism of central melanocortin receptors in vitro and in vivo by agouti-related protein.* Science, 1997. 278(5335): p. 135-8.

51.   Makimura, H., et al., *Reducing hypothalamic AGRP by RNA interference increases metabolic rate and decreases body weight without influencing food intake.* BMC Neurosci, 2002. 3: p. 18.

52.   Morris, B.J., *Neuronal localisation of neuropeptide Y gene expression in rat brain.* J Comp Neurol, 1989. 290(3): p. 358-68.

53.   Baltatzi, M., et al., *Neuropeptide Y and alpha-melanocyte-stimulating hormone: interaction in obesity and possible role in the development of hypertension.* Int J Clin Pract, 2008. 62(9): p. 1432-40.

54.   Morton, G.J. and M.W. Schwartz, *The NPY/AgRP neuron and energy homeostasis.* Int J Obes Relat Metab Disord, 2001. 25 Suppl 5: p. S56-62.

55.   Stanley, B.G. and S.F. Leibowitz, *Neuropeptide Y: stimulation of feeding and drinking by injection into the paraventricular nucleus.* Life Sci, 1984. 35(26): p. 2635-42.

56.   Stanley, B.G., et al., *Neuropeptide Y chronically injected into the hypothalamus: a powerful neurochemical inducer of hyperphagia and obesity.* Peptides, 1986. 7(6): p. 1189-92.

57.   Pages, N., et al., *Refeeding after 72 hour fasting alters neuropeptide Y and monoamines in various cerebral areas in the rat.* Comp Biochem Physiol Comp Physiol, 1993. 106(4): p. 845-9.

58.   Erickson, J.C., K.E. Clegg, and R.D. Palmiter, *Sensitivity to leptin and susceptibility to seizures of mice lacking neuropeptide Y.* Nature, 1996. 381(6581): p. 415-21.

59.   Qian, S., et al., *Neither agouti-related protein nor neuropeptide Y is critically required for the regulation of energy homeostasis in mice.* Mol Cell Biol, 2002. 22(14): p. 5027-35.

60.   Luquet, S., et al., *NPY/AgRP neurons are essential for feeding in adult mice but can be ablated in neonates.* Science, 2005. 310(5748): p. 683-5.

61.   Gropp, E., et al., *Agouti-related peptide-expressing neurons are mandatory for feeding.* Nat Neurosci, 2005. 8(10): p. 1289-91.

62.   Cowley, M.A., et al., *Leptin activates anorexigenic POMC neurons through a neural network in the arcuate nucleus.* Nature, 2001. 411(6836): p. 480-4.

63.   Tong, Q., et al., *Synaptic release of GABA by AgRP neurons is required for normal regulation of energy balance.* Nat Neurosci, 2008. 11(9): p. 998-1000.

64.   Sahm, U.G., et al., *The melanocortin (MC3) receptor from rat hypothalamus: photoaffinity labelling and binding of alanine-substituted alpha-MSH analogues.* FEBS Lett, 1994. 350(1): p. 29-32.

65.   Cowley, M.A., et al., *Integration of NPY, AGRP, and melanocortin signals in the hypothalamic paraventricular nucleus: evidence of a cellular basis for the adipostat.* Neuron, 1999. 24(1): p. 155-63.

66.   Plum, L., B.F. Belgardt, and J.C. Bruning, *Central insulin action in energy and glucose homeostasis.* J Clin Invest, 2006. 116(7): p. 1761-6.

67.   van Houten, M., et al., *Insulin-binding sites in the rat brain: in vivo localization to the circumventricular organs by quantitative radioautography.* Endocrinology, 1979. 105(3): p. 666-73.

68.   Cheung, C.C., D.K. Clifton, and R.A. Steiner, *Proopiomelanocortin neurons are direct targets for leptin in the hypothalamus.* Endocrinology, 1997. 138(10): p. 4489-92.

69.   Sipols, A.J., D.G. Baskin, and M.W. Schwartz, *Effect of intracerebroventricular insulin infusion on diabetic hyperphagia and hypothalamic neuropeptide gene expression.* Diabetes, 1995. 44(2): p. 147-51.

70.   Schwartz, M.W., et al., *Central nervous system control of food intake.* Nature, 2000. 404(6778): p. 661-71.

71.   Benoit, S.C., et al., *The catabolic action of insulin in the brain is mediated by melanocortins.* J Neurosci, 2002. 22(20): p. 9048-52.

72.   Elias, C.F., et al., *Leptin differentially regulates NPY and POMC neurons projecting to the lateral hypothalamic area.* Neuron, 1999. 23(4): p. 775-86.

73.   Kitamura, T., et al., *Forkhead protein FoxO1 mediates Agrp-dependent effects of leptin on food intake.* Nat Med, 2006. 12(5): p. 534-40.

74.   Morrison, C.D., et al., *Leptin inhibits hypothalamic Npy and Agrp gene expression via a mechanism that requires phosphatidylinositol 3-OH-kinase signaling.* Am J Physiol Endocrinol Metab, 2005. 289(6): p. E1051-7.

75.   Fekete, C., et al., *Differential effects of central leptin, insulin, or glucose administration during fasting on the hypothalamic-pituitary-thyroid axis and feeding-related neurons in the arcuate nucleus.* Endocrinology, 2006. 147(1): p. 520-9.

76.   da Silva, A.A., J.J. Kuo, and J.E. Hall, *Role of hypothalamic melanocortin 3/4-receptors in mediating chronic cardiovascular, renal, and metabolic actions of leptin.* Hypertension, 2004. 43(6): p. 1312-7.

77.   Mizuno, T.M. and C.V. Mobbs, *Hypothalamic agouti-related protein messenger ribonucleic acid is inhibited by leptin and stimulated by fasting.* Endocrinology, 1999. 140(2): p. 814-7.

78.   Schwartz, M.W., et al., *Leptin increases hypothalamic pro-opiomelanocortin mRNA expression in the rostral arcuate nucleus.* Diabetes, 1997. 46(12): p. 2119-23.

79.   Zhang, Y., et al., *Positional cloning of the mouse obese gene and its human homologue.* Nature, 1994. 372(6505): p. 425-32.

80.   Friedman, J.M., *Leptin at 14 y of age: an ongoing story.* Am J Clin Nutr, 2009. 89(3): p. 973S-979S.

81.   Chehab, F.F., M.E. Lim, and R. Lu, *Correction of the sterility defect in homozygous obese female mice by treatment with the human recombinant leptin.* Nat Genet, 1996. 12(3): p. 318-20.

82.   Harris, M., et al., *Transcriptional regulation of the thyrotropin-releasing hormone gene by leptin and melanocortin signaling.* J Clin Invest, 2001. 107(1): p. 111-20.

83.   Bornstein, S.R., et al., *Evidence for a novel peripheral action of leptin as a metabolic signal to the adrenal gland: leptin inhibits cortisol release directly.* Diabetes, 1997. 46(7): p. 1235-8.

84.   Pralong, F.P., et al., *Leptin inhibits directly glucocorticoid secretion by normal human and rat adrenal gland.* Endocrinology, 1998. 139(10): p. 4264-8.

85.   Rahmouni, K., W.G. Haynes, and A.L. Mark, *Cardiovascular and sympathetic effects of leptin.* Curr Hypertens Rep, 2002. 4(2): p. 119-25.

86.   Covey, S.D., et al., *The pancreatic beta cell is a key site for mediating the effects of leptin on glucose homeostasis.* Cell Metab, 2006. 4(4): p. 291-302.

87.   Bado, A., et al., *The stomach is a source of leptin.* Nature, 1998. 394(6695): p. 790-3.

88.   Masuzaki, H., et al., *Nonadipose tissue production of leptin: leptin as a novel placenta-derived hormone in humans.* Nat Med, 1997. 3(9): p. 1029-33.

89.   Herrid, M., T. O'Shea, and J.R. McFarlane, *Ontogeny of leptin and its receptor expression in mouse testis during the postnatal period.* Mol Reprod Dev, 2008. 75(5): p. 874-80.

90.   Considine, R.V., et al., *Serum immunoreactive-leptin concentrations in normal-weight and obese humans.* N Engl J Med, 1996. 334(5): p. 292-5.

91.   Hamilton, B.S., et al., *Increased obese mRNA expression in omental fat cells from massively obese humans.* Nat Med, 1995. 1(9): p. 953-6.

92.   Levy, J.R., et al., *Dual regulation of leptin secretion: intracellular energy and calcium dependence of regulated pathway.* Am J Physiol Endocrinol Metab, 2000. 278(5): p. E892-901.

93.   Mizuno, T.M., et al., *Obese gene expression: reduction by fasting and stimulation by insulin and glucose in lean mice, and persistent elevation in acquired (diet-induced) and genetic (yellow agouti) obesity.* Proc Natl Acad Sci U S A, 1996. 93(8): p. 3434-8.

94.   Saladin, R., et al., *Transient increase in obese gene expression after food intake or insulin administration.* Nature, 1995. 377(6549): p. 527-9.

95.   Walker, C.G., et al., *Insulin determines leptin responses during a glucose challenge in fed and fasted rats.* Int J Obes (Lond), 2005. 29(4): p. 398-405.

96.   Haynes, W.G., et al., *Receptor-mediated regional sympathetic nerve activation by leptin.* J Clin Invest, 1997. 100(2): p. 270-8.

97.   Friedman, J.M. and J.L. Halaas, *Leptin and the regulation of body weight in mammals.* Nature, 1998. 395(6704): p. 763-70.

98.   Halaas, J.L., et al., *Weight-reducing effects of the plasma protein encoded by the obese gene.* Science, 1995. 269(5223): p. 543-6.

99.   Vaisse, C., et al., *Leptin activation of Stat3 in the hypothalamus of wild-type and ob/ob mice but not db/db mice.* Nat Genet, 1996. 14(1): p. 95-7.

100.   Montague, C.T., et al., *Congenital leptin deficiency is associated with severe early-onset obesity in humans.* Nature, 1997. 387(6636): p. 903-8.

101.   Clement, K., et al., *A mutation in the human leptin receptor gene causes obesity and pituitary dysfunction.* Nature, 1998. 392(6674): p. 398-401.

102.   Campfield, L.A., et al., *Recombinant mouse OB protein: evidence for a peripheral signal linking adiposity and central neural networks.* Science, 1995. 269(5223): p. 546-9.

103.   Pelleymounter, M.A., et al., *Effects of the obese gene product on body weight regulation in ob/ob mice.* Science, 1995. 269(5223): p. 540-3.

104.   Licinio, J., et al., *Phenotypic effects of leptin replacement on morbid obesity, diabetes mellitus, hypogonadism, and behavior in leptin-deficient adults.* Proc Natl Acad Sci U S A, 2004. 101(13): p. 4531-6.

105.   Farooqi, I.S., et al., *Effects of recombinant leptin therapy in a child with congenital leptin deficiency.* N Engl J Med, 1999. 341(12): p. 879-84.

106.   Maffei, M., et al., *Leptin levels in human and rodent: measurement of plasma leptin and ob RNA in obese and weight-reduced subjects.* Nat Med, 1995. 1(11): p. 1155-61.

107.   Morris, D.L. and L. Rui, *Recent advances in understanding leptin signaling and leptin resistance.* Am J Physiol Endocrinol Metab, 2009. 297(6): p. E1247-59.

108.   Heymsfield, S.B., et al., *Recombinant leptin for weight loss in obese and lean adults: a randomized, controlled, dose-escalation trial.* JAMA, 1999. 282(16): p. 1568-75.

109.   Fogteloo, A.J., et al., *Effects of recombinant human leptin treatment as an adjunct of moderate energy restriction on body weight, resting energy expenditure and energy intake in obese humans.* Diabetes Nutr Metab, 2003. 16(2): p. 109-14.

110. Van Heek, M., et al., *Diet-induced obese mice develop peripheral, but not central, resistance to leptin.* J Clin Invest, 1997. 99(3): p. 385-90.
111. Tartaglia, L.A., *The leptin receptor.* J Biol Chem, 1997. 272(10): p. 6093-6.
112. Chua, S.C., Jr., et al., *Fine structure of the murine leptin receptor gene: splice site suppression is required to form two alternatively spliced transcripts.* Genomics, 1997. 45(2): p. 264-70.
113. Lee, G.H., et al., *Abnormal splicing of the leptin receptor in diabetic mice.* Nature, 1996. 379(6566): p. 632-5.
114. Lollmann, B., et al., *Detection and quantification of the leptin receptor splice variants Ob-Ra, b, and, e in different mouse tissues.* Biochem Biophys Res Commun, 1997. 238(2): p. 648-52.
115. Hoggard, N., et al., *Localization of leptin receptor mRNA splice variants in murine peripheral tissues by RT-PCR and in situ hybridization.* Biochem Biophys Res Commun, 1997. 232(2): p. 383-7.
116. Banks, A.S., et al., *Activation of downstream signals by the long form of the leptin receptor.* J Biol Chem, 2000. 275(19): p. 14563-72.
117. Devos, R., et al., *Ligand-independent dimerization of the extracellular domain of the leptin receptor and determination of the stoichiometry of leptin binding.* J Biol Chem, 1997. 272(29): p. 18304-10.
118. White, D.W., et al., *Leptin receptor (OB-R) signaling. Cytoplasmic domain mutational analysis and evidence for receptor homo-oligomerization.* J Biol Chem, 1997. 272(7): p. 4065-71.
119. Ghilardi, N. and R.C. Skoda, *The leptin receptor activates janus kinase 2 and signals for proliferation in a factor-dependent cell line.* Mol Endocrinol, 1997. 11(4): p. 393-9.
120. Hekerman, P., et al., *Pleiotropy of leptin receptor signalling is defined by distinct roles of the intracellular tyrosines.* FEBS J, 2005. 272(1): p. 109-19.
121. Li, C. and J.M. Friedman, *Leptin receptor activation of SH2 domain containing protein tyrosine phosphatase 2 modulates Ob receptor signal transduction.* Proc Natl Acad Sci U S A, 1999. 96(17): p. 9677-82.
122. Zhang, S.Q., et al., *Shp2 regulates SRC family kinase activity and Ras/Erk activation by controlling Csk recruitment.* Mol Cell, 2004. 13(3): p. 341-55.
123. Bjorbaek, C., et al., *Divergent roles of SHP-2 in ERK activation by leptin receptors.* J Biol Chem, 2001. 276(7): p. 4747-55.
124. Gong, Y., et al., *The long form of the leptin receptor regulates STAT5 and ribosomal protein S6 via alternate mechanisms.* J Biol Chem, 2007. 282(42): p. 31019-27.
125. Baumann, H., et al., *The full-length leptin receptor has signaling capabilities of interleukin 6-type cytokine receptors.* Proc Natl Acad Sci U S A, 1996. 93(16): p. 8374-8.
126. Stahl, N., et al., *Choice of STATs and other substrates specified by modular tyrosine-based motifs in cytokine receptors.* Science, 1995. 267(5202): p. 1349-53.
127. Darnell, J.E., Jr., *STATs and gene regulation.* Science, 1997. 277(5332): p. 1630-5.
128. Horvath, C.M., *The Jak-STAT pathway stimulated by interferon gamma.* Sci STKE, 2004. 2004(260): p. tr8.
129. Krebs, D.L. and D.J. Hilton, *SOCS: physiological suppressors of cytokine signaling.* J Cell Sci, 2000. 113 (Pt 16): p. 2813-9.
130. Nicholson, S.E. and D.J. Hilton, *The SOCS proteins: a new family of negative regulators of signal transduction.* J Leukoc Biol, 1998. 63(6): p. 665-8.
131. Bates, S.H., et al., *STAT3 signalling is required for leptin regulation of energy balance but not reproduction.* Nature, 2003. 421(6925): p. 856-9.

132. Cui, Y., et al., *Essential role of STAT3 in body weight and glucose homeostasis.* Mol Cell Biol, 2004. 24(1): p. 258-69.

133. Gao, Q., et al., *Disruption of neural signal transducer and activator of transcription 3 causes obesity, diabetes, infertility, and thermal dysregulation.* Proc Natl Acad Sci U S A, 2004. 101(13): p. 4661-6.

134. Jiang, L., et al., *Tyrosine-dependent and -independent actions of leptin receptor in control of energy balance and glucose homeostasis.* Proc Natl Acad Sci U S A, 2008. 105(47): p. 18619-24.

135. Niswender, K.D., et al., *Intracellular signalling. Key enzyme in leptin-induced anorexia.* Nature, 2001. 413(6858): p. 794-5.

136. Mirshamsi, S., et al., *Leptin and insulin stimulation of signalling pathways in arcuate nucleus neurones: PI3K dependent actin reorganization and KATP channel activation.* BMC Neurosci, 2004. 5: p. 54.

137. Fu, X.Y., et al., *The proteins of ISGF-3, the interferon alpha-induced transcriptional activator, define a gene family involved in signal transduction.* Proc Natl Acad Sci U S A, 1992. 89(16): p. 7840-3.

138. Lim, C.P. and X. Cao, *Structure, function, and regulation of STAT proteins.* Mol Biosyst, 2006. 2(11): p. 536-50.

139. Akira, S., *Functional roles of STAT family proteins: lessons from knockout mice.* Stem Cells, 1999. 17(3): p. 138-46.

140. Meraz, M.A., et al., *Targeted disruption of the Stat1 gene in mice reveals unexpected physiologic specificity in the JAK-STAT signaling pathway.* Cell, 1996. 84(3): p. 431-42.

141. Kaplan, D.H., et al., *Demonstration of an interferon gamma-dependent tumor surveillance system in immunocompetent mice.* Proc Natl Acad Sci U S A, 1998. 95(13): p. 7556-61.

142. Kaplan, M.H., et al., *Impaired IL-12 responses and enhanced development of Th2 cells in Stat4-deficient mice.* Nature, 1996. 382(6587): p. 174-7.

143. Takeda, K., et al., *Essential role of Stat6 in IL-4 signalling.* Nature, 1996. 380(6575): p. 627-30.

144. Nosaka, T., et al., *STAT5 as a molecular regulator of proliferation, differentiation and apoptosis in hematopoietic cells.* EMBO J, 1999. 18(17): p. 4754-65.

145. Liu, X., G.W. Robinson, and L. Hennighausen, *Activation of Stat5a and Stat5b by tyrosine phosphorylation is tightly linked to mammary gland differentiation.* Mol Endocrinol, 1996. 10(12): p. 1496-506.

146. Takeda, K., et al., *Targeted disruption of the mouse Stat3 gene leads to early embryonic lethality.* Proc Natl Acad Sci U S A, 1997. 94(8): p. 3801-4.

147. Sano, S., et al., *Keratinocyte-specific ablation of Stat3 exhibits impaired skin remodeling, but does not affect skin morphogenesis.* EMBO J, 1999. 18(17): p. 4657-68.

148. Chapman, R.S., et al., *Suppression of epithelial apoptosis and delayed mammary gland involution in mice with a conditional knockout of Stat3.* Genes Dev, 1999. 13(19): p. 2604-16.

149. Takeda, K., et al., *Enhanced Th1 activity and development of chronic enterocolitis in mice devoid of Stat3 in macrophages and neutrophils.* Immunity, 1999. 10(1): p. 39-49.

150. Takeda, K., et al., *Stat3 activation is responsible for IL-6-dependent T cell proliferation through preventing apoptosis: generation and characterization of T cell-specific Stat3-deficient mice.* J Immunol, 1998. 161(9): p. 4652-60.

151. Bowman, T., et al., *STATs in oncogenesis.* Oncogene, 2000. 19(21): p. 2474-88.

152. Kim, M.S., et al., *Role of hypothalamic Foxo1 in the regulation of food intake and energy homeostasis.* Nat Neurosci, 2006. 9(7): p. 901-6.

153. Xu, A.W., et al., *Inactivation of signal transducer and activator of transcription 3 in proopiomelanocortin (Pomc) neurons causes decreased pomc expression, mild obesity, and defects in compensatory refeeding.* Endocrinology, 2007. 148(1): p. 72-80.

154. Bromberg, J. and X. Chen, *STAT proteins: signal tranducers and activators of transcription.* Methods Enzymol, 2001. 333: p. 138-51.

155. Bromberg, J.F., *Activation of STAT proteins and growth control.* Bioessays, 2001. 23(2): p. 161-9.

156. Kisseleva, T., et al., *Signaling through the JAK/STAT pathway, recent advances and future challenges.* Gene, 2002. 285(1-2): p. 1-24.

157. Wong, M. and E.N. Fish, *RANTES and MIP-1alpha activate stats in T cells.* J Biol Chem, 1998. 273(1): p. 309-14.

158. Garcia, R. and R. Jove, *Activation of STAT transcription factors in oncogenic tyrosine kinase signaling.* J Biomed Sci, 1998. 5(2): p. 79-85.

159. Chung, J., et al., *STAT3 serine phosphorylation by ERK-dependent and -independent pathways negatively modulates its tyrosine phosphorylation.* Mol Cell Biol, 1997. 17(11): p. 6508-16.

160. Lim, C.P. and X. Cao, *Serine phosphorylation and negative regulation of Stat3 by JNK.* J Biol Chem, 1999. 274(43): p. 31055-61.

161. Rao, A., C. Luo, and P.G. Hogan, *Transcription factors of the NFAT family: regulation and function.* Annu Rev Immunol, 1997. 15: p. 707-47.

162. Yoshimura, A., *Negative regulation of cytokine signaling.* Clin Rev Allergy Immunol, 2005. 28(3): p. 205-20.

163. Brierley, M.M. and E.N. Fish, *Stats: multifaceted regulators of transcription.* J Interferon Cytokine Res, 2005. 25(12): p. 733-44.

164. Yasukawa, H., et al., *The JAK-binding protein JAB inhibits Janus tyrosine kinase activity through binding in the activation loop.* EMBO J, 1999. 18(5): p. 1309-20.

165. Dunn, S.L., et al., *Feedback inhibition of leptin receptor/Jak2 signaling via Tyr1138 of the leptin receptor and suppressor of cytokine signaling 3.* Mol Endocrinol, 2005. 19(4): p. 925-38.

166. Yoshimura, A., et al., *A novel cytokine-inducible gene CIS encodes an SH2-containing protein that binds to tyrosine-phosphorylated interleukin 3 and erythropoietin receptors.* EMBO J, 1995. 14(12): p. 2816-26.

167. Chung, C.D., et al., *Specific inhibition of Stat3 signal transduction by PIAS3.* Science, 1997. 278(5344): p. 1803-5.

168. Symes, A., et al., *The protein tyrosine phosphatase SHP-2 negatively regulates ciliary neurotrophic factor induction of gene expression.* Curr Biol, 1997. 7(9): p. 697-700.

169. Myers, M.P., et al., *TYK2 and JAK2 are substrates of protein-tyrosine phosphatase 1B.* J Biol Chem, 2001. 276(51): p. 47771-4.

170. Kiuchi, N., et al., *STAT3 is required for the gp130-mediated full activation of the c-myc gene.* J Exp Med, 1999. 189(1): p. 63-73.

171. Zhang, X., et al., *Interacting regions in Stat3 and c-Jun that participate in cooperative transcriptional activation.* Mol Cell Biol, 1999. 19(10): p. 7138-46.

172. Bromberg, J.F., et al., *Stat3 as an oncogene.* Cell, 1999. 98(3): p. 295-303.

173. Shen, Y., et al., *Constitutively activated Stat3 protects fibroblasts from serum withdrawal and UV-induced apoptosis and antagonizes the proapoptotic effects of activated Stat1.* Proc Natl Acad Sci U S A, 2001. 98(4): p. 1543-8.

174. Niu, G., et al., *Constitutive Stat3 activity up-regulates VEGF expression and tumor angiogenesis.* Oncogene, 2002. 21(13): p. 2000-8.

175. Leslie, K., et al., *Cyclin D1 is transcriptionally regulated by and required for transformation by activated signal transducer and activator of transcription 3.* Cancer Res, 2006. 66(5): p. 2544-52.

176. Azare, J., et al., *Constitutively activated Stat3 induces tumorigenesis and enhances cell motility of prostate epithelial cells through integrin beta 6.* Mol Cell Biol, 2007. 27(12): p. 4444-53.

177. Banting, F.G., et al., *Pancreatic extracts in the treatment of diabetes mellitus: preliminary report. 1922.* CMAJ, 1991. 145(10): p. 1281-6.

178. Davidson, H.W., C.J. Rhodes, and J.C. Hutton, *Intraorganellar calcium and pH control proinsulin cleavage in the pancreatic beta cell via two distinct site-specific endopeptidases.* Nature, 1988. 333(6168): p. 93-6.

179. Docherty, K. and J.C. Hutton, *Carboxypeptidase activity in the insulin secretory granule.* FEBS Lett, 1983. 162(1): p. 137-41.

180. Steiner, D.F., *Proinsulin and the biosynthesis of insulin.* N Engl J Med, 1969. 280(20): p. 1106-13.

181. Polonsky, K.S., B.D. Given, and E. Van Cauter, *Twenty-four-hour profiles and pulsatile patterns of insulin secretion in normal and obese subjects.* J Clin Invest, 1988. 81(2): p. 442-8.

182. Bagdade, J.D., E.L. Bierman, and D. Porte, Jr., *The significance of basal insulin levels in the evaluation of the insulin response to glucose in diabetic and nondiabetic subjects.* J Clin Invest, 1967. 46(10): p. 1549-57.

183. Birnbaum, M.J., *The insulin-sensitive glucose transporter.* Int Rev Cytol, 1992. 137: p. 239-97.

184. Cushman, S.W. and L.J. Wardzala, *Potential mechanism of insulin action on glucose transport in the isolated rat adipose cell. Apparent translocation of intracellular transport systems to the plasma membrane.* J Biol Chem, 1980. 255(10): p. 4758-62.

185. Poitout, V., et al., *Regulation of the insulin gene by glucose and fatty acids.* J Nutr, 2006. 136(4): p. 873-6.

186. Pilkis, S.J. and D.K. Granner, *Molecular physiology of the regulation of hepatic gluconeogenesis and glycolysis.* Annu Rev Physiol, 1992. 54: p. 885-909.

187. Kahn, C.R., *Banting Lecture. Insulin action, diabetogenes, and the cause of type II diabetes.* Diabetes, 1994. 43(8): p. 1066-84.

188. Marks, J.L., et al., *Localization of insulin receptor mRNA in rat brain by in situ hybridization.* Endocrinology, 1990. 127(6): p. 3234-6.

189. Porte, D., Jr. and S.C. Woods, *Regulation of food intake and body weight in insulin.* Diabetologia, 1981. 20 Suppl: p. 274-80.

190. Havrankova, J., J. Roth, and M. Brownstein, *Insulin receptors are widely distributed in the central nervous system of the rat.* Nature, 1978. 272(5656): p. 827-9.

191. Koch, L., et al., *Central insulin action regulates peripheral glucose and fat metabolism in mice.* J Clin Invest, 2008. 118(6): p. 2132-47.

192. Bruning, J.C., et al., *Role of brain insulin receptor in control of body weight and reproduction.* Science, 2000. 289(5487): p. 2122-5.

193. Konner, A.C., et al., *Insulin action in AgRP-expressing neurons is required for suppression of hepatic glucose production.* Cell Metab, 2007. 5(6): p. 438-49.

194. Braciale, V.L., J.R. Gavin, 3rd, and T.J. Braciale, *Inducible expression of insulin receptors on T lymphocyte clones.* J Exp Med, 1982. 156(2): p. 664-9.

195. Harbeck, M.C., et al., *Expression of insulin receptor mRNA and insulin receptor substrate 1 in pancreatic islet beta-cells.* Diabetes, 1996. 45(6): p. 711-7.

196. Kurokawa, K., et al., *Binding of 125I-insulin to the isolated glomeruli of rat kidney.* J Clin Invest, 1979. 64(5): p. 1357-64.

197. Bruning, J.C., et al., *A muscle-specific insulin receptor knockout exhibits features of the metabolic syndrome of NIDDM without altering glucose tolerance.* Mol Cell, 1998. 2(5): p. 559-69.

198. Jacobs, S., et al., *Insulin receptor: covalent labeling and identification of subunits.* Proc Natl Acad Sci U S A, 1979. 76(10): p. 4918-21.

199. Kasuga, M., et al., *The structure of insulin receptor and its subunits. Evidence for multiple nonreduced forms and a 210,000 possible proreceptor.* J Biol Chem, 1982. 257(17): p. 10392-9.

200. Goren, H.J., M.F. White, and C.R. Kahn, *Separate domains of the insulin receptor contain sites of autophosphorylation and tyrosine kinase activity.* Biochemistry, 1987. 26(8): p. 2374-82.

201. Kasuga, M., et al., *Insulin stimulates tyrosine phosphorylation of the insulin receptor in a cell-free system.* Nature, 1982. 298(5875): p. 667-9.

202. Schenker, E. and R.A. Kohanski, *Conformational states of the insulin receptor.* Biochem Biophys Res Commun, 1988. 157(1): p. 140-5.

203. Eck, M.J., et al., *Structure of the IRS-1 PTB domain bound to the juxtamembrane region of the insulin receptor.* Cell, 1996. 85(5): p. 695-705.

204. Burks, D.J., et al., *Heterologous pleckstrin homology domains do not couple IRS-1 to the insulin receptor.* J Biol Chem, 1997. 272(44): p. 27716-21.

205. Myers, M.G., Jr. and M.F. White, *Insulin signal transduction and the IRS proteins.* Annu Rev Pharmacol Toxicol, 1996. 36: p. 615-58.

206. Van Obberghen, E., et al., *Surfing the insulin signaling web.* Eur J Clin Invest, 2001. 31(11): p. 966-77.

207. Lima, M.H., et al., *Regulation of IRS-1/SHP2 interaction and AKT phosphorylation in animal models of insulin resistance.* Endocrine, 2002. 18(1): p. 1-12.

208. Hadari, Y.R., et al., *Insulin and insulinomimetic agents induce activation of phosphatidylinositol 3'-kinase upon its association with pp185 (IRS-1) in intact rat livers.* J Biol Chem, 1992. 267(25): p. 17483-6.

209. Ito, T., Y. Sasaki, and J.R. Wands, *Overexpression of human insulin receptor substrate 1 induces cellular transformation with activation of mitogen-activated protein kinases.* Mol Cell Biol, 1996. 16(3): p. 943-51.

210. Skolnik, E.Y., et al., *The function of GRB2 in linking the insulin receptor to Ras signaling pathways.* Science, 1993. 260(5116): p. 1953-5.

211. Terauchi, Y., et al., *Increased insulin sensitivity and hypoglycaemia in mice lacking the p85 alpha subunit of phosphoinositide 3-kinase.* Nat Genet, 1999. 21(2): p. 230-5.

212. Fruman, D.A., et al., *Hypoglycaemia, liver necrosis and perinatal death in mice lacking all isoforms of phosphoinositide 3-kinase p85 alpha.* Nat Genet, 2000. 26(3): p. 379-82.

213. Fruman, D.A., L.C. Cantley, and C.L. Carpenter, *Structural organization and alternative splicing of the murine phosphoinositide 3-kinase p85 alpha gene.* Genomics, 1996. 37(1): p. 113-21.

214. Whitman, M., et al., *Type I phosphatidylinositol kinase makes a novel inositol phospholipid, phosphatidylinositol-3-phosphate.* Nature, 1988. 332(6165): p. 644-6.

215. Skolnik, E.Y., et al., *Cloning of PI3 kinase-associated p85 utilizing a novel method for expression/cloning of target proteins for receptor tyrosine kinases.* Cell, 1991. 65(1): p. 83-90.

216. Yamada, K.M. and M. Araki, *Tumor suppressor PTEN: modulator of cell signaling, growth, migration and apoptosis.* J Cell Sci, 2001. 114(Pt 13): p. 2375-82.

217. Vanhaesebroeck, B. and D.R. Alessi, *The PI3K-PDK1 connection: more than just a road to PKB.* Biochem J, 2000. 346 Pt 3: p. 561-76.

218. Cheatham, B. and C.R. Kahn, *Insulin action and the insulin signaling network.* Endocr Rev, 1995. 16(2): p. 117-42.

219. Saltiel, A.R. and C.R. Kahn, *Insulin signalling and the regulation of glucose and lipid metabolism.* Nature, 2001. 414(6865): p. 799-806.

220. Weigel, D. and H. Jackle, *The fork head domain: a novel DNA binding motif of eukaryotic transcription factors?* Cell, 1990. 63(3): p. 455-6.

221. Clark, K.L., et al., *Co-crystal structure of the HNF-3/fork head DNA-recognition motif resembles histone H5.* Nature, 1993. 364(6436): p. 412-20.

222. Weigel, D., et al., *The homeotic gene fork head encodes a nuclear protein and is expressed in the terminal regions of the Drosophila embryo.* Cell, 1989. 57(4): p. 645-58.

223. Kaestner, K.H., W. Knochel, and D.E. Martinez, *Unified nomenclature for the winged helix/forkhead transcription factors.* Genes Dev, 2000. 14(2): p. 142-6.

224. Galili, N., et al., *Fusion of a fork head domain gene to PAX3 in the solid tumour alveolar rhabdomyosarcoma.* Nat Genet, 1993. 5(3): p. 230-5.

225. Hillion, J., et al., *AF6q21, a novel partner of the MLL gene in t(6;11)(q21;q23), defines a forkhead transcriptional factor subfamily.* Blood, 1997. 90(9): p. 3714-9.

226. Corral, J., et al., *Acute leukemias of different lineages have similar MLL gene fusions encoding related chimeric proteins resulting from chromosomal translocation.* Proc Natl Acad Sci U S A, 1993. 90(18): p. 8538-42.

227. Jacobs, F.M., et al., *FoxO6, a novel member of the FoxO class of transcription factors with distinct shuttling dynamics.* J Biol Chem, 2003. 278(38): p. 35959-67.

228. Furuyama, T., et al., *Identification of the differential distribution patterns of mRNAs and consensus binding sequences for mouse DAF-16 homologues.* Biochem J, 2000. 349(Pt 2): p. 629-34.

229. Biggs, W.H., 3rd, W.K. Cavenee, and K.C. Arden, *Identification and characterization of members of the FKHR (FOX O) subclass of winged-helix transcription factors in the mouse.* Mamm Genome, 2001. 12(6): p. 416-25.

230. Anderson, M.J., et al., *Embryonic expression of the tumor-associated PAX3-FKHR fusion protein interferes with the developmental functions of Pax3.* Proc Natl Acad Sci U S A, 2001. 98(4): p. 1589-94.

231. Biggs, W.H., 3rd, et al., *Protein kinase B/Akt-mediated phosphorylation promotes nuclear exclusion of the winged helix transcription factor FKHR1.* Proc Natl Acad Sci U S A, 1999. 96(13): p. 7421-6.

232. Brownawell, A.M., et al., *Inhibition of nuclear import by protein kinase B (Akt) regulates the subcellular distribution and activity of the forkhead transcription factor AFX.* Mol Cell Biol, 2001. 21(10): p. 3534-46.

233. Gilley, J., P.J. Coffer, and J. Ham, *FOXO transcription factors directly activate bim gene expression and promote apoptosis in sympathetic neurons.* J Cell Biol, 2003. 162(4): p. 613-22.

234. Greer, E.L. and A. Brunet, *FOXO transcription factors at the interface between longevity and tumor suppression.* Oncogene, 2005. 24(50): p. 7410-25.

235. Accili, D. and K.C. Arden, *FoxOs at the crossroads of cellular metabolism, differentiation, and transformation.* Cell, 2004. 117(4): p. 421-6.

236. van der Vos, K.E. and P.J. Coffer, *FOXO-binding partners: it takes two to tango.* Oncogene, 2008. 27(16): p. 2289-99.

237. Obsil, T. and V. Obsilova, *Structure/function relationships underlying regulation of FOXO transcription factors.* Oncogene, 2008. 27(16): p. 2263-75.

238. Hosaka, T., et al., *Disruption of forkhead transcription factor (FOXO) family members in mice reveals their functional diversification.* Proc Natl Acad Sci U S A, 2004. 101(9): p. 2975-80.

239. Ho, K.K., S.S. Myatt, and E.W. Lam, *Many forks in the path: cycling with FoxO.* Oncogene, 2008. 27(16): p. 2300-11.

240. Fu, Z. and D.J. Tindall, *FOXOs, cancer and regulation of apoptosis.* Oncogene, 2008. 27(16): p. 2312-9.

241. Peng, S.L., *Foxo in the immune system.* Oncogene, 2008. 27(16): p. 2337-44.

242. Partridge, L. and J.C. Bruning, *Forkhead transcription factors and ageing.* Oncogene, 2008. 27(16): p. 2351-63.

243. Puigserver, P., et al., *Insulin-regulated hepatic gluconeogenesis through FOXO1-PGC-1alpha interaction.* Nature, 2003. 423(6939): p. 550-5.

244. Nakae, J., et al., *Regulation of insulin action and pancreatic beta-cell function by mutated alleles of the gene encoding forkhead transcription factor Foxo1.* Nat Genet, 2002. 32(2): p. 245-53.

245. Matsumoto, M., et al., *Dual role of transcription factor FoxO1 in controlling hepatic insulin sensitivity and lipid metabolism.* J Clin Invest, 2006. 116(9): p. 2464-72.

246. Kitamura, T., et al., *The forkhead transcription factor Foxo1 links insulin signaling to Pdx1 regulation of pancreatic beta cell growth.* J Clin Invest, 2002. 110(12): p. 1839-47.

247. Kubota, N., et al., *Disruption of insulin receptor substrate 2 causes type 2 diabetes because of liver insulin resistance and lack of compensatory beta-cell hyperplasia.* Diabetes, 2000. 49(11): p. 1880-9.

248. Hribal, M.L., et al., *Regulation of insulin-like growth factor-dependent myoblast differentiation by Foxo forkhead transcription factors.* J Cell Biol, 2003. 162(4): p. 535-41.

249. Kamei, Y., et al., *Skeletal muscle FOXO1 (FKHR) transgenic mice have less skeletal muscle mass, down-regulated Type I (slow twitch/red muscle) fiber genes, and impaired glycemic control.* J Biol Chem, 2004. 279(39): p. 41114-23.

250. Sandri, M., et al., *Foxo transcription factors induce the atrophy-related ubiquitin ligase atrogin-1 and cause skeletal muscle atrophy.* Cell, 2004. 117(3): p. 399-412.

251. Furuyama, T., et al., *Forkhead transcription factor FOXO1 (FKHR)-dependent induction of PDK4 gene expression in skeletal muscle during energy deprivation.* Biochem J, 2003. 375(Pt 2): p. 365-71.

252. Burgering, B.M. and G.J. Kops, *Cell cycle and death control: long live Forkheads.* Trends Biochem Sci, 2002. 27(7): p. 352-60.

253. Furukawa-Hibi, Y., et al., *FOXO transcription factors in cell-cycle regulation and the response to oxidative stress.* Antioxid Redox Signal, 2005. 7(5-6): p. 752-60.

254. Nakae, J., et al., *The forkhead transcription factor Foxo1 regulates adipocyte differentiation.* Dev Cell, 2003. 4(1): p. 119-29.

255. Plum, L., et al., *The obesity susceptibility gene Cpe links FoxO1 signaling in hypothalamic pro-opiomelanocortin neurons with regulation of food intake.* Nat Med, 2009. 15(10): p. 1195-201.

256. Vogt, P.K., H. Jiang, and M. Aoki, *Triple layer control: phosphorylation, acetylation and ubiquitination of FOXO proteins.* Cell Cycle, 2005. 4(7): p. 908-13.

257. Huang, H. and D.J. Tindall, *Dynamic FoxO transcription factors.* J Cell Sci, 2007. 120(Pt 15): p. 2479-87.

258. Van Der Heide, L.P., M.F. Hoekman, and M.P. Smidt, *The ins and outs of FoxO shuttling: mechanisms of FoxO translocation and transcriptional regulation.* Biochem J, 2004. 380(Pt 2): p. 297-309.

259. Brunet, A., et al., *Akt promotes cell survival by phosphorylating and inhibiting a Forkhead transcription factor.* Cell, 1999. 96(6): p. 857-68.

260. Brunet, A., et al., *14-3-3 transits to the nucleus and participates in dynamic nucleocytoplasmic transport.* J Cell Biol, 2002. 156(5): p. 817-28.

261.   Zhang, X., et al., *Phosphorylation of serine 256 suppresses transactivation by FKHR (FOXO1) by multiple mechanisms. Direct and indirect effects on nuclear/cytoplasmic shuttling and DNA binding.* J Biol Chem, 2002. 277(47): p. 45276-84.

262.   Tang, E.D., et al., *Negative regulation of the forkhead transcription factor FKHR by Akt.* J Biol Chem, 1999. 274(24): p. 16741-6.

263.   Rena, G., et al., *Two novel phosphorylation sites on FKHR that are critical for its nuclear exclusion.* EMBO J, 2002. 21(9): p. 2263-71.

264.   Woods, Y.L., et al., *The kinase DYRK1A phosphorylates the transcription factor FKHR at Ser329 in vitro, a novel in vivo phosphorylation site.* Biochem J, 2001. 355(Pt 3): p. 597-607.

265.   Brunet, A., et al., *Stress-dependent regulation of FOXO transcription factors by the SIRT1 deacetylase.* Science, 2004. 303(5666): p. 2011-5.

266.   Essers, M.A., et al., *FOXO transcription factor activation by oxidative stress mediated by the small GTPase Ral and JNK.* EMBO J, 2004. 23(24): p. 4802-12.

267.   Oh, S.W., et al., *JNK regulates lifespan in Caenorhabditis elegans by modulating nuclear translocation of forkhead transcription factor/DAF-16.* Proc Natl Acad Sci U S A, 2005. 102(12): p. 4494-9.

268.   Lehtinen, M.K., et al., *A conserved MST-FOXO signaling pathway mediates oxidative-stress responses and extends life span.* Cell, 2006. 125(5): p. 987-1001.

269.   van der Heide, L.P. and M.P. Smidt, *Regulation of FoxO activity by CBP/p300-mediated acetylation.* Trends Biochem Sci, 2005. 30(2): p. 81-6.

270.   Motta, M.C., et al., *Mammalian SIRT1 represses forkhead transcription factors.* Cell, 2004. 116(4): p. 551-63.

271.   Fukuoka, M., et al., *Negative regulation of forkhead transcription factor AFX (Foxo4) by CBP-induced acetylation.* Int J Mol Med, 2003. 12(4): p. 503-8.

272.   Daitoku, H., et al., *Silent information regulator 2 potentiates Foxo1-mediated transcription through its deacetylase activity.* Proc Natl Acad Sci U S A, 2004. 101(27): p. 10042-7.

273.   van der Horst, A., et al., *FOXO4 transcriptional activity is regulated by monoubiquitination and USP7/HAUSP.* Nat Cell Biol, 2006. 8(10): p. 1064-73.

274.   Matsuzaki, H., et al., *Insulin-induced phosphorylation of FKHR (Foxo1) targets to proteasomal degradation.* Proc Natl Acad Sci U S A, 2003. 100(20): p. 11285-90.

275.   Hu, M.C., et al., *IkappaB kinase promotes tumorigenesis through inhibition of forkhead FOXO3a.* Cell, 2004. 117(2): p. 225-37.

276.   Huang, H., et al., *Skp2 inhibits FOXO1 in tumor suppression through ubiquitin-mediated degradation.* Proc Natl Acad Sci U S A, 2005. 102(5): p. 1649-54.

277.   Aoki, M., H. Jiang, and P.K. Vogt, *Proteasomal degradation of the FoxO1 transcriptional regulator in cells transformed by the P3k and Akt oncoproteins.* Proc Natl Acad Sci U S A, 2004. 101(37): p. 13613-7.

278.   Plas, D.R. and C.B. Thompson, *Akt activation promotes degradation of tuberin and FOXO3a via the proteasome.* J Biol Chem, 2003. 278(14): p. 12361-6.

279.   Nakae, J., et al., *The forkhead transcription factor Foxo1 (Fkhr) confers insulin sensitivity onto glucose-6-phosphatase expression.* J Clin Invest, 2001. 108(9): p. 1359-67.

280.   Nakae, J., V. Barr, and D. Accili, *Differential regulation of gene expression by insulin and IGF-1 receptors correlates with phosphorylation of a single amino acid residue in the forkhead transcription factor FKHR.* EMBO J, 2000. 19(5): p. 989-96.

281.   Belgardt, B.F., et al., *PDK1 deficiency in POMC-expressing cells reveals FOXO1-dependent and -independent pathways in control of energy homeostasis and stress response.* Cell Metab, 2008. 7(4): p. 291-301.

282. Sambrook, J., Russel, D.W., *Molecular cloning: a laboratory manual*. Vol. 2344 pp pp. 2001: CSHL Press.

283. Inoue, H., H. Nojima, and H. Okayama, *High efficiency transformation of Escherichia coli with plasmids*. Gene, 1990. 96(1): p. 23-8.

284. Birnboim, H.C., *A rapid alkaline extraction method for the isolation of plasmid DNA*. Methods Enzymol, 1983. 100: p. 243-55.

285. Zhou, C., Y. Yang, and A.Y. Jong, *Mini-prep in ten minutes*. Biotechniques, 1990. 8(2): p. 172-3.

286. Wunderlich, F.T., Rajewski, K. , *unpublished data*. 2002.

287. Schmidt-Supprian, M., *unpublished data*.

288. Okabe, M., et al., *'Green mice' as a source of ubiquitous green cells*. FEBS Lett, 1997. 407(3): p. 313-9.

289. Lui, J., Accili, D., *unpublished data*.

290. Pasparakis, M., Kollias G., *Production of cytokine transgenic and knockout mice. In Cytokines: A Practical Approach. F.R. Balkwill, ed.* Oxford, Oxford University Press, 1995: p. 297-324.

291. Sanger, F., S. Nicklen, and A.R. Coulson, *DNA sequencing with chain-terminating inhibitors*. Proc Natl Acad Sci U S A, 1977. 74(12): p. 5463-7.

292. Mullis, K.B. and F.A. Faloona, *Specific synthesis of DNA in vitro via a polymerase-catalyzed chain reaction*. Methods Enzymol, 1987. 155: p. 335-50.

293. Saiki, R.K., et al., *Enzymatic amplification of beta-globin genomic sequences and restriction site analysis for diagnosis of sickle cell anemia*. Science, 1985. 230(4732): p. 1350-4.

294. Chomczynski, P. and P.K. Qasba, *Alkaline transfer of DNA to plastic membrane*. Biochem Biophys Res Commun, 1984. 122(1): p. 340-4.

295. Feinberg, A.P. and B. Vogelstein, *"A technique for radiolabeling DNA restriction endonuclease fragments to high specific activity". Addendum*. Anal Biochem, 1984. 137(1): p. 266-7.

296. Mao, X., Y. Fujiwara, and S.H. Orkin, *Improved reporter strain for monitoring Cre recombinase-mediated DNA excisions in mice*. Proc Natl Acad Sci U S A, 1999. 96(9): p. 5037-42.

297. Hogan, B., Costantini, F., Lacey, E., *Manipulation the mouse embryo: A Laboratory Manual*. Cold Spring Harbor Laboratory Press, 1986.

298. Todaro, G.J. and H. Green, *Cell growth and the initiation of transformation by SV40*. Proc Natl Acad Sci U S A, 1966. 55(2): p. 302-8.

299. Eggan, K. and R. Jaenisch, *Differentiation of F1 embryonic stem cells into viable male and female mice by tetraploid embryo complementation*. Methods Enzymol, 2003. 365: p. 25-39.

300. Torres, R.M., Kühn, R. , *Laboratory Protocols for Conditional Gene Targeting*. Oxford, Oxford University Press, 1997.

301. Peitz, M., et al., *Ability of the hydrophobic FGF and basic TAT peptides to promote cellular uptake of recombinant Cre recombinase: a tool for efficient genetic engineering of mammalian genomes*. Proc Natl Acad Sci U S A, 2002. 99(7): p. 4489-94.

302. Horn, R. and A. Marty, *Muscarinic activation of ionic currents measured by a new whole-cell recording method*. J Gen Physiol, 1988. 92(2): p. 145-59.

303. Akaike, N. and N. Harata, *Nystatin perforated patch recording and its applications to analyses of intracellular mechanisms*. Jpn J Physiol, 1994. 44(5): p. 433-73.

304. Lindau, M. and J.M. Fernandez, *IgE-mediated degranulation of mast cells does not require opening of ion channels*. Nature, 1986. 319(6049): p. 150-3.

305.   Rae, J., et al., *Low access resistance perforated patch recordings using amphotericin B.* J Neurosci Methods, 1991. 37(1): p. 15-26.

306.   Dodt, H.U. and W. Zieglgansberger, *Visualizing unstained neurons in living brain slices by infrared DIC-videomicroscopy.* Brain Res, 1990. 537(1-2): p. 333-6.

307.   Parton, L.E., et al., *Glucose sensing by POMC neurons regulates glucose homeostasis and is impaired in obesity.* Nature, 2007. 449(7159): p. 228-32.

308.   Claret, M., et al., *AMPK is essential for energy homeostasis regulation and glucose sensing by POMC and AgRP neurons.* J Clin Invest, 2007. 117(8): p. 2325-36.

309.   Dhillon, H., et al., *Leptin directly activates SF1 neurons in the VMH, and this action by leptin is required for normal body-weight homeostasis.* Neuron, 2006. 49(2): p. 191-203.

310.   Kloppenburg, P., et al., *Heterogeneous effects of dopamine on highly localized, voltage-induced Ca2+ accumulation in identified motoneurons.* J Neurophysiol, 2007. 98(5): p. 2910-7.

311.   Janoschek, R., et al., *gp130 signaling in proopiomelanocortin neurons mediates the acute anorectic response to centrally applied ciliary neurotrophic factor.* Proc Natl Acad Sci U S A, 2006. 103(28): p. 10707-12.

312.   Seibler, J., et al., *Rapid generation of inducible mouse mutants.* Nucleic Acids Res, 2003. 31(4): p. e12.

313.   Friedrich, G. and P. Soriano, *Promoter traps in embryonic stem cells: a genetic screen to identify and mutate developmental genes in mice.* Genes Dev, 1991. 5(9): p. 1513-23.

314.   Schubert, M., et al., *Role for neuronal insulin resistance in neurodegenerative diseases.* Proc Natl Acad Sci U S A, 2004. 101(9): p. 3100-5.

315.   Plum, L., et al., *Enhanced PIP3 signaling in POMC neurons causes KATP channel activation and leads to diet-sensitive obesity.* J Clin Invest, 2006. 116(7): p. 1886-901.

316.   Lilie, R., *Histopathologic Technic and Practical Histochemistry.* McGraw-Hill Book Co., New York, 1965. 3rd edition.

317.   Banny, T.M. and G. Clark, *The new domestic cresyl echt violet.* Stain Technol, 1950. 25(4): p. 195-6.

318.   Gavrieli, Y., Y. Sherman, and S.A. Ben-Sasson, *Identification of programmed cell death in situ via specific labeling of nuclear DNA fragmentation.* J Cell Biol, 1992. 119(3): p. 493-501.

319.   Laemmli, U.K., *Cleavage of structural proteins during the assembly of the head of bacteriophage T4.* Nature, 1970. 227(5259): p. 680-5.

320.   Silver, D.L., *Mouse genetics: concepts and applications.* Vol. 375 pp pp. 1995: Oxford University press.

321.   Casola, S., et al., *Tracking germinal center B cells expressing germ-line immunoglobulin gamma1 transcripts by conditional gene targeting.* Proc Natl Acad Sci U S A, 2006. 103(19): p. 7396-401.

322.   Balthasar, N., et al., *Leptin receptor signaling in POMC neurons is required for normal body weight homeostasis.* Neuron, 2004. 42(6): p. 983-91.

323.   Tronche, F., et al., *Disruption of the glucocorticoid receptor gene in the nervous system results in reduced anxiety.* Nat Genet, 1999. 23(1): p. 99-103.

324.   Koralov, S.B. and K. Rajewsky, *unpublished data.*

325.   Mesaros, A., et al., *Activation of Stat3 signaling in AgRP neurons promotes locomotor activity.* Cell Metab, 2008. 7(3): p. 236-48.

326.   Emanuelli, B., et al., *SOCS-3 is an insulin-induced negative regulator of insulin signaling.* J Biol Chem, 2000. 275(21): p. 15985-91.

327.   Rui, L., et al., *SOCS-1 and SOCS-3 block insulin signaling by ubiquitin-mediated degradation of IRS1 and IRS2.* J Biol Chem, 2002. 277(44): p. 42394-8.

328. Lam, E.W., R.E. Francis, and M. Petkovic, *FOXO transcription factors: key regulators of cell fate.* Biochem Soc Trans, 2006. 34(Pt 5): p. 722-6.

329. Dijkers, P.F., et al., *Expression of the pro-apoptotic Bcl-2 family member Bim is regulated by the forkhead transcription factor FKHR-L1.* Curr Biol, 2000. 10(19): p. 1201-4.

330. Stahl, M., et al., *The forkhead transcription factor FoxO regulates transcription of p27Kip1 and Bim in response to IL-2.* J Immunol, 2002. 168(10): p. 5024-31.

331. Zhu, Y., et al., *Ablation of NF1 function in neurons induces abnormal development of cerebral cortex and reactive gliosis in the brain.* Genes Dev, 2001. 15(7): p. 859-76.

332. Gilyarov, A.V., *Nestin in central nervous system cells.* Neurosci Behav Physiol, 2008. 38(2): p. 165-9.

333. Myers, M.G., Jr., et al., *The geometry of leptin action in the brain: more complicated than a simple ARC.* Cell Metab, 2009. 9(2): p. 117-23.

334. Obici, S., et al., *Hypothalamic insulin signaling is required for inhibition of glucose production.* Nat Med, 2002. 8(12): p. 1376-82.

335. Mao, X., et al., *Activation of EGFP expression by Cre-mediated excision in a new ROSA26 reporter mouse strain.* Blood, 2001. 97(1): p. 324-6.

336. Soriano, P., *Generalized lacZ expression with the ROSA26 Cre reporter strain.* Nat Genet, 1999. 21(1): p. 70-1.

337. Sauer, B., *Inducible gene targeting in mice using the Cre/lox system.* Methods, 1998. 14(4): p. 381-92.

338. Lin, S., et al., *Development of high fat diet-induced obesity and leptin resistance in C57Bl/6J mice.* Int J Obes Relat Metab Disord, 2000. 24(5): p. 639-46.

339. El-Haschimi, K., et al., *Two defects contribute to hypothalamic leptin resistance in mice with diet-induced obesity.* J Clin Invest, 2000. 105(12): p. 1827-32.

340. Martin, T.L., et al., *Diet-induced obesity alters AMP kinase activity in hypothalamus and skeletal muscle.* J Biol Chem, 2006. 281(28): p. 18933-41.

341. Seeley, R.J., et al., *Melanocortin receptors in leptin effects.* Nature, 1997. 390(6658): p. 349.

342. Munzberg, H., et al., *Role of signal transducer and activator of transcription 3 in regulation of hypothalamic proopiomelanocortin gene expression by leptin.* Endocrinology, 2003. 144(5): p. 2121-31.

343. Myers, M.G., M.A. Cowley, and H. Munzberg, *Mechanisms of leptin action and leptin resistance.* Annu Rev Physiol, 2008. 70: p. 537-56.

344. Bjorbaek, C., et al., *Identification of SOCS-3 as a potential mediator of central leptin resistance.* Mol Cell, 1998. 1(4): p. 619-25.

345. Bjorbak, C., et al., *SOCS3 mediates feedback inhibition of the leptin receptor via Tyr985.* J Biol Chem, 2000. 275(51): p. 40649-57.

346. Ueki, K., T. Kondo, and C.R. Kahn, *Suppressor of cytokine signaling 1 (SOCS-1) and SOCS-3 cause insulin resistance through inhibition of tyrosine phosphorylation of insulin receptor substrate proteins by discrete mechanisms.* Mol Cell Biol, 2004. 24(12): p. 5434-46.

347. Howard, J.K., et al., *Enhanced leptin sensitivity and attenuation of diet-induced obesity in mice with haploinsufficiency of Socs3.* Nat Med, 2004. 10(7): p. 734-8.

348. Kievit, P., et al., *Enhanced leptin sensitivity and improved glucose homeostasis in mice lacking suppressor of cytokine signaling-3 in POMC-expressing cells.* Cell Metab, 2006. 4(2): p. 123-32.

349. Reed, A.S., et al., *Functional role of Socs3 up-regulation in hypothalamic leptin resistance and long-term energy homeostasis.* Diabetes.

350. Parekh, P.I., et al., *Reversal of diet-induced obesity and diabetes in C57BL/6J mice.* Metabolism, 1998. 47(9): p. 1089-96.

351. Munzberg, H., J.S. Flier, and C. Bjorbaek, *Region-specific leptin resistance within the hypothalamus of diet-induced obese mice.* Endocrinology, 2004. 145(11): p. 4880-9.

352. Enriori, P.J., et al., *Diet-induced obesity causes severe but reversible leptin resistance in arcuate melanocortin neurons.* Cell Metab, 2007. 5(3): p. 181-94.

353. Gout, J., et al., *Leptin infusion and obesity in mouse cause alterations in the hypothalamic melanocortin system.* Obesity (Silver Spring), 2008. 16(8): p. 1763-9.

354. Lin, S., L.H. Storlien, and X.F. Huang, *Leptin receptor, NPY, POMC mRNA expression in the diet-induced obese mouse brain.* Brain Res, 2000. 875(1-2): p. 89-95.

355. Tups, A., et al., *Photoperiodic regulation of leptin sensitivity in the Siberian hamster, Phodopus sungorus, is reflected in arcuate nucleus SOCS-3 (suppressor of cytokine signaling) gene expression.* Endocrinology, 2004. 145(3): p. 1185-93.

356. Krol, E. and J.R. Speakman, *Regulation of body mass and adiposity in the field vole, Microtus agrestis: a model of leptin resistance.* J Endocrinol, 2007. 192(2): p. 271-8.

357. Mori, H., et al., *Socs3 deficiency in the brain elevates leptin sensitivity and confers resistance to diet-induced obesity.* Nat Med, 2004. 10(7): p. 739-43.

358. Rosenbaum, M., et al., *Leptin reverses weight loss-induced changes in regional neural activity responses to visual food stimuli.* J Clin Invest, 2008. 118(7): p. 2583-91.

359. Schwartz, M.W. and K.D. Niswender, *Adiposity signaling and biological defense against weight gain: absence of protection or central hormone resistance?* J Clin Endocrinol Metab, 2004. 89(12): p. 5889-97.

360. Berthoud, H.R., *Mind versus metabolism in the control of food intake and energy balance.* Physiol Behav, 2004. 81(5): p. 781-93.

361. Fukuda, M., et al., *Monitoring FoxO1 localization in chemically identified neurons.* J Neurosci, 2008. 28(50): p. 13640-8.

362. Iskandar, K., et al., *PDK1/ FoxO1 pathway in POMC neurons regulates Pomc expression and food intake.* Am J Physiol Endocrinol Metab.

363. Yang, G., et al., *FoxO1 inhibits leptin regulation of pro-opiomelanocortin promoter activity by blocking STAT3 interaction with specificity protein 1.* J Biol Chem, 2009. 284(6): p. 3719-27.

364. Modur, V., et al., *FOXO proteins regulate tumor necrosis factor-related apoptosis inducing ligand expression. Implications for PTEN mutation in prostate cancer.* J Biol Chem, 2002. 277(49): p. 47928-37.

365. Tran, H., et al., *DNA repair pathway stimulated by the forkhead transcription factor FOXO3a through the Gadd45 protein.* Science, 2002. 296(5567): p. 530-4.

366. Barthelemy, C., C.E. Henderson, and B. Pettmann, *Foxo3a induces motoneuron death through the Fas pathway in cooperation with JNK.* BMC Neurosci, 2004. 5: p. 48.

367. Yuan, Z., et al., *Regulation of neuronal cell death by MST1-FOXO1 signaling.* J Biol Chem, 2009. 284(17): p. 11285-92.

368. Kawano, T., et al., *Decreased akt activity is associated with activation of forkhead transcription factor after transient forebrain ischemia in gerbil hippocampus.* J Cereb Blood Flow Metab, 2002. 22(8): p. 926-34.

369. Fukunaga, K., T. Ishigami, and T. Kawano, *Transcriptional regulation of neuronal genes and its effect on neural functions: expression and function of forkhead transcription factors in neurons.* J Pharmacol Sci, 2005. 98(3): p. 205-11.

370. Beal, M.F., *Aging, energy, and oxidative stress in neurodegenerative diseases.* Ann Neurol, 1995. 38(3): p. 357-66.

371. Davila, D. and I. Torres-Aleman, *Neuronal death by oxidative stress involves activation of FOXO3 through a two-arm pathway that activates stress kinases and attenuates insulin-like growth factor I signaling.* Mol Biol Cell, 2008. 19(5): p. 2014-25.

372. Kops, G.J., et al., *Forkhead transcription factor FOXO3a protects quiescent cells from oxidative stress.* Nature, 2002. 419(6904): p. 316-21.

373. Schilback, K. and M. Schubert, *unpublished data.*

374. Hommel, J.D., et al., *Leptin receptor signaling in midbrain dopamine neurons regulates feeding.* Neuron, 2006. 51(6): p. 801-10.

8 Acknowledgements

I am sincerely grateful to Prof. Dr. Jens C. Brüning for providing me with this interesting project, giving me the opportunity to work in his lab and his support.

I would like to thank Prof. Dr. Peter Kloppenburg, Prof. Dr. Siegfried Roth and Dr. Frank Thomas Wunderlich for agreeing to form my thesis committee.

Furthermore, I would like to thank Dr. Debora Grosskopf-Kroiher for excellent help during the Interdisciplinary Postgraduate Program Molecular Medicine.

I thank all former and present members of the Brüning lab for creating a friendly and productive environment, for help with experiments and for discussions. In particular, I would like to sincerely thank Jens Alber for aiding with mouse handling, Sonja Becker for blastocysts injections, Brigitte Hampel for immunohistochemical stainings, Dr. Claudia Wunderlich for *in situ* hybridisation, Sigrid Irlenbusch for ELISA and aiding with ES and EF cell culture, Christoph Göttlinger for cell sorting, Dr. Andrea Mesaros for discussions about STAT3-C, and AG Kloppenburg for electrophysiology. Furthermore, I thank all proofreaders of this manuscript and my labmates Jens Alber, Dr. Nora Redemann, and Bruno Klisch. Additionally, I am especially thankful to Dr. Gabriele Spohn for her support and friendship.

Special thanks to Dr. Frank Thomas Wunderlich for his support and letting me bug him about all the little things.

I remain indebted to my family, my parents Brigitte and Hans Dieter Ernst, my sister Sylvia Ernst-Kühn, and Jens Alber for their never-ending love and support, patience, and encouragement.

9 Erklärung

Ich versichere, dass ich die von mir vorgelegte Dissertation selbständig angefertigt, die benutzten Quellen und Hilfsmittel vollständig angegeben und die Stellen der Arbeit - einschließlich Tabellen, Karten und Abbildungen -, die anderen Werken im Wortlaut oder dem Sinn nach entnommen sind, in jedem Einzelfall als Entlehnung kenntlich gemacht habe; dass diese Dissertation noch keiner anderen Fakultät oder Universität zur Prüfung vorgelegen hat; dass sie - abgesehen von unten angegebenen Teilpublikationen - noch nicht veröffentlicht worden ist sowie, dass ich eine solche Veröffentlichung vor Abschluss des Promotionsverfahrens nicht vornehmen werde. Die Bestimmungen dieser Promotionsordnung sind mir bekannt. Die von mir vorgelegte Dissertation ist von Prof. Dr. Jens C. Brüning betreut worden.

Köln, Februar 2010   Marianne Bettina Ernst

Teilpublikationen

Ernst MB, Wunderlich CM, Hess S, Paehler M, Mesaros A, Koralov SB, Kleinridders A, Husch A, Münzberg H, Hampel B, Alber J, Kloppenburg P, Brüning JC, Wunderlich FT. Enhanced Stat3 activation in POMC neurons provokes negative feedback inhibition of leptin and insulin signaling in obesity. J Neurosci. 2009 Sep 16; 29 (37): 11582-93.

Belgardt BF, Husch A, Rother E, **Ernst MB**, Wunderlich FT, Hampel B, Klöckener T, Alessi D, Kloppenburg P, Brüning JC. PDK1 deficiency in POMC-expressing cells reveals FOXO1-dependent and –independent pathways in control of energy homeostasis and stress response. Cell Metab. 2008 Apr; 7 (4): 291-301.

10 Curriculum Vitae

Persönliche Daten

Name   Marianne Bettina Ernst

Geburt   28.03.1980

Adresse   Blankenheimerstraße 3, 50937 Köln

Email   marianne.ernst@web.de

Nationalität   deutsch

Schulische Ausbildung

1986-1990   Grundschule, Gladbeck

1990 - 1999   Ratsgymnasium, Gladbeck
                Abschluss: Allgemeine Hochschulreife

Studium

1999 - 2003   Studium Chemie (Diplom) an der Fachhochschule Gelsenkirchen

2001 - 2002   Praxissemester in der Zentralen Forschung, Ressort Synthese, Abteilung
                Enzymtechnologie der Bayer AG, Leverkusen

2003   Diplomarbeit in der Abteilung Mikrobielle Physiologie des Instituts für
                Biotechnologie des Forschungszentrums Jülich zum Thema:
                „Enantioselektive enzymatische Reduktion von Carbonylverbindungen
                mit Cofaktor-Regeneration in rekombinanten *Escherichia coli*

2003 - 2005   Studium Molekulare Biologie (Master of Science) an der Fachhochschule
                Gelsenkirchen

2004 - 2005   Research Project in der Abteilung Mausgenetik und Metabolismus des
                Instituts für Genetik der Universität zu Köln

2005   Master Arbeit in der Abteilung Mausgenetik und Metabolismus des
                Instituts für Genetik der Universität zu Köln zum Thema: „Konditionale
                Ausprägung von Foxo1-Varianten in der Maus"

seit 12/2005   Promotion in der Abteilung Mausgenetik und Metabolismus des Instituts
                für Genetik der Universität zu Köln

Publikationen

2010   Belgardt BF, Mauer J, Wunderlich FT, **Ernst MB**, Pal M, Spohn G, Brönneke H, Brodesser S, Hampel B, Schauss AC, Bruning J.Hypothalamic and Pituitary JNK1 Signaling Coordinately Regulates Glucose Metabolism. PNAS. (accepted).

2009   **Ernst MB**, Wunderlich CM, Hess S, Paehler M, Mesaros A, Koralov SB, Kleinridders A, Husch A, Münzberg H, Hampel B, Alber J, Kloppenburg P, Brüning JC, Wunderlich FT. Enhanced Stat3 activation in POMC neurons provokes negative feedback inhibition of leptin and insulin signaling in obesity. J Neurosci. 2009 Sep 16; 29 (37): 11582-93.

2008   Belgardt BF, Husch A, Rother E, **Ernst MB**, Wunderlich FT, Hampel B, Klöckener T, Alessi D, Kloppenburg P, Brüning JC. PDK1 deficiency in POMC-expressing cells reveals FOXO1-dependent and – independent pathways in control of energy homeostasis and stress response. Cell Metab. 2008 Apr; 7 (4): 291-301.

2008   Mesaros A, Koralov SB, Rother E, Wunderlich FT, **Ernst MB**, Barsh GS, Rajewsky K, Brüning JC. Activation of Stat3 signaling in AgRP neurons promotes locomotor activity. Cell Metab. 2008 Mar; 7 (8): 236-48.

2005   **Ernst M**, Kaup B, Müller M, Bringer-Meyer S, Sahm H. Enantioselective redution of carbonyl compounds by whole-cell biotransformation, combining a formate dehydrogenase and a (R)-specific alcohol dehydrogenase. Appl Microbiol Biotechnol. 2005 Mar; 66 (6): 629-34.